UNIVERSITY OF CALIFORNIA
RIVERSIDE

The Kinetic Mechanism of Flavin-Based Electron Bifurcation (FBEB) in the Crotonyl-CoA-Dependent NADH:ferredoxin Oxidoreductase Complex From the Bacterium *Megasphaera elsdenii*

A Dissertation submitted in partial satisfaction
of the requirements for the degree of

Doctor of Philosophy

in

Biophysics

by

Wayne W Vigil Jr

June 2024

Dissertation Committee:
Dr. Russ Hille, Chairperson
Dr. Richard Debus
Dr. Yanran Li

The Dissertation of Wayne W Vigil Jr. is approved:

_____

_____

_____

Committee Chairperson

University of California, Riverside

Acknowledgements

First and foremost, I would like to thank Dr. Russ Hille for giving me the opportunity to learn to be a scientist under his tutelage. His advice, mentorship and support during my time at UC Riverside are things that I will forever be grateful for. I would like to express my deepest gratitude as the guidance and independence granted during my doctoral journey were monumental in not only my professional but personal development as well. I hope to become a scientist that can live up to the standards of excellence that I have been shown.

I would also like to thank Dimitri Niks for his assistance, extensive knowledge, and the many conversations in lab (even the tangential ones). My time in lab was enriched by sharing time with Dimitri and my lab mates during my journey and I would like to thank those past and present (in no particular order): Steve Ortiz, Derek Nguyen, Sheron Hakopian, Jessica Tran, Kevin Menjivar and Alexandre Uzel. I would like to extend a special thanks to Dr. Sophie Franz-Badur, although my time under her mentorship was short, I am grateful for the knowledge and experience she shared with me in that time as it really set the tone for my journey.

Finally, I would like to thank Dr. Richard Debus and Dr. Yanran Li for being my thesis committee as their expertise and knowledge always pushed me to be as prepared as possible in presenting my research.

The text of this dissertation is in part, a reprint of material as it appears the in the following publications:

- Chapter 3 will contain material from, “Spectral deconvolution of redox species in the crotonyl-CoA-dependent NADH:ferredoxin oxidoreductase from *Megasphaera elsdenii*. A flavin-dependent bifurcating enzyme”, April 2021.
- Chapter 4 will contain material from, “The reductive half-reaction of two bifurcating electron-transferring flavoproteins”, June 2022.
- Chapter 6 will contain material from, “Rapid-reaction kinetics of the butyryl-CoA dehydrogenase component of the electron-bifurcating crotonyl-CoA-dependent NADH:ferredoxin oxidoreductase from *Megasphaera elsdenii*”, July 2023.
- Chapter 8 will contain material from, “The Rapid-reaction Kinetics of an Electron-Bifurcating Flavoprotein. The crotonyl-CoA-dependent NADH:ferredoxin oxidoreductase”, currently in the process of submission.

The co- authors Dr. Russ Hille and Dimitri Niks listed in the above publications directed and supervised the research that forms the basis of this dissertation.

Dedication

To my family, friends, Linh, and those who never had the opportunity.

We are all in the gutter,

but some of us are looking at the stars.

Oscar Wilde

ABSTRACT OF THE DISSERTATION

The Kinetic Mechanism of Flavin-Based Electron Bifurcation (FBEB) in the Crotonyl-CoA-Dependent NADH:ferredoxin Oxidoreductase Complex From the Bacterium *Megasphaera elsdenii*

by

Wayne W Vigil Jr

Doctor of Philosophy, Graduate Program in Biophysics
University of California, Riverside, June 2024
Dr. Russ Hille, Chairperson

Flavin-based electron bifurcation (FBEB) is an evolutionarily ancient mode of energy conservation found in a multitude of archaea and bacteria. FBEB allows these organisms to conserve energy by coupling the generation of low-potential reducing equivalents to the reduction of a high-potential electron acceptor/pathway. The thermodynamics of these separate pathways and the bifurcating cofactor (flavin adenine dinucleotide or FAD) have all been previously well-studied. However, in the context of FBEB the kinetics and nature of electron transfer (ET) in the system remain unknown.

The present work serves to elucidate the discrete steps of ET involved in bifurcation of the crotonyl-CoA-dependent NADH:ferredoxin oxidoreductase complex from the bacterium *Megasphaera elsdenii*. The complex consists of two flavoenzymes, an electron transferring flavoprotein (EtfAB) and a butyryl-CoA dehydrogenase (bcd).

The kinetics of the reductive and oxidative half-reactions of the individual proteins, the intact-complex, and the reduction of ferredoxin have been investigated. The various techniques that have been employed include: spectral deconvolution of the UV-vis spectra, kinetic steady-state assays, rapid-reaction kinetics, enzyme monitored turnover and electron paramagnetic resonance (EPR) spectroscopy.

The work has revealed, despite the favorability of transfer of the low-potential electron into the high-potential pathway, this does not occur in an enzymatic time-frame. There is no "leakage" into the high-potential pathway that would "short-circuit" bifurcation. Spectral deconvolution and EPR analysis have confirmed not only the presence, but also the importance of, the flavin semiquinone in ET. Rapid-reaction kinetic studies of both reductive and oxidative half-reactions have revealed that after the initial reduction by NADH there are a series of slower ETs in the high-potential pathway that impede the immediate transfer of the low-potential electrons, thus preserving the fidelity of ferredoxin reduction. Enzyme-monitored turnover and steady-state studies have shown that the rate of ferredoxin reduction is significantly slower than the initial reduction of the complex.

The experimental findings provide evidence supporting the rate of bifurcation being preserved through controlled, slow ET into the high-potential pathway, with the FAD constituting the first site in the high-potential pathway operating exclusively between the semiquinone and hydroquinone oxidation states.

Table of Contents

List of Figures

Chapter 1

Introduction

1.1 General background

1.1.1 Electron bifurcation

Flavin-Based Electron Bifurcation (FBEB) is an evolutionarily ancient but only relatively recently discovered method of energy conservation found in a multitude of organisms ranging from archaea to bacteria organisms of varying oxygen tolerance. General electron bifurcation is conventionally defined as simply the splitting of electrons from any two-electron donor onto two separate high- and low-potential pathway, and has been researched as early as the 1970s when the oxidoreduction of cytochrome *b* in the presence of antimycin was observed. This reaction occurs in the mitochondrial membrane of mammals, has been described as "oxidant-induced reduction" and is a prime example of electron bifurcation in an aerobic organism (1). The critical assertion that needs to be made in regards to FBEB specifically is that the pathways the electrons proceed along are thermodynamically dissimilar with respect to their distinctive high- and low-potential acceptors.

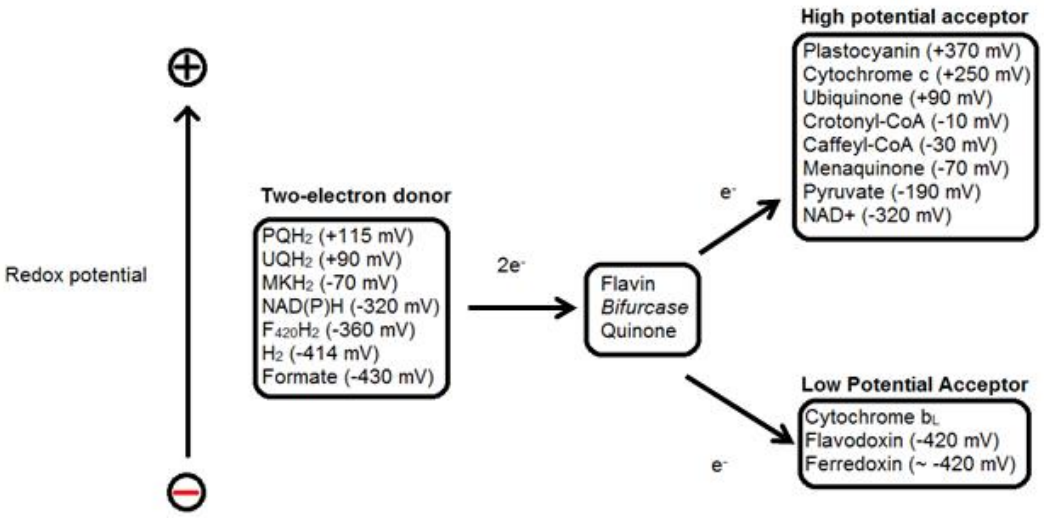

Figure 1. Simplistic overview of known electron bifurcation systems. Two-electron donors are on the left, bifurcating centers middle, high-potential acceptors top right, and low-potential electron acceptors bottom right. The numbers in parenthesis are the accepted midpoint reduction potential (E_m at pH 7). Modified from Buckel and Thauer to represent the change in reduction potential (4).

The defining feature of FBEB is the flavin adenine dinucleotide cofactor (FAD) where the two electrons are split and then sent along their respective high- and low-potential pathways. Bifurcating flavoproteins constitute a newly discovered class of complex flavoenzymes and are hallmarked by their multiple redox-active centers. They play crucial roles in the bioenergetics of anaerobic archaea and bacteria by allowing the organism to conserve energy by keeping the generation of the low-potential reducing equivalents needed to fix carbon or nitrogen close to thermodynamic equilibrium by the coupling of the high- and low-potential electron acceptors/pathways. Examples of these donors are the pyridine nucleotides NADH and NADPH, and even formate. Examples of high-potential acceptors include but are not limited to: crotonyl-CoA, caffeyl-CoA, NADH, pyruvate and various quinones (mena-, ubi- etc.) which are important substrates/intermediates in metabolic pathways such as fatty-acid synthesis and general

electron transfer. The low-potential reducing equivalents generated by FBEB are used to generate reduced ferredoxin and flavodoxin which in turn are used to drive a plethora of intracellular reactions that are dependent on the organism such as: H_2 evolution, fixation of N_2 and O_2, methano- and acetogenesis, and synthesis of adenosine triphosphate (ATP) (2-5). At present, there are a total of twelve different FBEB systems have been identified. Among the more complex systems are the *mvh* NiFe hydrogenase, consisting of six subunits containing twelve redox-active centers (6), and the *hyt* formate/hydrogen lyase that has seven subunits and twenty-one redox-active centers (7), both these examples being from *Clostridium autoethanogenum*. These systems are far too complex to undergo a detailed spectroscopic analysis and thus there is a need to identify simpler, more readily accessible systems for detailed study.

1.2 Flavoenzymes

1.2.1 Electron transferring flavoproteins

Simpler systems that not only utilize FBEB but are more amenable to spectroscopic deconvolution do exist. Many are primarily composed of an electron-transferring flavoprotein (or ETF) that includes the site of bifurcation providing egress to the high- and low-potential pathways. ETFs are well characterized in the literature, as they are important in many biological processes for both vertebrate and microbial organisms, and have been described as early as 1954 (8). There are two types of ETFs that are structurally homologous. The first are the “simple” ETFs which do not engage in bifurcation and second are the bifurcating ETFs, which do. Examples of “simple” ETFs

are the porcine and *Methylophilus methylotrophus* ETFs ; the former is integral to mitochondrial fatty-acid oxidation (8-9), and latter to biological electron transfer from trimethylamine dehydrogenase into the respiratory chain (10). Examples of bifurcating ETFs include the EtfAB components from the menaquinone-dependent NADH:ferredoxin oxidoreductase *Pyrobaculum aerophilum* or *Thermotoga maritima* (11) as well the *Megasphaera elsdenii* crotonyl-CoA-dependent NADH:ferredoxin oxidoreductase (12).

Non-bifurcating and bifurcating ETFs are structurally very similar, being heterodimers with one equivalent of FAD in the **α** subunit and either an adenosine mononucleotide phosphate (AMP) or FAD in the **β** subunit. The primary distinction between the non-bifurcating and bifurcating ETFs is whether or not AMP (for the non-bifurcating) or FAD (for bifurcating ETFs) is bound in the **β** subunit. Structural analyses have shown that the domain of the **α** subunit that contains the FAD in common with bifurcating and non-bifurcating ETFs (the et FAD) is highly mobile in non-bifurcating and bifurcating alike (10, 13-14). The field of flavoenzymes is well-studied and ever evolving. Bifurcating ETFs are one of the many examples of previously identified flavoproteins that have been "rediscovered" as an entirely new class of enzymes. With this in mind it is important to take a look at the history of both flavins and flavoproteins themselves.

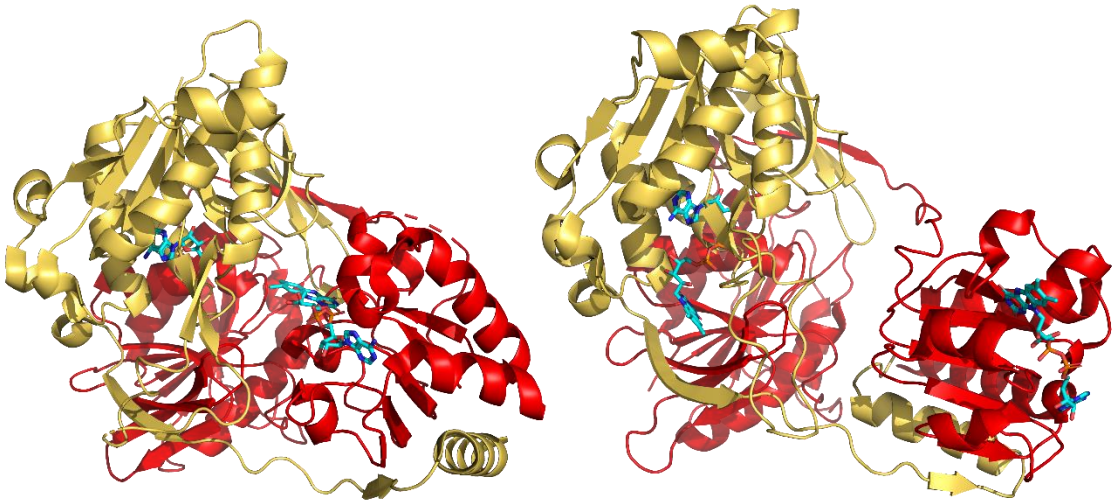

Figure 2. Comparison of the structures of the simple EtfAB from *Methylophilus methylotrophus* left (PDB 1O96) and the bifurcating EtfAB from *Clostridium difficile* right (PDB 5OL2). The α subunits are in red and ß in yellow (10, 14). In *M. methylotrophus* EtfAB the AMP and FAD cofactors can be seen in the ß and α subunits respectively. FAD can be seen in both subunits of the EtfAB from *Clostridium difficile*.

1.2.2 Discovery of flavoenzymes

The initial discovery of flavin-containing proteins was made in 1879 when a yellow pigment was isolated from cow's milk and named lactoflavin (lacto- for milk and the flavus for yellow). It wasn't until the 1930s that Paul Kerrer and Richard Kuhn were able to determine the structure of the yellow pigment, identifying it as riboflavin, or vitamin B_2, which is the precursor to FAD (15). In the following years, the identification of more "yellow" pigments and their role in catalysis included but was in no way limited to; Otto Warburg's 1932 discovery of the class of "Old Yellow Enzymes" (OYEs) which underwent both oxidation and reduction while oxidizing glucose-6-phosphate (16), Hugo Theorell's discovery of the yellow pigment's role in activity of said enzyme and its structure as flavin mononucleotide (FMN) in 1935 and 1937 (17-18), and Otto Warburg and Walter Christian's discovery of $_D$-amino acid oxidase and identification of its cofactor

as FAD in 1938 (19). These discoveries were the first identification of the class of molecules known as, coenzymes, illustrating the importance of vitamins in the context of their role's enzyme catalysis and not just overall metabolism (20).

1.2.3 Flavin Biosynthesis

As previously mentioned, the precursor to FAD is riboflavin (or Vitamin B_2), which must be synthesized prior to the conversion of the more structurally complex FMN and FAD. The overall biosynthetic pathway requires one equivalent of guanosine-5'-triphosphate (GTP) and two of ribulose-5-phosphate, (hence the ribo- in riboflavin) is broadly conserved across plants, fungi, and most prokaryotes. The system we are working with is from the bacterium *Megasphaera elsdenii* in origin and recombinantly expressed in *Escherichia coli*, and the enzymes described in the synthesis of riboflavin by *E.* coli are encoded by the *ribA-E* genes (21). There are five enzymes and six reactions that are responsible for the synthesis of riboflavin (with the pyrimidine deaminase and reductase being a singular bifunctional enzyme constituting steps 2 and 3 of the synthesis): 1. the ribA GTP cyclohydrolase II that catalyzes the first committed step of the pathway, the release of pyrophosphate from GTP resulting in formation of 2,5-diamino-6-ribosylamino-4(3*H*)-pyrimidinone 5'-phosphate (22); 2, the ribD pyrimidine deaminase that catalyzes the deamination of the of the NH_2 group at position two of guanine, resulting in conversion to 5-amino-6-ribosylamino-4 (3*H*)-pyrimidine 5′-phosphate (23); 3, The ribD pyramidine reductase that, with NADPH, converts the deaminated product to 5-amino-6- ribitylamino-2,4(1*H*,3*H*)-pyrimidinedione 5′-phosphate (23); 4, The ribB 3,4-dihydroxy-2-butanone 4-phosphate synthase that

converts the reduced pyrimidine to the pteridine 6,7-dimethyl-8-ribityllumazine, using a four-carbon fragment originating from pentose-phosphate pool (24); 5, the ribE 6,7-dimethyl-8-ribityllumazine synthase that condenses, 3,4-dihydroxy-2-butanone 4-phosphate with 5-amino-6- ribitylamino-2,4(1*H*,3*H*)-pyrimidinedione (25); and lastly 6, the ribC riboflavin synthase that catalyzes the disproportionation of two molecules of 6,7-dimethyl-8-ribityllumazine, resulting in the exchange of a 4-carbon unit leading to one equivalent of riboflavin and one of 5-amino-6- ribitylamino-2,4(1*H*,3*H*)-pyrimidinedione (26).

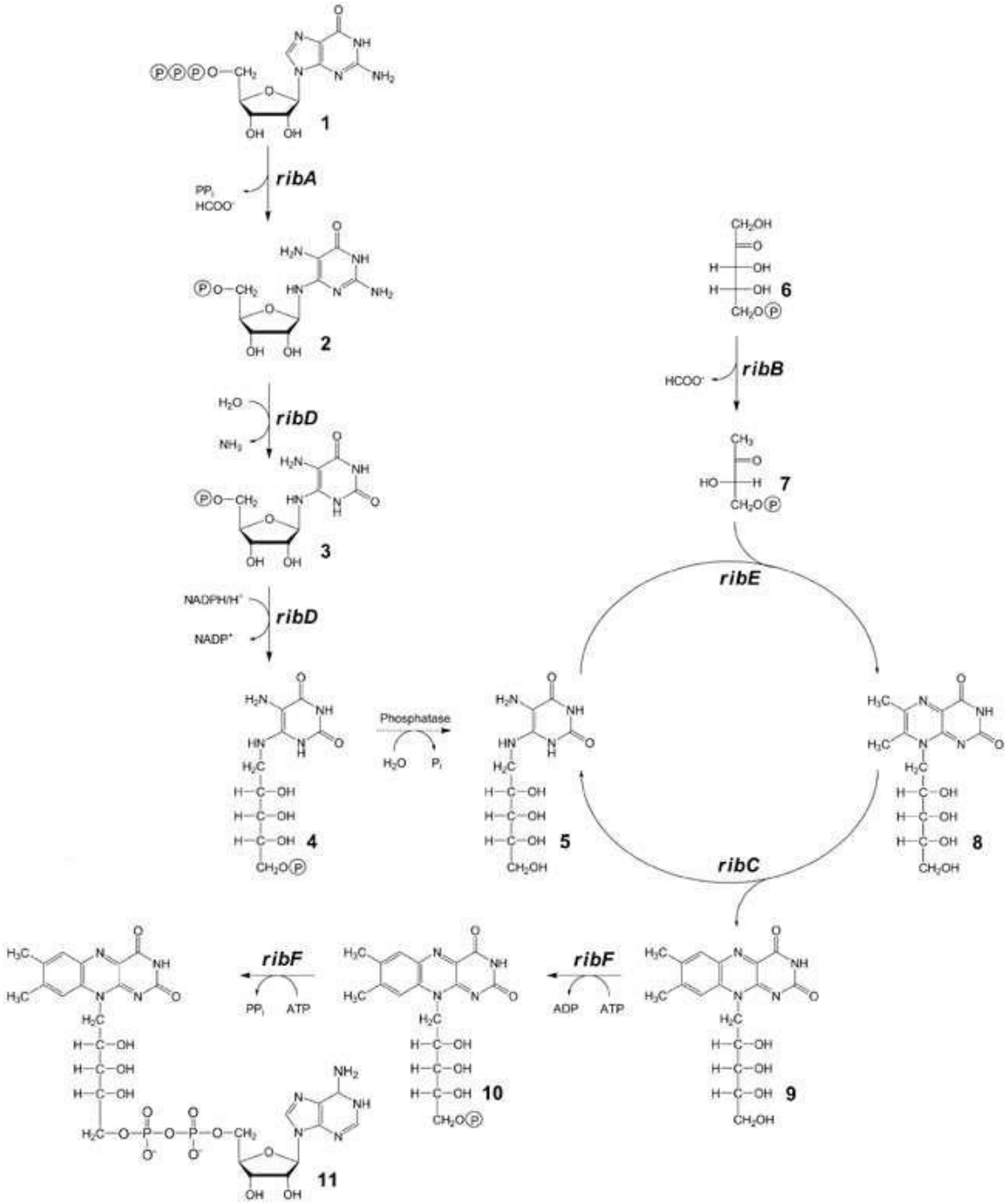

Figure 3. Biosynthesis of riboflavin. Starting from GTP and ribulose-5-phosphate as described above (23).

In bacteria, the conversion of riboflavin to FMN is catalyzed by riboflavin kinase and FAD by FAD synthetase (27-28). Riboflavin kinase catalyzes the irreversible phosphorylation of riboflavin at the 5' position of the ribityl chain using adenosine triphosphate (ATP) to make FMN. FMN is then converted to FAD, again using ATP, by a reversible adenylylation catalyzed FAD synthetase (or FMN adenylyltransferase) (29). As previously mentioned, the biosynthetic pathway through to FAD is well conserved across multiple taxa and as a result the utilization of flavin-containing enzymes is wide-spread.

1.2.4 Flavin Chemistry

FAD is well known for its ability to facilitate both one- and two-electron transfer reactions due to the three distinct oxidation states it can assume in the biological pH range. These are the oxidized quinone (FAD or (Q)), the one-electron reduced semiquinones (SQ, which can be either the neutral FADH• or anionic $FAD•^-$), and the two-electron reduced hydroquinone (HQ, either $FADH_2$ or $FADH^-$). The semiquinone hydroquinone states have pKa values of 8.3 (between FADH• and $FAD•^-$) and 6.7 (between $FADH_2$ and $FADH^-$), respectively. This means in a neutral pH solvent, the predominant forms of the oxidation states will be FADH• and $FADH^-$, but the local environment of the protein active site can greatly influence the local pH of the FAD so all four states can be observed in one system or another (30). It should also be noted that the semiquinone of free flavins only accumulate to ~10% in the course of reductive titrations, although it can be greatly stabilized in some flavoproteins. $FAD•^-$ can occasionally be generated in some flavoproteins, if only transiently, upon photoreduction by an

intraprotein electron transfer involving the oxidation of a nearby aromatic amino-acid residue by the highly oxidizing FAD* excited state (31). In free solution, the photogenerated radical undergoes rapid intramolecular electron transfer to the adenine moiety from the isoalloxazine ring in a time frame of 9 picoseconds (32). The relative thermodynamic stability of the three flavin oxidation states is dictated by the half-potentials for the two one-electron half-potentials for the quinone/semiquinone (Q/SQ) and the semiquinone/hydroquinone (SQ/HQ) couples, with the midpoint potential for the two-electron Q/HQ being the average of the two half-potentials. For free FAD, the Q/SQ half-potential is significantly more negative than the SQ/HQ half-potential (- 314 ± mV and - 124 mV, respectively) resulting in a thermodynamically unfavorable SQ, as explained in greater detail in the next section (33).

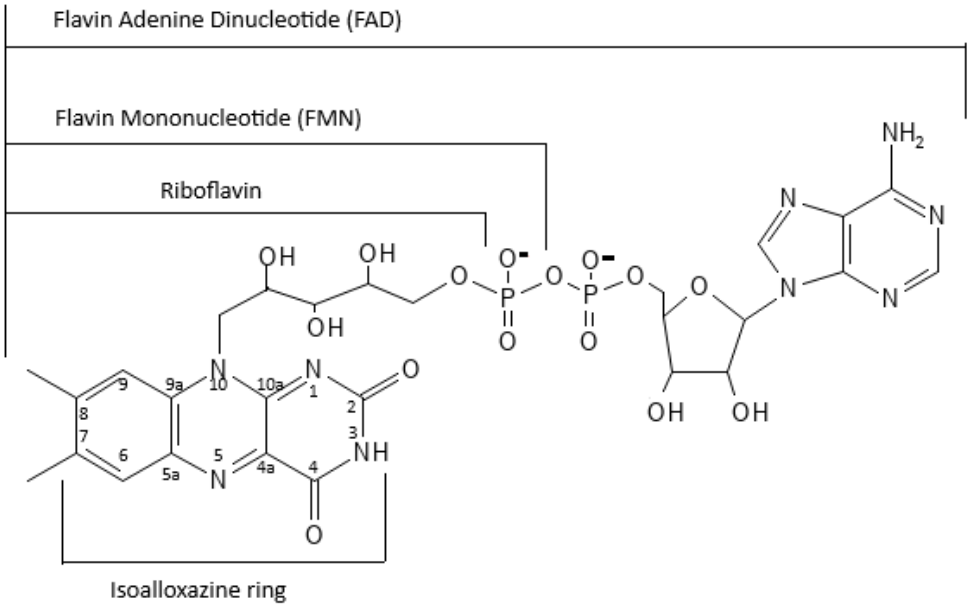

Figure 4. The structure of oxidized FAD. The isoalloxazine, RF, and FMN components of FAD are labelled as well as the numbering of the isoalloxazine ring.

1.3 Biological electron transfer

Although initially, oxidation-reduction reactions were described in terms of oxygen content, the definition soon broadened to include all reactions in which there was a loss or gain of electrons. For such reactions to be thermodynamic it is important for the total energy of the transfer of electrons to result in a net-zero energy change in the donor/acceptor pair. This phenomenon is an application of the Franck-Condon principle in which there exists a barrier to the exchange of electrons due to the energy of the hydration shell not transferring as quickly as the electrons in the donor-acceptor complex. This is because the ions of the complex are in different arrangements, either geometrically or energetically, and there is an intrinsic energetic discrepancy between the pair (34). Once the symmetrical arrangement of the electronic states in the hydration shells of both ions of the complex occurs, rapid electron transfer is observed as the complex is considered to now be "activated" as the change in energy is now net-zero. This is a distance-dependent relationship, in which the barrier to the electron transfer event lessens as donor and acceptor approach but is still further than the interatomic distances needed for molecular rearrangement (35-37). It is in this context that we define the electron transfer reactions of the FAD that are integral to this thesis, including both two-electron hydride transfer reactions and the individual one-electron steps. The Nernst equation describes the relationship of the observed reduction potentials to the intrinsic thermodynamics of the system, as discussed in the next section.

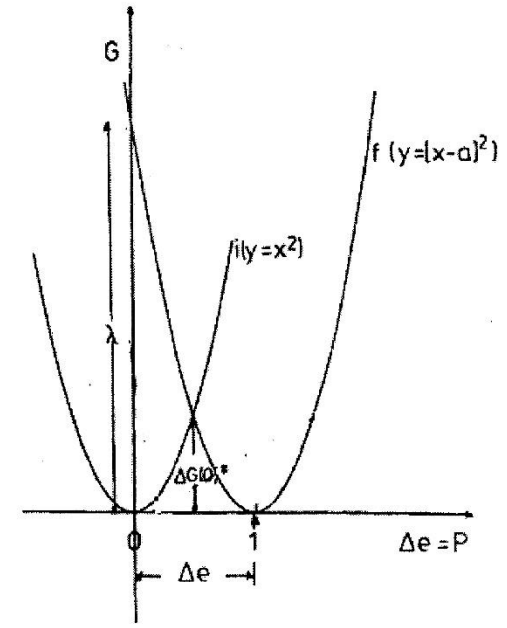

Figure 5. Marcus parabolas describing the relation of the reorganization of energy of the two spheres. Where Δe is equal 0.5 it corresponds to the self-exchange of charge.

1.3.1 Nernst Equation

The thermodynamics of the redox-active cofactors of the system investigated in this thesis have been previously determined via electrochemical titrations that resulted in the elucidation of the half-potentials of the cofactors (33). The equation that relates the observed reduction potential and the standard potential is the Nernst Equation (eq. 1):

$$E_{cell} = E^{\circ}_{cell} - \frac{RT}{nF} lnQ$$

E_{cell} is the potential at the measured temperature

E°_{cell} is the standard cell potential

R is the universal gas constant: (8.31446261815324 J K^{-1} mol^{-1})

T is the temperature in Kelvins

n is number of electrons in the transfer reaction (1 or 2)

F is the Faraday constant (96 485.3321233100184 C mol^{-1})

Q is the ratio of the concentration of reduced and oxidized species ([Reduced]/[Oxidized])

This equation dictates that every difference of 60 mV corresponds to a factor of ten shift in the equilibrium constant for a one-electron transfer process (30 mV for a two-electron transfer). The observed ratio of the oxidation states is inherently tied to the stability of the semiquinone radical and said stability is integral to the bifurcating function of the enzyme.

1.3.2 Crossed vs. Uncrossed half-potentials

The terms "crossed" and "uncrossed" describe the overall thermodynamic stability for the semiquinone oxidation state by way of relating the half-potentials of the Q/SQ and SQ/HQ couples. The stability of semiquinone formation can be represented mathematically as (eq. 2): $K_S = [SQ]^2 \times ([Q] \times [HQ])^{-1}$ where K_s is the stability constant, SQ is the semiquinone, Q is the quinone, and HQ the hydroquinone concentrations. The stability constant is related to the difference of the measured potentials (Nernst Equation) using the following relation (eq. 3):

$$\Delta E_m = E_{mQ/SQ} - E_{mSQ/HQ} = 2.3RT(F)^{-1} log K_s$$

$$\Delta E_m = 0.059 log K_s$$

From this equation, the calculated stability from the difference in the half-potentials is used to determine the extent to which the half-potentials of the flavin are "crossed" or "uncrossed", highly crossed half-potentials giving a thermodynamically unstable semiquinone and highly uncrossed a stabilized semiquinone. It is important to note that

as logK_s increases the half-potentials for the first step and second steps decrease linearly and when K_s is equal to 1 the lines will intersect. "Crossed" flavins are those where K_s is less than 1 and as a result the semiquinone is both, thermodynamically unfavorable and unstable transiently and the logKs for the two half-potentials cross in a plot of logK_s vs reduction potential. This unstable semiquinone constitutes the low-potential electron generated in the course of bifurcation and is what make reduction of the low-potential acceptor possible. "Uncrossed" flavins are those in which the stability constant is greater than 1 and thus a stable semiquinone is observed (4).

1.4 *Megasphaera elsdenii*

The obligate anaerobe *Megasphaera elsdenii* is a filamentous bacterium that was first discovered in the caecum of sheep in 1953 and only referred to as the isolate LC, or large coccus (39). It wasn't until 1959 that it was characterized as the new species *Peptostreptococcus elsdenii* (40), and in 1971 given its current name as it did not fully align with the *Peptostreptococcus* genus description (41). *Megasphaera elsdenii* plays a crucial role in fatty-acid synthesis, lactate fermentation and butyrate synthesis in the bovine and ovine rumen (39, 42-44). The production of H_2 gas has been observed in cultures of *Megasphaera elsdenii* ever since its initial discovery in 1953 and has ultimately been linked to the reduction of ferredoxin in the organism (45).

Electron-transfer reactions in *Megasphaera elsdenii* have been studied even before the specific ETF enzymes involved in the crotonyl-CoA-dependent NADH:ferredoxin oxidoreductase complex was identified in 1964 by Ransom Baldwin

and Roy Emery (46). Baldwin and Emery analyzed cell-free fractions from *M. elsdenii* and subjected them to dye-dependent reduction assays to determine acyl-CoA dehydrogenase activity. This was accomplished using the reduction of 2,6-Dichlorophenolindophenol (DCPIP) in the presence of NADH and then in the presence of butyryl-CoA so as to avoid contamination by the high levels of NADH oxidation found in the fractions. One fraction in particular exhibited four times the NADH oxidation activity of other fractions but zero butyryl-CoA activity. Interestingly, this Fraction II contained an FAD protein resembling the ETFs found in mammalian tissues. Combination of Fraction II and the acyl-CoA dehydrogenase fraction demonstrated the presence of a ferredoxin-linked NAD^+ reductase activity, which we now attribute to the bifurcation of the intact crotonyl-CoA-dependent NADH:ferredoxin oxidoreductase complex. The involvements of ETFs in these early studies of rumen anaerobes were not surprising as a substantial amount of not only FAD, but other flavin derivatives had been isolated from cell-free extractions as early as the 1950s by JL Peel (47).

1.5 Electron-transferring flavoprotein and butyryl-CoA dehydrogenase

The electron-transferring flavoprotein (EtfAB) and butyryl-CoA dehydrogenase (bcd) components of the *Megasphaera elsdenii* system have been the subject of investigation well before their known involvement in the bifurcating complex as evidenced above. The native purification and characterization of EtfAB from *Megasphaera elsdenii* was performed by Carolyn Whitfield and Vincent Massey in 1974 where it was noted that the enzyme binds more FAD compared to other flavoenzymes

and had “marked changes in the absorption spectrum” (48). A more in-depth analysis of the recombinantly expressed EtfAB and its “unusual spectrum” was carried out by Kiyoshi Sato in 2003 where both the electron-transferring FAD (et-FAD) and bifurcating FAD (bif-FAD) from the α and ß subunits of the holo-enzyme were spectroscopically characterized (49). Reduction potentials of the protein were determined by Sato again in 2013 (50). In both wild-type and recombinant systems the overall spectral changes associated with reduction were observed and included the accumulation of anionic semiquinone.

The native purification and characterization of bcd was carried out by Paul Engel and Vincent Massey in 1971 (51). Reduction potentials of isolated bcd were determined by Fink *et al.* in 1986 and regulation behavior by substrate and product binding by Stankovich *et al.* in 1987 (52, 53). The accumulation of the neutral semiquinone was noted during these experiments and the metabolic scheme of electron-transfer from NADH to crotonyl-CoA was proposed. Using said reduction potentials, Buckel and Thauer were able to propose the scheme for bifurcation in EtfAB (4).

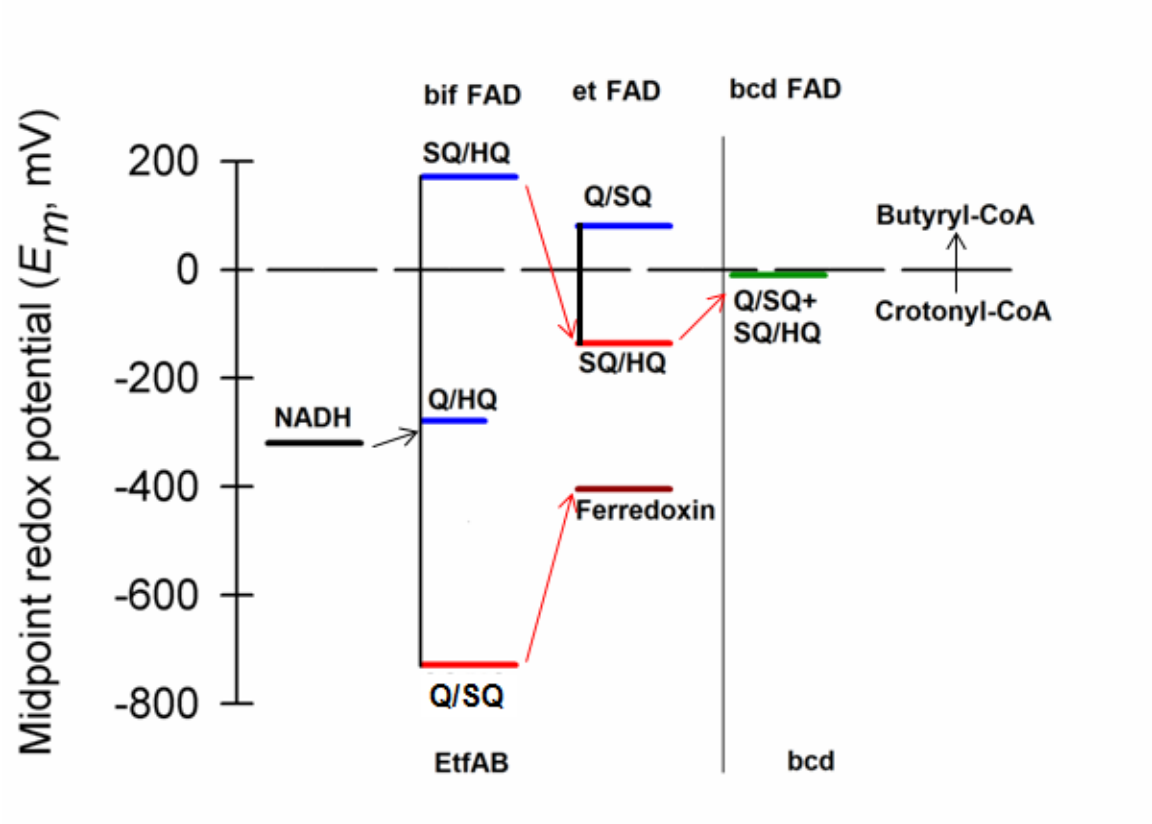

Figure 6. The proposed scheme of electron transfer modified from Buckel and Thauer 2018 using the reduction potentials (4). The high-potential pathway is exergonic overall in relation to the NADH midpoint potential, but the first electron transfer step is endergonic. The low-potential pathway is endergonic in the reduction of ferredoxin, but the discrete et from EtfAB to ferredoxin is exergonic due to the bf FAD's crossed half-potentials.

Structural characterization of the intact complex was determined in the homologous system from *Clostridium difficile* by Demmer *et al.* in 2017 (14). It was observed that EtfAB:bcd forms a tetramer of heterotrimeric protomers. EtfAB are arranged tetrahedrally about a bcd core as $[EtfAB:bcd]_4$. The overall topical structure and simplified protomer are shown in Figure 7 below.

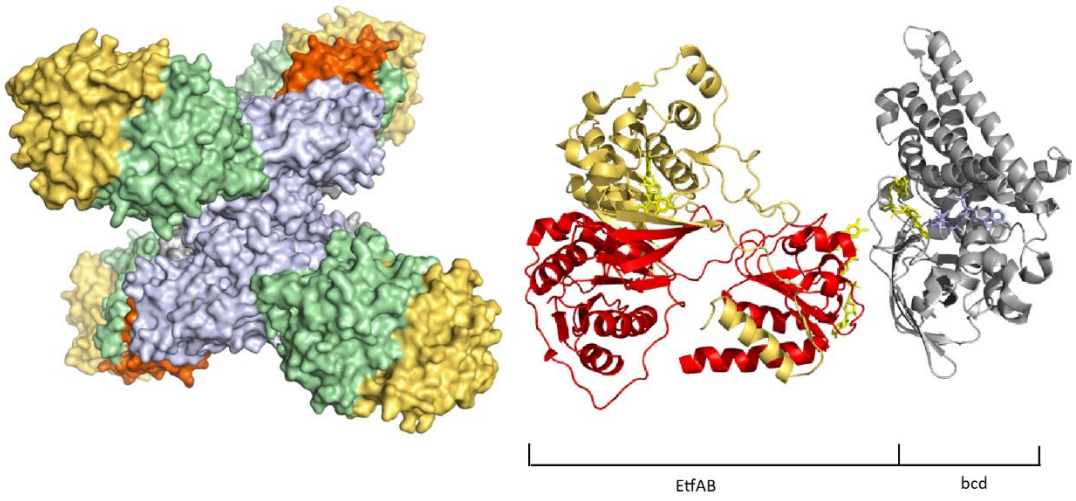

Figure 7. Structures of EtfAB:bcd heterotrimer and catalytic protomer. Left, space filling model of the heterotrimeric structure of $[EtfAB:bcd]_4$ from *C difficile* (protein data bank 5OL2) where bcd is grey and EtfAB is green, yellow and red. Right, the simplified protomer of only EtfAB:bcd where the bcd again is in grey and the α-subunit, or electron transferring, is in red and the ß-subunit, or bifurcating, is in yellow (14).

The overall stoichiometry modified from Hermann *et al.* (2), of the complex is as follows (eqn. 4):

$$2\ \text{NADH} + \text{crotonyl-CoA} + 2\ \text{ferredoxin}_{ox} \rightleftharpoons 2\ \text{NAD}^{+} + \text{butyryl-CoA} + 2\ \text{ferredoxin}_{red}$$

Thus in the context of electron bifurcation, the median potential donor is NADH, crotonyl-CoA is the high-potential acceptor and ferredoxin is the low-potential acceptor. The high-potential pathway consists of et from the reduced bif-FAD via NADH oxidation through the et-FAD, bcd FAD and ultimately onto crotonyl-CoA. The low-potential pathway is composed of only et from the low-potential bif-$FAD^{\bullet -}$ to ferredoxin. As previously stated, the reduction potentials of the half-reactions have been determined and shown in Figure 6.

1.6 Last Universal Common Ancestor

The last universal common ancestor (LUCA), is the proposed common ancestor to all extant archaeal, bacterial and eukaryotic organisms today. The likely metabolism of LUCA has been inferred from a meta-analysis of over six million protein-encoding genes (from 1,817 bacterial and 134 archaeal genomes and 286,514 distinct protein families) (54), it being concluded that LUCA was likely a thermophilic anaerobe with a DNA-based genome and ribosome-mediated protein synthesis, and could fix nitrogen with a nitrogenase and carbon via the Wood-Ljungdahl pathway. LUCA is speculated to have arisen approximately 3.85 Ga (giga annum) years ago based on an interrogation of carbon isotopic data, and existed well after the arrival of the first living organisms at around 4.4 Ga (55) but well before the development of photosynthesis (56).

It has been proposed that LUCA employed FBEB as a means to generate low-potential reducing equivalents to reduce the ferredoxin required for both nitrogen and carbon fixation. This is in part due to the evidence that LUCA utilized the cofactors necessary for FBEB, including NADH, GTP, FMN, and importantly FAD. The pathway for CO_2 fixation that was employed by LUCA generates acetyl-CoA via the Wood-Ljungdahl pathway and is significant in the context of the present work in that this is a common link to the metabolism of *M. elsdenii*. As was discussed above, the discovery of *M. elsdenii* was due in part to its acyl-CoA dehydrogenase activity (46, 55). On the other hand, it has been argued that FBEB did not arise until after the divergence of the archaeal and bacterial taxa as it has been observed not only in anaerobic organisms of the former but in different taxa of aerobes and facultative anaerobes as well (57). It is possible that

FBEB was present in LUCA and also arose independently in archaea and bacteria, however it is nevertheless clear that FBEB is an evolutionarily ancient mechanism of energy conservation.

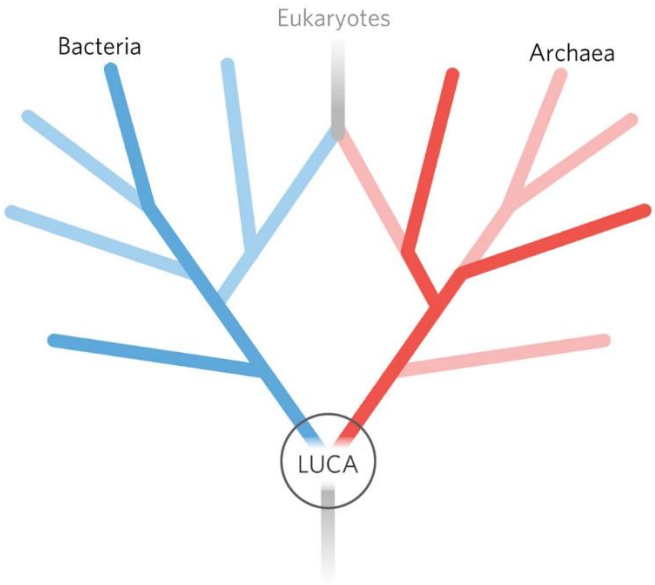

Figure 8. Phylogenetic tree for LUCA's genes. Genes found in multiple members of both bacteria and archaea and showed recovery of monophyly in both were identified and attributed to LUCA (54).

1.7 Enzyme Kinetics

1.7.1 Historical Background

LUCA's evolutionary success can be attributed to the enzymes it had in its employ, as they allowed it to efficiently carry out the biological functions necessary for success. Regardless of whether or not one's view of life's origin aligns with the "genetics first" or "metabolism first" school of thought (58), the use of enzymes as catalysts for necessary biologic reactions can be considered crucial for evolution. The laws of

thermodynamics are inviolable rules that everything must adhere to and in being so, are useful in predicting the spontaneity of chemical and biological reactions. This is because the sign of the change of Gibbs free energy, $\Delta G^{\circ\prime}$, can be either negative or positive and indicates whether the reaction is spontaneous or non-spontaneous, respectively. Enzymes function as catalysts for biochemical reactions not by altering the relative energies of the initial and final states (i.e. substrates and products) but rather by lowering the activation barrier separating them. This results in a change in the path of the reaction and results in the conservation of energy as it strictly adheres to the First and Second Laws of Thermodynamics. For an adiabatic process (*i.e.*, on in thermal equilibrium with its environment), the catalyzed reaction only proceeds with a lower barrier to reaction provided by the enzyme (for unfavorable reactions, either by coupling the reaction to a more thermodynamically favorable one, or as a step in an overall favorable metabolic pathway).

Enzymes' roles as catalysts in biological reactions has been extensively investigated, and the observation that substrate and enzyme need to first combine in order to initiate the reaction goes back to the late nineteenth century., when researchers such as Cornelius O'Sullivan and Frederick Tompson reported on the inversion of cane sugar via the organized ferment, invertase (59). These workers also made several discoveries which, in hindsight, remain fundamental in enzymatic research including: the rate of activity can always be expressed by a "time-curve" that is constant until substrate concentration is lowered; the reaction is pH dependent; there are significant temperature effects on the overall rate of reaction; and, most importantly, the enzyme remains

unchanged at the end of the reaction. The substrate concentration's role in this "time-curve" was further investigated by Adrian Brown who showed that a plot of the velocity of an enzyme-catalyzed reaction against the substrate concentration took the form of a rectangular hyperbola. Brown determined that enzyme-catalyzed reactions displayed zero- and first order-kinetics in the low- and high [substrate] regimes, respectively, rather than following a simple law of mass action (60). Another critical discovery was made in 1903 by Victor Henri, that enzymes do not alter the equilibrium constant for a reaction but do affect the reaction rate as a function of concentration (61). Henri also brought to light the fact that in typical steady-state kinetic studies the substrate's concentration is in excess of the enzyme's and proposed an equation predicting the relationship between rate of reaction and substrate concentration. However, there were two crucial errors in Henri's analysis in that he did not account for the pH of the reaction or the slow anomerization of the product of the invertase reaction, and could not accurately predict product accumulation. These needed to be accounted for before an equation could be codified.

1.7.2 Steady State Kinetics

Leonor Michaelis and Maud Menten did so in 1923, where they proposed the mathematical explanation of enzyme kinetics and asserted that in equilibrium, enzyme and substrate form a loose complex (62). This relation can generally be represented as such (eqn. 5):

$$E + S \overset{K_s}{\rightleftharpoons} ES \xrightarrow{kcat} E + P$$

E is the free enzyme

S is the substrate

ES is the complex of enzyme and substrate

P is the product formed from the reaction

K_s is the dissociation constant of the complex

k_{cat} is the rate of catalysis of the product

It had been previously determined that after addition of substrate to initiate the reaction the rate of catalysis constant for an extended period of time before substrate was exhausted, a steady-state. Michaelis and Menten famously utilized the initial velocity of the reaction as a function of [substrate] as they have been historically credited, but they also included analysis of the full-time course using the integrated form of the rate equation. This accounted for product inhibition well before product inhibition in enzyme catalysis was properly formalized (63). The monumental work done by Michaelis and Menten has yielded us the following rate equation in the form that yields the rectangular hyperbola (eqn. 6):

$$v = \frac{k_{cat}[S]}{K_m + [S]}$$

v is the initial velocity of the reaction

S is again substrate

K_m is the specificity constant

k_{cat} is the rate of catalysis

It is important to note that when undertaking steady-state kinetic studies that not only is product inhibition a potential factor in the mechanism of reaction but the reverse reaction of E + P to ES can also occur, thus (eqn. 7):

$$E + S \underset{k_{-1}}{\overset{k_1}{\rightleftharpoons}} ES \underset{k_{-2}}{\overset{k_2}{\rightleftharpoons}} E + P$$

k_1 and k_{-1} are the rate constants of the forward and reverse reactions respectively

k_2 and k_{-2} are the rate constants of the forward and reverse reactions, respectively and can be represented by the rate of catalysis, k_{cat}, as seen in eqn. 5.

From this the equilibrium constant can be expressed as the ratio of the product of the forward microscopic rate constants divided by the product of the reverse as so (eqn. 8):

$$K_{eq} = \frac{k_1 k_2}{k_{-1} k_{-2}}$$

This was presented by George Briggs and John Haldane in order to combine the Michaelis-Menten approach with an equilibrium treatment for the reaction (64). The main assumption presented by Briggs and Haldane was that the [ES] rapidly approaches a steady-state in which after the initial burst phase of turnover the [ES] will not change to any appreciable amount until a significant amount of substrate has been consumed, thus $\frac{d[ES]}{dt} = 0$. The rate of product formation can then be related to velocity, by stating the total enzyme concentration, $[E_T]$, to the sum of [E] and [ES]. This allowed for the derivation of the following relation (eqn. 9):

$$v = k_{cat}[ES] = \frac{k_{cat}[E_T][S]}{\left(\frac{k_{-1}+k_{cat}}{k_1}\right)+[S]}$$

By relating the maximum reaction velocity at saturating substrate [S], V_{max}, to the product of k_{cat} [E_t] and the specificity constant, $K_M = \left(\frac{k_{-1}+k_{cat}}{k_1}\right)$. By substituting these terms into eqn. 9 we arrive at eqn. 10:

$$v = \frac{V_{max}[S]}{K_m+[S]}$$

With both approaches we end up with an equation describing velocity of product formation. With Michaelis-Menten, the rapid equilibrium of the ES complex is faster than catalysis and K_M is close to K_d. While the Briggs-Haldane approach arrives at the same conclusion without assuming the k_{cat} and k_{-1} relation. Thus, whether the ES complex concentration is constant due to the equilibrium or steady-state conditions the initial velocity behavior remains the same. With this, the full picture of the steady-state enzyme turnover is shown as the formation of the ES remains constant during catalysis.

1.8 Pre Steady-State Rapid Reaction Kinetics

1.8.1 Background

Steady-state studies of enzyme turnover has proven to be a valuable tool in investigating the kinetic properties of enzymes both past and present. However, the main limitations of this methodology boil down to speed; the initial velocity of the reaction and the rate at which the E + S = E•S equilibrium is attained. Methods to disturb the equilibrium of a system and measure the rate of re-equilibration were developed as early as the 1920s by Hamilton Hartridge and Francis Roughton. These workers developed a continuous-flow device to measure the dissociation of oxygen from hemoglobin via

photolysis (65). They then worked to homogenously and rapidly mix fluids to measure changes occurring before the ES equilibrium was established (66), and to measure the temperature of two reactants in solution that correspond to the overall changes in temperature of the reaction (67). Because, as in their words, "A perusal of the literature shows that previous investigators have, in the main, restricted themselves to the study of slow reaction…" (66). This line of thought helped give birth to the study of reactions (both biological and chemical) in the pre steady-state regime, prior to equilibration of E + S and E•S. The scope and application of such work only increased with the technological advances, as we will see.

1.8.2 Stopped-Flow Spectrophotometry

The development and subsequent commercial availability of instrumentation and methodology to collect data relevant to many biochemical processes, including enzymatic reactions, helped to significantly advance the field of enzymology. One such method, ultraviolet-visible absorption spectroscopy (UV-vis), became first commercially available in 1942 as the Varian Cary II spectrophotometer (68). This proved to be an extremely powerful tool for enzymologists, as many proteins incorporated cofactors absorbed in the UV-visible range and reactions often involved the transient formation of spectroscopically distinct intermediates such as Schiff bases from pyridoxal phosphate-utilizing enzymes (69) and different oxidation states of flavin and hemes with distinct absorption characteristics of their own (70). With new spectroscopic and fluorescent methods, researchers were able to investigate reactions in a manner that fully incorporated this new technology. Echoing the approach of Hamilton and Roughton,

once the research on “slower” reactions had been exhausted, the need for rapid and reliable methods of measuring spectroscopic data arose. Quentin Gibson and Leslie Milnes achieved this in 1964 with their construction of a stopped-flow apparatus that involved mixing solutions of equal volume and following UV-visible spectral changes in the course of reaction with half-lives as short as milliseconds (71). The combination of homogenous mixing and rapid data collection made it possible to track many previously unobservable processes, including the kinetics associated with the approach to equilibrium of the E•S complex, formation and role of intermediates in enzymes with redox-active cofactors such as the aforementioned flavins, and the overall mechanism of action of proteins including the half-reactions not normally observed in the steady-state (72-73).

The primary strength of pre-steady state rapid-reaction kinetics was it yielded information about the reaction on the approach to equilibrium by tracking the observed rate of reaction of the enzyme and substrate on a very fast time scale. Analytical and computational work by Sidney Strickland, Graham Palmer, and Vincent Massey in 1975 established that it was very possible to ascertain rate constants for the reaction and determine the microscopic rate constants constant from the data obtained. This was due to two pivotal observations: first, the product of reaction appeared with first-order kinetics and; and second, the apparent rate constant for the reaction varied hyperbolically with increasing substrate concentration, asymptoting to a maximum rate at high [substrate], just as the steady-state k_{cat} did (74). The steady-state solution and relevant mechanism that described this behavior as well as enabled the extraction of the observed

rate constants for formation of an intermediate, C, and the equilibrium constants for each step in the mechanism (eqn. 11):

$$A + B \underset{k_{-1}}{\overset{k_1}{\rightleftharpoons}} C \underset{k_{-2}}{\overset{k_2}{\rightleftharpoons}} D$$

A is the enzyme

B is the substrate

C is an intermediate in the mechanism

D is the product formed from the reaction which the observed rate of reaction is measured

k_1 and k_{-1} are the rate constants of the forward and reverse reactions respectively

k_2 and k_{-2} are the rate constants of the forward and reverse reactions respectively

In order to derive an equation that relates the rate of formation of D, k_{obs}, to the concentration of substrate and the microscopic rate constants of the forward and reverse rate constants for each step, there were several crucial criteria and assertions that needed to be met. First, A and D needed to be spectroscopically distinct and thus formation/loss could be tracked (while A and C were indistinguishable). Second, under saturating substrate conditions there should be an instantaneous conversion of A → C and a slower, rate-limiting conversion of C → D which can be followed spectroscopically. With these conditions satisfied; applying the steady-state condition to [C], rearranging the equation to solve for $\frac{d[D]}{dt}$, and assuming $[B_o] >> [A_o]$ gave the following equation relating $\frac{d[D]}{dt}$ (k_{obs}) to the rate constants was reached (eqn. 12):

$$k_{obs} = \frac{k_1[B](k_2+k_{-2})+k_{-1}k_{-2}}{k_1[B]+k_{-1}+k_2}$$

As the equilibrium condition required that $k_{-1} >> k_2$ and the irreversible formation of product requiring k_{-2} being negligibly small or equal to zero the numerator and denominator are simplified and Strickland *et al*. were able to give us the hyperbolic dependence of k_{obs} to substrate concentration, as shown below (eqn. 13):

$$k_{obs} = \frac{k_1 k_2 [B]}{k_1 [B] + k_{-1}}$$

It was now possible to reliably relate the hyperbolic fit of k_{obs} vs [B] and extrapolate to an infinite [B] to yield the kinetic parameters of the limiting rate of reduction, k_{red} and K_d of the reaction without the need to deconvolute the specific microscopic rate constants. Kinetic studies including deuterated isotope effects, enzyme monitored turnover experiments and many others could now be carried out efficiently and reproducibly.

1.9 Electron Paramagnetic Resonance Spectroscopy (EPR)

1.9.1 Background

The discovery of reaction intermediates, which eventually would be shown to be paramagnetic, was made early in the history of physical organic chemistry. Such free radical species ranged from early gas-phase chemistry with the formation of cyanogen by heating mercuric cyanide as reported by Gay-Lussac in 1815 (75) to the condensed-phase research by Gomberg in 1900 with triphenylmethyl in 1900 (76). It wasn't until 1945 however, when Yevgeny Zavoisky obtained the first EPR signal of manganese chloride tetrahydrate using a spectrometer of his own construction that the paramagnetic properties could be measured (77). The theory behind electron paramagnetic resonance (EPR) follows the same fundamental principles as nuclear magnetic resonance (NMR), as

both methodologies require the sample to be contained in a magnetic field where the absorption of electromagnetic energy induces a reorientation of one or more magnetic moments (of an unpaired electron in the case of EPR, of nuclei such as ^{1}H or ^{19}F that have nuclear moments). NMR typically makes use of electromagnetic radiation in the radio frequency range (MHz), while EPR utilizes the microwave radiation frequency (GHz). The microwave frequencies in EPR are designated by historically designated "bands", where X-band (~ 9.5 GHz) is the most common due to the widespread availability of microwave sources in this range in the post World War II period when the technique became popularized. As the electrons in most molecules are paired in chemical bonds, and as a result most molecules are not EPR active. However, organic radical species and many transition metal ions in one oxidation state or another are EPR active. Such species are frequently intermediates in enzyme-catalyzed reactions, particularly oxidation-reduction reactions, making EPR a valuable tool in deconvoluting reaction mechanisms in a wide array of biochemical processes (78).

1.9.2 Electron Zeeman interaction

One of the fundamental physical principles that defines EPR, is the interaction between the externally applied magnetic field and the magnetic moment of the unpaired electron. The magnetic moment will orient itself in just one of two orientations, either parallel or antiparallel, relative to the magnetic field. The parallel orientation is the more stable, and the energy gap between these two states is proportional to the strength of the magnetic field. At any given field strength, when the energy gap between parallel and antiparallel orientations matches the energy of the incident microwave frequency light, a

photon is absorbed that results in the inversion of the two states, creating a resonant condition. The combination of field strength and microwave frequency that give rise to resonance is defined by a parameter called the "*g*" value that defines a given system. *g* values can be useful in identifying paramagnetic species as they describe the intrinsic resonance of the unpaired electron and its environment. The *g* value associated with an EPR-active species can be compared that for the free electron for reference, g_e, which has a value of 2.0023. The *g* value for a given EPR-active species is often shifted from g_e as a result of the interaction between the intrinsic angular momentum of the electron and the orbital angular momentum of the orbital in which the electron resides. As EPR samples are typically solid-state samples (either powder or frozen solution), the g value can have as many as three distinct values that depend on the orientation of the paramagnetic species in the applied magnetic field and its overall degree of asymmetry. The degree anisotropy of the *g* values, represented as (g_1, g_2, g_3) or (g_z, g_y, g_x), range from isotropic where all three *g* values are the same, to axial signals where two values are the same and the third is distinct, to rhombic where all three values differ.

The interaction that describes the applied magnetic field and the moment of the electron is known as the Zeeman effect and is dependent on the strength of the applied magnetic field. As the *g* values are a representation of the local environment of the electron, we first need to define the spin angular momentum of said electron as (eqn. 14):

$$spin\ angular\ momentum = \sqrt{S(S+1)}\,\frac{h}{2\pi}$$

S is the associated spin angular momentum

h is Planck's constant, $6.626 \times 10^{-34} Js$

Next, we need to define the strength of the unpaired electron's magnetic moment parallel to the externally applied magnetic field, arbitrarily defined as the z axis, that is associated with the spin angular momentum above (eqn. 15):

$$\mu_z = -g_e \mu_B M_S$$

g_e is the free electron g value

μ_B is the Bohr magneton

M_S is the spin quantum number, which is $\pm \frac{1}{2}$.

Consequently, the electron can now have two different magnetic momentum and two different spin states. In the absence of a magnetic field, these two states are prone to degenerate and become EPR silent. Once in the presence of a magnetic field, the separate states will interact with the applied field and have different energy levels. This is the Zeeman interaction and can be described as such (eqn. 16):

$$E = \pm \frac{1}{2} g_e \mu_B B$$

B is the strength of the applied magnetic field

This results in the two energy levels shown in Figure 10 below that diverge linearly as the field strength is increased, an effect known as Zeeman splitting. The individual levels corresponding to the M_s +1/2 and -1/2 quantum numbers are referred to as Zeeman levels (79).

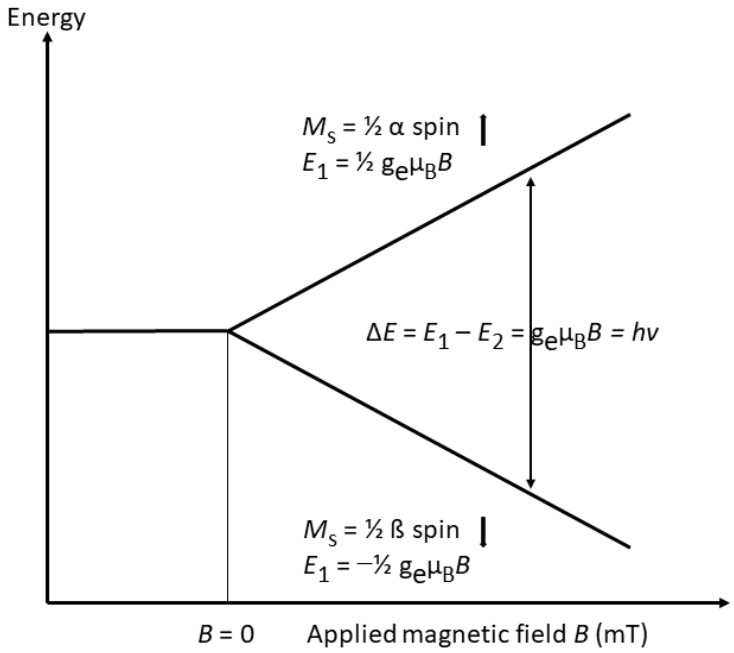

Figure 9. The Zeeman effect. Diagram illustrating after the application of the magnetic field (B_0) the different spin states ($M_s \pm ½$) are no longer degenerate. The α and ß are used to denote the up and down directions of the spins, respectively (79).

1.9.3 Electron-nuclear hyperfine interaction

In addition to the Zeeman interaction described above, EPR signals can also be influenced by electron-nuclear hyperfine interactions, which describe the interaction between the magnetic moment of the unpaired electron and the nuclear moment of nearby nuclei (such as ^{1}H and ^{19}F). This manifests spectroscopically in two distinct ways: 1, the isotropic hyperfine, which is a result of the polarization of finite unpaired electron spin density in inner s atomic orbitals by the nuclear magnetic moment, which can provide insight on the nature of said orbital; and 2, the anisotropic hyperfine *A*, due to magnetic dipole-dipole interactions between the electron and a nearby nucleus, which is influenced

by the electron's distance from and orientation to the nucleus. And as with the g value, A can have as many as three distinct components (A_x, A_y, A_z) which can provide useful spatial information (78).

1.9.4 Electron-electron coupling

Another interaction that is important to consider in EPR spectroscopy is the possible interaction between multiple unpaired electrons in a complex. These are known as zero-field interactions and arise when S, the total spin angular momentum of the system is greater than $\frac{1}{2}$. This results in the loss of degeneracy from the (2S +1) factor expected in the ground state as each electron has dipolar and spin-orbit coupling interactions. Known as Zero-field splitting, as this is present even in the absence of an applied magnetic field. The two parameters that affect the coupling are the average distance between the electrons and the deviation of the system from its cubic symmetry (78).

1.9.5 FAD EPR

The one-electron reduced FAD semiquinone has two possible ionization states, FADH• and $FAD^{\bullet -}$ and both are EPR active. The EPR spectra of both species has been extensively investigated and can be reliably used to distinguish the two species from one another due to the characteristic linewidths of their EPR spectra (80-81). Both signals have approximately isotropic X-band spectra, but the anionic $FAD^{\bullet -}$ has a typical linewidth of 14-15 Gauss whereas the neutral FADH• has a somewhat broader linewidth of 18-20 Gauss in the X-band spectrometer, again dependent on system.

Chapter 2

Experimental procedures

2.1 Organisms and growth conditions of flavoproteins

Plasmids containing genes for EtfAB (*Mels*_2126 + *Mels*_2127) and bcd (*Mels*_2128) from *Megasphaera elsdenii* were constructed, described, and received by Chowdhury *et al.* (12). Plasmids were derived from pASG-IBA3 (IBA GmbH) vector to include a C-terminal Strep II tag for purification. Plasmids were transformed into chemically competent *Escherichia coli* BL21 cells and grown in Terrific Broth (TB) with 100 µL/mL of ampicillin with shaking at 180 rpm, 30 °C for 6 hours. Glycerol stocks were made by the addition of 80 % sterile glycerol to the media for a final concentration of 50 % $\frac{v}{v}$. Stocks were then flash frozen in liquid nitrogen and stored at -80 °C until further use.

For growth and expression of both EtfAB and bcd; a preculture was prepared with cells taken from appropriate glycerol stocks and placed in 10 mL TB with 100 µg/mL of ampicillin. Cells were grown overnight with shaking at 220 rpm, 37 °C and typically reached an absorbance of 15-16 OD at 600 nm ($A_{600\ nm}$). Large-scale growth was carried out in 6 L Erlenmeyer flasks with 2 L of TB and 100 µg/mL ampicillin. Flasks were inoculated with the preculture at a starting $A_{600\ nm}$ of 0.0125 and grown for ~ 6 h with shaking at 180 rpm at 37 °C. Once $A_{600\ nm}$ reached 0.5, the temperature was reduced to 21 °C and shaking continued at 180 rpm until an $A_{600\ nm}$ of 0.8 was reached. At which point, 0.1 mM anhydrotetracycline was added to induce protein expression and cells were

grown overnight (approximately 18 hours until an $A_{600\ nm}$ of 14). Cell harvesting was performed by a 20-minute centrifugation at 5500×g and 4 °C. the resulting pellets were collected, weighed (typical wet pellet weight was ~ 15g/L), flash frozen in liquid nitrogen and stored at -80 °C until purification.

2.2 Purification of EtfAB and bcd

All purification steps were performed aerobically and at 0 – 4 °C (unless otherwise stated) using a procedure modified from Chowdhury *et al*. (12). Previously frozen cells were thawed and suspended in 0.5 – 1 g/mL of lysis buffer, 50 mM Tris-HCl, 150 mM NaCl, pH 8.0 (for EtfAB) or 50 mM, Tris-HCl, 150 mM NaCl, pH 7.5 (for bcd) supplemented with 1 mM NaF, 1 mM benzamidine, 0.5 mM phenylmethylsulfonyl fluoride (PMSF), and catalytic amounts of lysozyme and DNase I. The cells were incubated 4 °C for 1 hour with stirring before breaking. Cell lysis was performed at 4 °C via 1 to 2 passages through a French Pressure Cell at 10,000 psi. Cell lysate was centrifuged at 200,000×g for 60 minutes at 4 °C to removed cell debris. The supernatant was collected, flash frozen in liquid nitrogen and stored at -80 °C until purification.

During previous purifications of EtfAB, it was observed that FAD associated with the electron-transferring (et FAD) and not the bifurcating (bf FAD) dissociates during the loading and washing steps of purification. To limit how long protein was bound to the column, thawed supernatant was bound via batching where 6 mL of Strep-Tactin XT Superflow resin (IBA GmbH) pre-equilibrated with wash buffer was rotated at 4 °C for 60 minutes. The column was then washed at 2 mL/min with 30 column volumes of wash

buffer, 50 mM Tris-HCl, 150 mM NaCl, pH 8.0, supplemented with 100 µM of FAD to limit the depletion of FAD. Protein was eluted at a rate of 0.5 mL/min with 50 mM Biotin, 50 mM HEPES, pH 7.5 and concentrated to a volume of less than 1 mL. Elution was supplemented with excess FAD to limit et FAD dissociation during centrifugation and concentration was performed using an Amicon Ultra 4 (Millipore) with a molecular weight cut off of 60,000 Da. To remove excess FAD and buffer exchange protein into Buffer A (50 mM, Tris-HCl, 150 mM NaCl, pH 7.5), an 8.3 mL PD-10 (GE Healthcare) desalting column equilibrated with Buffer A was used. Purified protein prepared in this manner was typically > 95 % replete in its electron transferring FAD and 100 % replete in its bifurcating FAD, as confirmed by SDS denaturation. Buffer exchanged protein was then aliquoted, flash frozen via liquid nitrogen and stored at -80 °C until use.

Purification of bcd was performed in the same manner as EtfAB. With the wash buffer changed to Buffer A and the Amicon Ultra 4 (Millipore) with a 40,000 Da molecular weight cutoff. Even though the butyryl-CoA dehydrogenase FAD (bcd FAD) does not dissociate during purification like the et FAD of EtfAB, washing buffer was still supplemented with excess FAD as it did not negatively impact the purification. After elution, it was observed that the bcd would sometimes exhibit a "greening" when purified. This was a result of a long-wavelength absorption at 710 nm due to the charge-transfer complex (CTC) between a cellular CoA persulfide and oxidized enzyme (82). The CTC was removed by first making the protein sample anaerobic via five cycles on an Argon train as previously described by Djordjevic *et al.* (83) and reducing the sample excess with anaerobic sodium dithionite. Once the sample was left at room temperature

for ~ 15 minutes the excess FAD and sodium dithionite were removed and protein buffer exchanged with an 8.3 mL PD-10 (GE Healthcare) desalting column as previously described. Protein was aliquoted, flash frozen via liquid nitrogen and stored at -80 °C until use.

2.3 Plasmid construction of ferredoxin

The gene for a four-iron four-sulfur ferredoxin ([4Fe-4S]) from *Megasphaera elsdenii* (NCBI: locus tag C6Y28_RS04440) was used to construct a plasmid derived from a pTrcHisB vector with the 6xHis-linker-6xHis tag replaced with an N-terminal Strep-II tag. The plasmid was transformed into chemically competent *Escherichia coli* CLK002 cells (MG1655 Δ*isc* Δ*metJ*; Frank Sargent, Newcastle University, personal communication) and glycerol stocks were created and stored in the manner described above.

2.4 Growth and purification of ferredoxin

Growth was performed semi-anaerobically, with both preculture and initial large-scale grown aerobically before switching to anaerobic conditions for induction. Preculture was prepared with cells taken from the appropriate glycerol stocks and placed in 80 mL of rich media consisting of 20 g/L tryptone, 10 g/L yeast, 5 g/L $NaHPO_4$, 4 g/L glucose, 16 mL/L of 50 % glycerol (TGYEP) and 100 µg/mL of ampicillin. Cells were grown overnight with shaking at 220 rpm, 37 °C. Large-scale growth was carried out in 6 L Erlenmeyer flasks with 3 L of TGYEP and 100 µg/mL ampicillin. Flasks were inoculated with the preculture to a starting $A_{600\ nm}$ of ~ 0.2 and grown for ~ 6 h with

shaking at 180 rpm, 30 °C. Once $A_{600\ nm}$ reached 1.5, cells were transferred to another 3 L flask for the anerobic portion of the growth. 100 µL of antifoam B emulsion (Sigma-Aldrich), 2 mM of isopropyl ß-D-1-thiogalactopyranoside (IPTG) and 0.25 g/L of L-cysteine and 0.2 g/L of ferric ammonium citrate were added, with the latter 2 added for iron-sulfur reconstitution and expression (84). Flasks were then sealed and cells were grown anaerobically for 36 hours with constant stirring and Argon bubbling. Cells were harvested by a 20-minute centrifugation at 5500×g and 4 °C. The resulting pellets were collected, flash frozen in liquid nitrogen, and stored at -80 °C until purification.

Cell lysis and purification performed anaerobically and at 4 – 10 °C in an anaerobic glovebox (Coy Labs) with an atmosphere including 2.5 – 3 % H_2. Frozen cells were thawed and resuspended in lysis buffer, 50 mM, Tris-HCl, 150 mM NaCl, pH 8.0, with 1 mM NaF, 1 mM benzamidine, 0.5 mM PMSF, and catalytic amounts of lysozyme and DNase I and incubated for 60 minutes. In addition to the lysis components; 10 mM of glucose, 80 nM of glucose oxidase from *Aspergillus niger* (Sigma Type VII), and 8 nM of bovine liver catalase (Sigma stock #C-40) were added to continually scrub the samples of residual oxygen. Incubated cells were broken via passage through an EmulsiFlex-B15 cell homogenizer (Avestin, Inc.). Lysate was centrifuged at 200,000×g for 60 minutes at 4 °C to removed cell debris. Supernatant was loaded onto a pre-equilibrated 5 mL Strep-Tactin XT Superflow column with 50 mM Tris-HCl, 150 mM NaCl, pH 8.0 at a rate of 0.5 mL/min. 50 mM HEPES, pH 7.5 buffer was used to wash the column for 20 column volumes after which protein was eluted directly onto a Q-Sepharose column via the same buffer supplemented with 50 mM biotin. The Q-Sepharose column was washed in the

same manner and eluted with 50 mM HEPES, pH 7.5, 0.5 M NaCl. Protein was aliquoted, flash frozen and stored in liquid nitrogen until further use.

2.5 SDS denaturation and flavin quantification

Total flavin quantification via denaturation of *Megasphaera elsdenii* EtfAB and bcd as well as *Azotobacter vinelandii* flavodoxin was conducted using the method previously described by Aliverti *et al.* (85). Protein solutions containing ~ 10 µM of enzyme in Buffer A had 20 % sodium dodecyl sulfate (SDS) added to a final concentration of 1 % $\frac{v}{v}$. The solutions were monitored spectroscopically for changes in the 280 nm and 450 nm maxima. The initial and final spectra of the released FAD were compared to established free FAD spectra and concentration was calculated using $\varepsilon_{450\ nm}$ = 11.3 $mM^{-1}\ cm^{-1}$ (49, 86).

2.6 Removal of the et FAD from EtfAB

Between the electron transferring (et FAD) and the bifurcating (bf FAD) of EtfAB, it was observed that the et-FAD partially dissociates during purification and must be reconstituted prior to experimentation by incubation in the presence of free FAD. A modified method used to deplete the et FAD was previously described by Sato *et al.* (49) in which a centrifugal concentration was performed alternating between reaction buffer and reaction buffer with the addition of 2 M of KBr (a chaotropic salt). The flowthrough after each concentration was checked for the presence of FAD and concentration ceased when no FAD was detected, typically after four rounds. After concentration, the enzyme was checked both spectroscopically and by SDS quantification to determine FAD

saturation. Protein was buffer exchanged with an 8.3 mL PD-10 (GE Healthcare) desalting column equilibrated with Buffer A and stored as described above.

2.7 Synthesis and purification of pro-R and pro-S NADD

Synthesis of deuterated nicotinamide adenine dinucleotide at the pro-R and pro-S protons of the 4-position were carried out in a modified procedure from Viola *et al.* 1979 (87). Pro-R was synthesized by mixing 3 mM Ethanol-d_6, 25 mM NAD^+, 50 units of alcohol dehydrogenase from *Saccharomyces cerevisiae*, 100 units of yeast aldehyde dehydrogenase in 10 mL of 10 mM NH_4OH, pH 9 buffer at 25 ºC. The reaction was monitored at 340 nm until absorbance changes ceased (typically overnight). Percentage of conversion was determined by the ratio between the 260 and 340 nm peaks, where a A_{260}/A_{340} of 2.3 represented complete conversion. Enzymes were separated from the NADD/ NAD^+ mixture by centrifugal concentration with a 10,000 MW cutoff, as the flowthrough contained the mixture and was frozen and stored at – 80 ºC until purification.

Pro-S was synthesized by first preparing 10 mM Glucose-1-d and 25 mM NAD^+ in 6 mL of 10 mM KPO_4, pH 8 buffer with 4 mL of DMSO at 25 ºC, 1000 units of glucose-6-phosphate dehydrogenase from *Leuconostoc mesenteroides* was added to the initiate the reaction (reaction was typically complete after 2 hours). Extent of conversion and completion of reaction was again monitored at 340 nm and yield was calculated by

the A_{260}/A_{340} ratio. Separation of enzyme and NADD/ NAD^+ was performed as described above and stored at – 80 ºC until purification.

Separation of either pro-R or pro-S NADD from NAD^+ was performed via HPLC with a 5 mL DEAE anion exchange chromatography (Sigma-Millipore) column equilibrated with 10 mM NH_4OH, pH 8. DEAE was used as NADD would weakly bind while NAD^+ would not. NADD/ NAD^+ solution was loaded at 0.5 mL/min and washed at 1 mL/min with 10 mM NH_4OH, pH 8 for 50 mL and elution was performed by a 500 mL linear gradient at 1 mL/min with 10 mM NH_4OH, 1M NaCl, pH 8. Chromatography was monitored at 260 & 340 nm and NADD would typically elute at 20 % (200 mM NaCl). As NADD purified in this manner was concentrated enough to allow direct dilution into reaction buffer (~ 10 – 20 mM) aliquots were frozen and stored – 80 ºC until use.

2.8 UV-visible absorbance measurements

All static anaerobic titrations, SDS quantifications, ferredoxin reduction assays and routine spectrophotometry were conducted with a Hewlett-Packard 8452A diode-array spectrophotometer equipped with a thermostatted cell holder. Molar extinction coefficients as reported by Toogood *et al* of $\varepsilon_{450\ nm}$ = 21.1 mM^{-1} cm^{-1} and $\varepsilon_{450\ nm}$ = 11.8 mM^{-1} cm^{-1} were used to calculate concentration of EtfAB and bcd, respectively (88). Static titrations were performed in a quartz cuvette sealed with a rubber septum. Anaerobicity of the cuvette containing protein samples was achieved using an Argon wet

or dry train as previously described by Niks *et al.* (89) with the addition of 80 nM of glucose oxidase from *Aspergillus niger* (Sigma Type VII), and 8 nM of bovine liver catalase (Sigma stock #C-40) in the protein solution. After anaerobicity was achieved, 10 mM glucose was added to continually scrub the sample of oxygen. Another permutation of this method used when the protein precipitated during the time it took to make the solution anaerobic is described as so: buffer containing glucose would be bubbled directly and protein containing the glucose oxidase:catalase mixture would be directly injected into the anaerobic buffer and allowed to scrub for 15 – 30 minutes on ice. The substrates used: NADH (Thermo Scientific J61638.03), sodium dithionite (Reagents C2316300), butyryl-CoA (Sigma B1508), or crotonyl-CoA (Sigma C6146), were also made anaerobic on the Argon train minus the glucose oxidase:catalase solution. Introduction of anaerobic substrates was achieved by directly piercing the rubber septum with a Hamilton syringe. The interface between the body of the needle and the septum was sealed with Apiezon N vacuum grease. After the collection of oxidized spectra, an aliquot of reductant/oxidant would be added, then a spectrum immediately after addition of substrate and a spectrum 5 to 10 minutes following the addition to ensure complete reaction would be collected. Aliquots of substrate were added in this manner until the measured spectra matched those of published reduced enzyme spectra.

2.9 Photoreduction of EtfAB

In anaerobic solution, photoreduction of et FAD to one-electron reduced semiquinone was observed with sufficient light intensity. The et FAD was photoreduced to the semiquinone and would not reduce further nor photoreduction in any capacity of

the bf FAD was observed regardless of duration of exposure. To generate the one-electron reduced EtfAB, solution was made anaerobic in either a sidearm cuvette or anaerobic quartz cuvette as described above and exposed to either an 80 W Xenon lamp or direct sunlight for one-minute duration. Extent of photoreduction and semiquinone accumulation was monitored via UV-vis at 450 and 377 nm, respectively and exposure repeated until absorbance changes ceased.

2.10 Ferredoxin reduction assay

All activity assay measurements and absorbance spectra were carried out as described above with the temperature-controlled cell holder set to 25 °C in Buffer A unless otherwise stated. The reduction of ferredoxin in the absence of hydrogenase via the oxidation of NADH by the EtfAB:bcd complex was previously established by Chowdhury *et al.* and the rate of steady-state reduction was 0.29 s^{-1} *(*12). Using a procedure modified from Chowdhury *et al.*, a solution containing 15 µM ferredoxin, 1 µM EtfAB:bcd, 50 µM crotonyl-CoA and 80 nM glucose oxidase:8 nM catalase was made anaerobic as described above. After anaerobiosis was achieved, the solution was tipped into one arm of the sidearm quartz cuvette containing 10 mM glucose and the solution was allowed to scrub for 15 minutes. After scrubbing, the solution was then tipped into the sidearm containing 250 µM NADH and tipped back into the cuvette and data collection began. Direct reduction of ferredoxin was followed at 427 nm, collecting spectra every 5 s for 10 minutes or until no more change in absorbance was observed. Calculations were performed using the following equation as follows (eqn. 16):

$$k_{cat} = \frac{\Delta A_{427}}{\Delta \varepsilon_{427} \times [EtfAB]}$$

Where, ΔA_{427} was obtained by line of best fit analysis on the linear portion of the measured trace and $\Delta \varepsilon_{427}$ of 8.3 mM^{-1} cm^{-1} was used as determined by difference spectroscopy as shown by Ortiz *et al.* (90) and compared to [4Fe-4S] oxidized absorption and reduced EPR spectra of similar ferredoxins as published (91).

2.11 Rapid-reaction kinetics

Rapid reaction kinetics experiments were performed using an SX-20 stopped-flow spectrophotometer (Applied Photophysics Ltd., Leatherhead, Surrey, UK) equipped with either photodiode array (PDA) or photomultiplier tube (PMT) detection and ProData SX 2.2.5.6 data acquisition software. PDA data acquisition was used for the full spectral range of 230—740 nm, while PMT was used for faster observed rates of reaction such as the concentration dependences and at done at a single wavelength.

Anaerobiosis of stopped-flow apparatus was achieved the day prior to experimentation by washing with Argon-bubbled water through the device and subsequent washing with anaerobic reaction buffer containing glucose and glucose oxidase:catalase and continually scrubbing overnight. For reactions where mixing was only between enzyme and substrate, protein would be made anaerobic in an iced tonometer on a dry Argon train and substrate would be directly bubbled with Argon gas before mounting on the apparatus. In the case of protein mixed with protein experiments, either one of or both protein solutions would be made anaerobic in v-vials with glucose oxidase:catalase, transferred into a COY anaerobic glovebox, loaded into pre-wet

syringes with reaction buffer/10 mM glucose and then loaded into the stopped flow apparatus. The light intensity when using the PDA detector often resulted in the formation of anionic semiquinone (FAD•⁻) in EtfAB and photobleaching of bcd after 10 seconds of exposure. To account for this, when data collection extended past 10 seconds the integration time of the device was increased from 1 to 10 ms and light intensity was decreased significantly. In this manner, FAD•⁻ accumulation and photobleaching as a result of photoirradiation was ceased. However, the acquisition time of the first spectra increased from 1 to 10 milliseconds. PMT detection time remained sub 1 ms as data collection started immediately allowing for reliable collection of transients for kinetic traces as the intensity of light did not induce photo-irradiative effects. Experiments were performed at: 5, 10, and 25 °C depending on the observed rate of reaction.

Analysis of the fast phases of reaction involving EtfAB and NADH and bcd with crotonyl-CoA/butyryl-CoA utilized only the first 10 to 500 ms immediately following mixing. For reactions with a k_{obs} slower than 100 s^{-1}, the resulting time course that corresponded to exponential change were instead used. Transients obtained were analyzed by ProData Viewer 4.2.0 and exponentially fit by a nonlinear least squares regression using the following (eqn. 17):

$$A_t = A_\infty \pm \sum A_n \exp\left(\frac{-t}{k_n}\right)$$

n is the number of kinetic phases

For the reduction of EtfAB via NADH, the sum of two exponentials was used while any of the bcd reduction/oxidation processes used a single-exponential. For concentration dependences, the observed rate constants at each [substrate] were plotted against one another and the resultant rectangular hyperbola was fit with the following equation (eqn. 18):

$$k_{obs} = \frac{k_{red}[S]}{(K_d + [S])}$$

The limiting rate constant for reduction, k_{red}, and dissociation constant, K_d, could be extracted.

2.12 EPR spectroscopy

Electron paramagnetic resonance (EPR) spectra were recorded using a Bruker Magnettech ESR500 spectrometer running ESRStudio 1.80.0 acquisition software. Samples measured a 50 mL liquid nitrogen Dewar flask was used for samples measured at 77 K, while a liquid nitrogen variable temperature controller was used for samples at 80 K to 150 K. Samples were measured with a modulation amplitude of 0.6 mT and power of 0.02 mW. All reactions were performed in 50 mM Tris-HCl, 150 mM NaCl, pH 7.5 unless otherwise noted and frozen in PQ tubes for quantification. Quantification was carried out by a double integration of the first-derivative spectra acquired and compared to a sample of *Azotobacter vinelandii* flavodoxin with a known neutral semiquinone (FADH•) concentration. Titrations, standard quantifications, and enzyme monitored turnover samples were made directly in PQ EPR tubes previously flushed with argon and

with reductant/oxidant added anaerobic via Hamilton syringe and monitored via UV-vis spectroscopy. Fast mixing of samples was achieved by making enzyme and substrate anaerobic in v-vials as previously described and transferred into COY anaerobic chamber. Small volumes of substrate were added to the anaerobic tubes via Hamilton syringe and sealed with rubber septa as a separate Hamilton syringe containing enzyme was sealed as well. Sealed samples were transferred into a 4 °C cold room and incubated on ice for 5 to 10 minutes. Enzyme was added rapidly via Hamilton syringe to substrate and immediately quenched in a dry ice/ethanol solution before placing in liquid nitrogen. Samples prepared in this manner were typically frozen 600 ms after the start of reaction.

Chapter 3

Spectral deconvolution of redox species

The following work is a reprint of material published in "Spectral deconvolution of redox species in the crotonyl-CoA-dependent NADH:ferredoxin oxidoreductase from *Megasphaera elsdenii*. A flavin-dependent bifurcating enzyme", April 2021 (92). The co- authors Dr. Nilanjin Chowdhury and Dr. Wolfgang Buckel were collaborators who performed plasmid construction, expression and purification of the proteins (12). Dr. Sophie Franz-Badur performed the initial purification and expression of the proteins along with preliminary stopped-flow experiments, not included in this thesis.

3.1 Spectral deconvolution of the contributions of each FAD in EtfAB:bcd

Despite the presence of three FAD molecules in the EtfAB/bcd complex, deconvolution of the spectral changes attributable to each was in fact more straightforward than might initially be expected for two reasons. First, the oxidized et FAD had a perturbed absorption spectrum that made it readily distinguishable from either the bifurcating or bcd FAD (Figure 10A, red spectrum), making it possible to deconvolute the absorption spectra for the bifurcating and et FADs of EtfAB. Our results agreed very well with a similar deconvolution performed previously by Sato et al. (49). Second, and more importantly, it was possible to deconvolute the contributions of the et FAD•$^{-}$ and bcd FADH• given their distinct spectroscopic signatures; the two are thus readily distinguishable; the bifurcating FAD was distinct in not forming a stable semiquinone at all, owing to its highly crossed half-potentials. This was important in

analyzing future kinetic results as most of the key electron-transfer events of bifurcation were one-electron processes. The bifurcating FAD did not form a stable semiquinone owing to its extremely crossed reduction potentials. As shown in Figure 10A, we have deconvoluted the relevant component spectral changes involved, demonstrating that the spectral changes associated with reduction of each of the three flavins were in fact sufficiently distinct as to allow accurate deconvolution.

The several spectra and difference spectra shown in Figure 10 were obtained as follows: The spectra of oxidized and fully reduced bcd were obtained with the as-isolated and dithionite-reduced protein, with the FADH• semiquinone (characterized by its extended absorption above 500 nm) essentially quantitatively formed as an intermediate at low pH; the spectral changes associated with formation and decay of the FADH• were obtained straightforwardly by subtraction. The spectrum of oxidized ETF had been deconvoluted by subtracting the spectrum of depleted EtfAB, which gave the absorption spectrum of the bifurcating FAD, from that of the as-isolated protein to give the contribution of the et FAD, which was indicated above as quite distinct from the spectra of either the bifurcating or bcd FAD. The spectral changes associated with formation and decay of the et $FAD^{\bullet -}$ were obtained from quantitative titrations of replete EtfAB with sodium dithionite, in which the et $FAD^{\bullet -}$ (with its characteristic absorption band at 370 nm) accumulated essentially quantitatively (correcting for the spectral change associated with reduction of the bifurcating FAD from the quinone to the hydroquinone). It was evident that the difference spectra thus obtained, Figure 10B were

quite distinct, permitting deconvolution of experimentally obtained spectra and spectral changes.

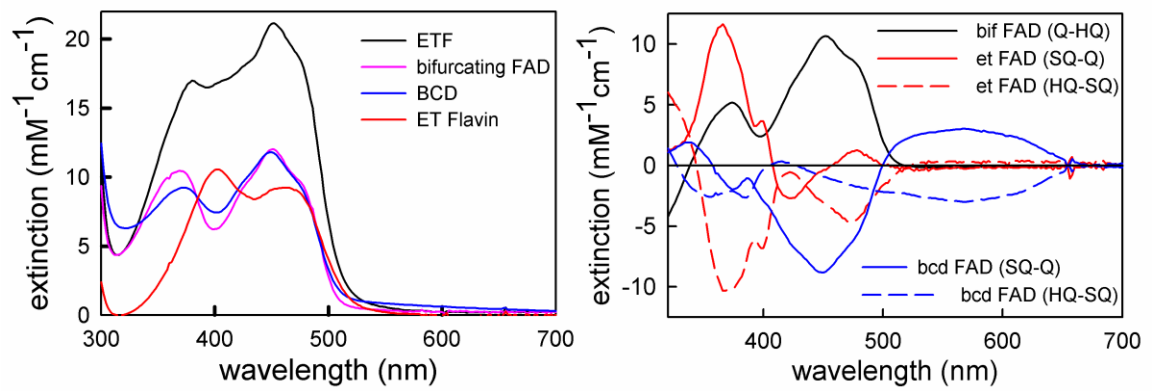

Figure 10. Absorption spectra of the component flavins of EtfAB:bcd. Left, absorption spectra of: replete EtfAB (black); EtfAB depleted of the et FAD, yielding the spectrum of the bifurcating FAD (magenta); the et FAD, obtained by subtracting the spectrum of the bifurcating FAD from that for replete EtfAB (red); as-isolated bcd (blue). Right, difference spectra seen for reduction of each flavin (two-electron for the bifurcating FAD, sequential one-electron reduction in the case of the et and bcd FADs).

3.2 Absence of a reduced EtfAB:NAD$^+$ charge-transfer complex in the *M. elsdenii* system

In contrast to other bifurcating flavin systems, (93-95) no charge-transfer complexes between reduced EtfAB and NAD$^+$ were observed with the *M. elsdenii* EtfAB. This was illustrated in Figure 11, where it was seen that addition of NAD$^+$ up to concentrations of 2.5 mM did not elicit any significant long wavelength absorbance in dithionite-reduced EtfAB. The spectral changes that were observed, with increases in absorbance at ~470 nm and ~360 nm, arose from a slight reoxidation of the protein by the added NAD$^+$ due to mass action; the concomitant accumulation of a small amount of NADH was reflected in the increased absorbance at ~360 nm. The oxidized-minus-

reduced difference spectrum for EtfAB was shown in the inset to Figure 11B for comparison. We also found that no long wavelength absorbance was observed on addition of NAD^+ to depleted, dithionite-reduced EtfAB (data not shown), but do note that weak long-wavelength absorbance (ε_{700} <1,000 $M^{-1}cm^{-1}$) had been observed previously on reduction of the *M. elsdenii* ETF by NADH, although this work was done at pH 5.5 (47).

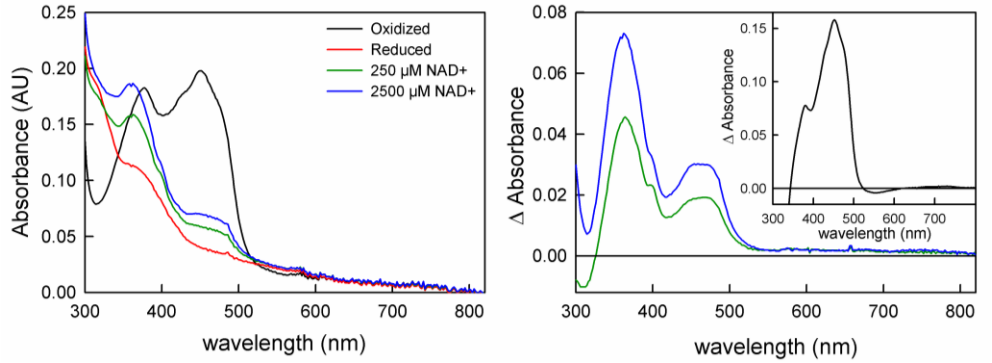

Figure 11. The effect of NAD^+ on the absorption spectrum of dithionite-reduced EtfAB. Left, the absorption spectra of oxidized (black) and dithionite-reduced (red) EtfAB, and the spectra seen after addition of 250 µM (green) and 2.5 mM (blue) NAD^+. Right, the difference spectra observed, illustrating the absence of any substantial absorbance above 600 nm, using the same color scheme.

3.3 The bifurcating FAD of depleted EtfAB forms abundant FAD•⁻

Quite unexpectedly, we observed accumulation of significant amounts of FAD•⁻ in the course of a reductive titration of depleted EtfAB with sodium dithionite, as reflected in the transient accumulation of absorbance in the 370 nm range in the course of the titration, as shown in Figure 12A. Formation of FAD•⁻ was confirmed by EPR, with a prominent semiquinone spectrum observed with a linewidth of 15 G (Figure 12B, upper spectrum). The EPR signal seen upon partial reduction of replete EtfAB with sodium

dithionite, in which the FAD•⁻ of the et FAD accumulates, was also shown for comparison (Figure 12B, lower spectrum). Together with the 370 nm absorbance increase, the narrow linewidth of the EPR signal indicates that it was the anionic rather than neutral semiquinone that was formed (80). The extremely rapid reduction of the depleted EtfAB by NADH indicated unequivocally that it was the bifurcating FAD that was retained after the KBr treatment, despite the close similarity of the FAD•⁻ signals arising from the bifurcating and electron-transferring FADs. The appearance of a strong semiquinone signal attributable to the bifurcating FAD of depleted EtfAB indicated that removal of the electron-transferring FAD resulted in an uncrossing of the half-potentials of the bifurcating FAD. This resulted in the (at least partial) stabilization of the semiquinone oxidation state. The FAD•⁻ that accumulated upon partial reduction of the depleted EtfAB with dithionite persisted indefinitely, and was thermodynamically rather than kinetically stabilized; it did not protonate to the neutral FADH•.

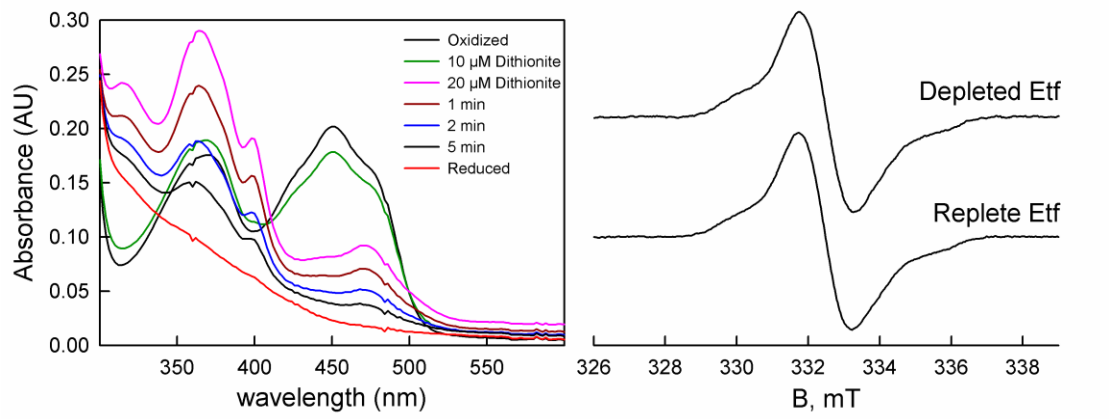

Figure 12. The accumulation of FAD•⁻ in EtfAB depleted of its et FAD. Left, a reductive titration of depleted EtfAB with sodium dithionite. The transient increase in absorbance in the 370 nm region is indicative of accumulation of FAD•- in the course of the titration. Right, X-band EPR of partially reduced, depleted EtfAB, along with the signal seen in the course of a dithionite titration of replete EtfAB, with the signal arising from the FAD•- of the electron-transferring FAD.

3.4 Discussion

The spectral deconvolution undertaken here demonstrated that the spectral contributions of the three FADs of EtfAB/bcd were quite distinct, due in large part to the fact that much of the intraprotein electron transfer was taking place in one-electron steps (as reflected in the transient accumulation of semiquinone states) and that the et FAD formed the anionic semiquinone while the bcd FAD formed the neutral species. Deconvolution was further facilitated by the perturbed spectrum of the oxidized et FAD.

It was at first surprising that removal of the et FAD from EtfAB resulted in the uncrossing of the half-potentials for the bifurcating FAD that remained in the protein, resulting in significant accumulation of the anionic semiquinone in the course of reductive titrations with sodium dithionite. This was particularly the case since strongly crossed half-potentials were widely considered to be a general property common to all bifurcating flavoproteins (including those where the bifurcating FAD is not part of an EtfAB unit). It was important to recognize, however, that there was considerable domain-swapping evident in the crystal structures of both the EtfAB portion of the *C. difficile* EtfAB:bcd complex (left) and the isolated *A. fermentans* EtfAB (14, 96) . As shown in Figure 13, both subunits of EtfAB in fact contributed to the domains in which the two FADs are bound, particularly in the "closed" structure in which the *A. fermentans* protein was found, with the et FAD proximal to the bifurcating FAD. Thus, while the et and bifurcating FADs were frequently referred to in the literature as the α FAD and ß

FAD, respectively, this was somewhat misleading. The adenosine diphosphate portion of the et FAD did interact primarily with the EtfA (or α) subunit, but its isoalloxazine ring interacted extensively with the body of the EtfB subunit; conversely while the adenosine diphosphate of the bifurcating FAD interacted principally with EtfB (or ß), its isoalloxazine ring interacted extensively with the EtfA subunit, at least in the "closed" configuration seen with the *A. fermentans* protein. The differing positions of the domain containing the et FAD was a manifestation of the dynamic behavior. The domain-swapping evident in the structures provided a structural rationale as to how removal of the et FAD might affect the environment of the bifurcating FAD.

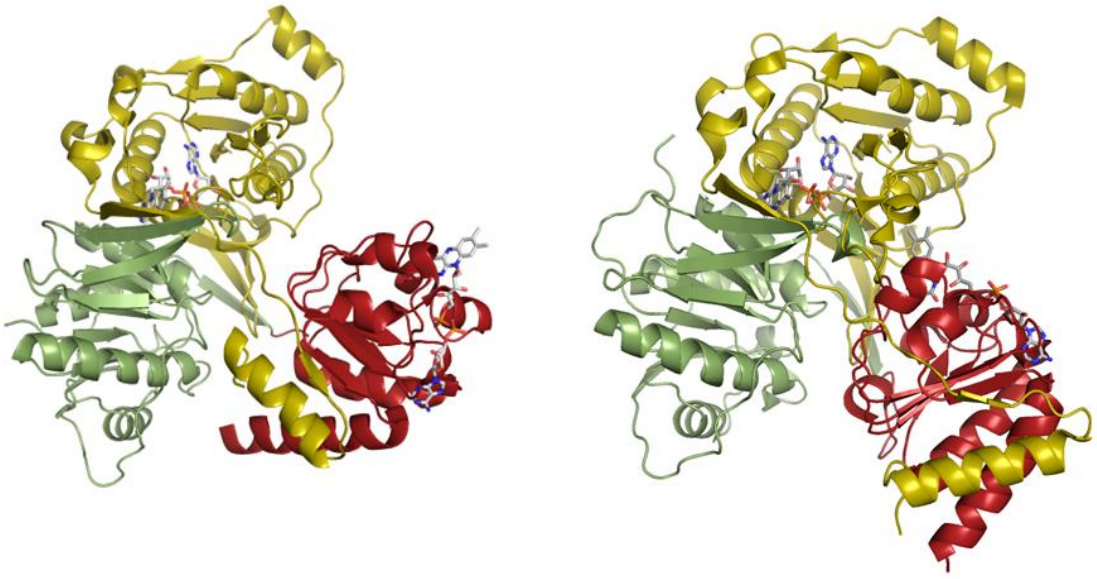

Figure 13. Comparison of the two configurations of et FAD in EtfAB. The structure of EtfAB within the *C. difficile* EtfAB:bcd complex (left), and the isolated EtfAB from *A fermentans* (14, 96). The color scheme and orientation are the same in both cases, center: the N-terminal domain of EtfA in green, and its C-terminal domain in red. The EtfB subunit is in yellow. The two FAD molecules are rendered in stick mode in CPK coloring. The bifurcating FAD is sandwiched between the N-terminal domain of EtfA (green) and the body of EtfB (yellow). The electron-transferring FAD is in a domain that consists principally of the C-terminal portion of EtfA (red), but includes the C-terminal α-helix of EtfB (yellow). It is apparent from a comparison of the two structures that the overall folds of each domain in the two proteins are very similar, as it is for all ETFs, but the orientation of the domain possessing the et FAD is mobile and can assume different orientations relative to the remainder of the protein, as illustrated here. In the C. difficile structure at left, the C-terminal domain of EtfA and the et FAD are oriented away from EtfB (yellow) and face the bcd component of the complex (not shown for clarity), while in the A. fermentans structure at right, the C-terminal domain of EtfA (red) and the et FAD pack closely against the body of EtfB (yellow) and in proximity to the bifurcating FAD. The differing orientations are a reflection of the dynamic properties of the domain harboring the et FAD, as mentioned in the text

Chapter 4

The reductive half-reaction of EtfAB

The following work is a reprint of material published in "The reductive half-reaction of two bifurcating electron-transferring flavoproteins", June 2022 (97). The co-author Jessica Tran did experiments on EtfAB from *Pyrobaculum aerophilum* which are not be included in this dissertation. Co- authors Dr. Gerrit Schut, Dr. Xiaoxuan Ge and Dr. Michael Adams collaborated with Jessica Tran and purified the *P. aerophilum* EtfAB.

4.1 Reductive titrations of EtfAB with NADH and sodium dithionite

We first undertook reductive titrations of replete EtfAB (i.e., protein containing both the bifurcating and et FADs) with either NADH or dithionite. With NADH, a transient increase in the 360 to 377 nm region was observed that was consistent with formation of anionic semiquinone, $FAD^{\bullet -}$ (Figure 14A); $FAD^{\bullet -}$ accumulation is even greater in the course of titrations with sodium dithionite, as shown in Figure 14B, which reflected partial reduction of the et FAD. The formation of a long-wavelength absorbing charge–transfer complex between the reduced protein and NAD^+ was not observed. These results were consistent with previous reports with *M. elsdenii* (48-50) and underscored the fact that formation of a charge–transfer complex is not critical to the bifurcation process.

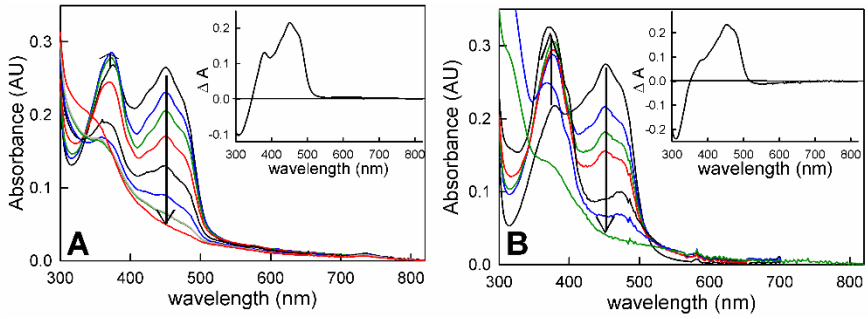

Figure 14. Reductive titrations of the replete EtfAB. A, titration of oxidized (bold black) EtfAB with NADH at 25 °C. Bold blue and red spectra correspond to maximum FAD•⁻and reduced spectra, respectively, in the course of the titration. Arrows at 377 nm indicate FAD•⁻ accumulation and 450 nm flavin reduction. Inset, difference spectrum, reduced minus oxidized. Negative features indicate flavin reduction. B, titration of oxidized (bold black) EtfAB with sodium dithionite at 25 °C. Lower bold black and green spectra correspond to maximum FAD•⁻ and reduced spectra, respectively. Inset, difference spectrum, reduced minus oxidized. Negative features indicate flavin reduction.

We next examined the behavior of the protein that had been depleted of the et FAD by incubation with potassium bromide (KBr). FAD•⁻ wasn't exhibited in the course of titration with NADH, as shown in Figure 15A which was to be expected since reaction of NADH with the remaining bf FAD was expected to proceed directly to the fully reduced flavin hydroquinone (HQ). Surprisingly, and contrary to expectation if the half-potentials of the bf FAD are highly crossed, there was substantial accumulation of FAD•⁻ at intermediate points in the course of titration of depleted protein with sodium dithionite (Figure 15B). Based on the extinction coefficient for the FAD•⁻ state of 17 mM^{-1} cm^{-1} at 365 nm (98), the amount of FAD•⁻ accumulation at maximum in the course of the titration was approximately 80% (the remainder of the protein presumably having been fully reduced on to the HQ). It was indicative of the uncrossing of the half-potentials of the bf FAD.

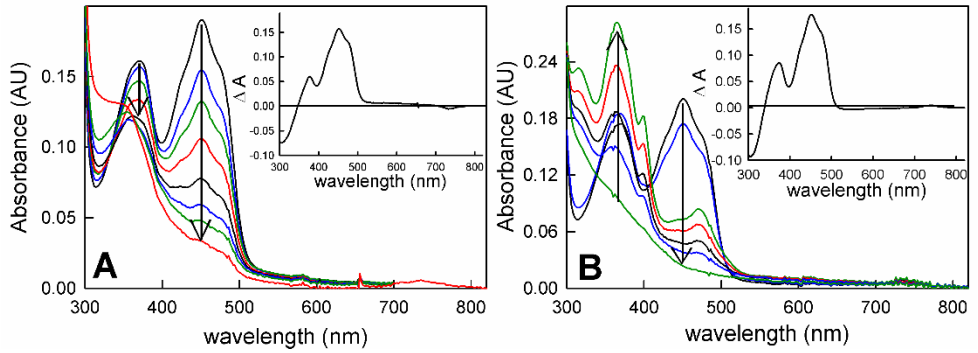

Figure 15. Reductive titrations of the depleted EtfAB. A, titration of oxidized (bold black) EtfAB with NADH at 25 °C. Bold blue and red spectra correspond to maximum FAD•⁻ and reduced spectra, respectively, in the course of the titration. Arrows at 377 nm indicate FAD•⁻ accumulation (or lack thereof in A) and 450 nm flavin reduction. Inset, difference spectrum, reduced minus oxidized. Negative features indicate flavin reduction. B, titration of oxidized (bold black) EtfAB with sodium dithionite at 25 °C. Lower bold black and green spectra correspond to maximum FAD•⁻ and reduced spectra, respectively. Inset, difference spectrum, reduced minus oxidized. Negative features indicate flavin reduction.

4.2 Kinetics of reduction of EtfAB with NADH

We next examined the reductive half-reaction of the two EtfABs by stopped-flow spectrophotometry, beginning with the depleted form that had only the bf FAD so as to examine the intrinsic kinetics of reduction of the bf FAD without the complication of subsequent electron transfer events to the et FAD. Following the reaction at 450 nm, ~90% of the total absorbance change seen Figure 16A occurred in a single phase, with a rate constant that was hyperbolically dependent on [NADH]. Hyperbolic fits to the plot of k_{obs} versus [NADH] yielded a K_d of 96 μM and limiting k_{red} of 1600 s^{-1} at 5 °C. We note that this value was obtained by extrapolation in the plot of rate constant versus [NADH] to infinite [NADH] and that the fastest experimentally determined rate constant is 1000 s^{-1}. This remained at the limit of modern stopped-flow devices, there remains sufficient observed absorbance change at the highest NADH concentrations used to

reliably determine that rate constant for reduction. Having thus characterized the rate of reduction of the bf FAD alone, the reaction of the replete EtfAB with NADH was next examined. Unfortunately, following any transient accumulation of $FAD^{\bullet -}$ in the 377 nm region, as seen in the equilibrium titrations, was not possible owing to the strong absorbance of NADH (which was always present in pseudo–first order excess). As expected, however, the transients seen at 450 nm were considerably more complex than those seen with the depleted systems. Three phases are apparent: a very fast phase that is complete within 20 ms; an intermediate phase that extends out to 1 s; and a slow phase that occurs on the 100 s timescale. The fastest phase was [NADH]-dependent and accounts for approximately half of the total absorbance change at 450 nm. This was attributed to the initial reduction of the bf FAD, with a K_d of 30 μM and limiting k_{red} of 590 s^{-1} at 5 °C (Figure 16B). The intermediate phase accounted for only ∼15% of the total absorbance change at 450 nm but as shown below correlated with accumulation of a significant amount of $FAD^{\bullet -}$, as discussed further. The slowest phase of the reaction resulted in full reduction of the protein, again consistent with the equilibrium titration with NADH.

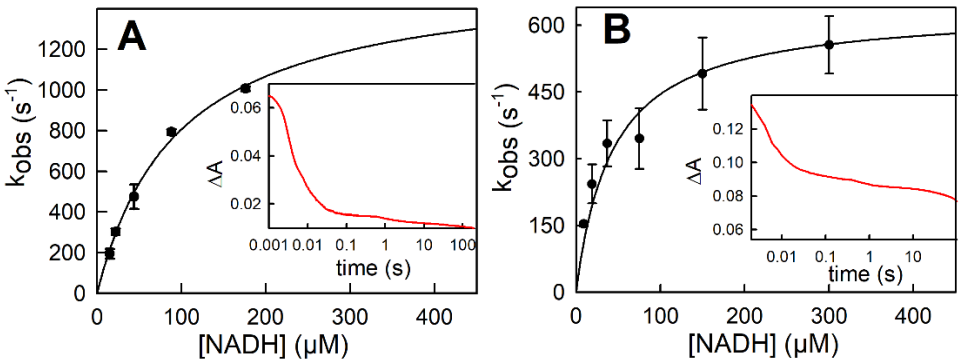

Figure 16. Reduction of depleted and replete EtfAB by NADH. The reaction of 7 μM depleted EtfAB with increasing NADH concentrations monitored at 450 nm at 5 °C. The K_d and limiting k_{red} from hyperbolic fits to the data are 96 μM and 1600 s^{-1}, respectively. The inset shows a representative transient out to 200 s.

In order to follow absorbance changes that might be associated with FAD•⁻ accumulation in the course of the reaction, it was necessary to perform the stopped-flow kinetics at greatly reduced concentrations of NADH. While the reaction will not be exponential under conditions that are not pseudo–first order, it was nevertheless possible to examine the time scale on which various processes occur. Figure 17 showed the results of experiments in EtfAB was reacted with one equivalent of NADH. With the protein depleted of the electron-transferring FAD (panel A), the reaction was monophasic and took place on the 10 to 100 ms timescale, with no accumulation of SQ. With the replete protein (panels B), the kinetics were again substantially more complex. As with the depleted protein, the fast phase of the transient observed at 450 nm occurred on the same 10 to 100 ms time. The transients seen at 377 nm exhibited absorbance increases on comparable timescales to reduction at 450 nm because of the accumulation of FAD•⁻. At the end of the fast phase, the one equivalent of NADH was consumed. On a longer

timescale, a decrease in the absorption because of FAD•⁻ as judged by the decrease of absorbance at 377 nm; this was accompanied by an increase in absorbance at 450 nm.

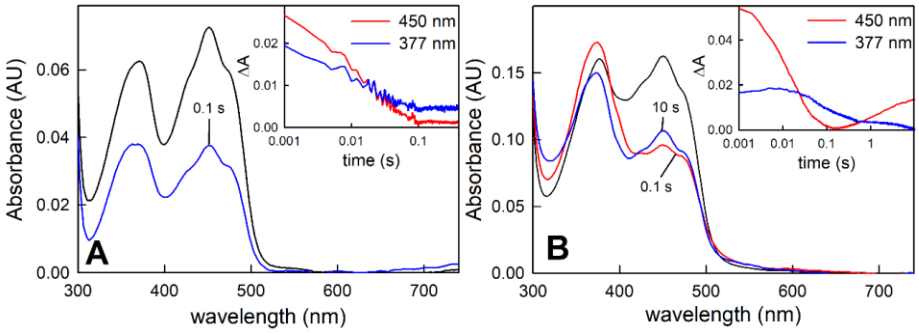

Figure 17. The reaction of EtfAB with stoichiometric concentrations of NADH. A, stopped-flow spectra of 7.5 μM of depleted EtfAB reacted with 7.5 μM of NADH at 10 °C show that in the pre-steady state there is no accumulation of FAD•⁻ seen in the first 200 ms of the reaction with the oxidized spectrum shown in black and 100 ms spectrum in blue. Inset, the 450 and 377 nm time courses extracted from the full-wavelength spectra out to 200 ms. B, stopped-flow spectra of 3 μM replete EtfAB reacted with 3 μM of NADH at 10 °C shows that in the pre-steady state there is rapid accumulation of FAD•⁻ seen in the first 200 ms of the reaction with the oxidized spectrum shown in black and 100 ms spectrum in red. Blue spectrum indicates loss of FAD•⁻ and reoxidation of the bifurcating flavin at 10 s. Inset, the 450 and 377 nm time courses extracted from the full-wavelength spectra out to 10 s.

This was likely a consequence of the intramolecular electron transfer between a pair of SQs in a single protomer ultimately yielding oxidized bifurcating flavin and reduced electron-transferring flavin (intermolecular electron transfer occurred on a much longer timescale Fig. 6B). This intramolecular electron transfer, necessarily entailed the transfer of the (nominally) low-potential electron into the high-potential pathway (which must be slow for successful bifurcation). The accumulation of FAD•⁻ on intermediate timescales in the reaction of the EtfAB component of the *A. fermentans* EtfAB:bcd system, highly homologous to that from *M. elsdenii* studied here, has been observed previously (99) and attributed to intermolecular electron transfer from two-electron reduced protein to

oxidized protein to yield two equivalents of one-electron reduced enzyme in which the $FAD•^-$ would arise from the et FAD, which is known to form a stable anionic SQ. The timescale on which $FAD•^-$ accumulates in both our and the previous study would require that such an intermolecular electron transfer process would have to occur at a rate near the diffusion-controlled limit. In order to examine rates of intermolecular electron transfer, two different experiments were performed. In the first, EtfAB depleted of et FAD was reacted with a substoichiometric concentration of NADH. As shown in Figure 18, intermolecular electron transfer with the depleted occurred over the course of hours (Panel A). In a second experiment, fully reduced replete EtfAB was reacted with an equal concentration of fully oxidized protein, and the kinetics were followed by stopped-flow spectrophotometry. The et FAD was known to have a high Q/SQ half-potential (49), and the expectation was that eventually the system must equilibrate via intermolecular electron transfer to yield the $FAD•^-$ of the et FAD. In this case, intermolecular electron transfer involving either flavin could be followed. As shown in the insets to Figure 18B, intermolecular electron transfer, as reflected in formation of $FAD•^-$, occurred on a timescale of 100 s.

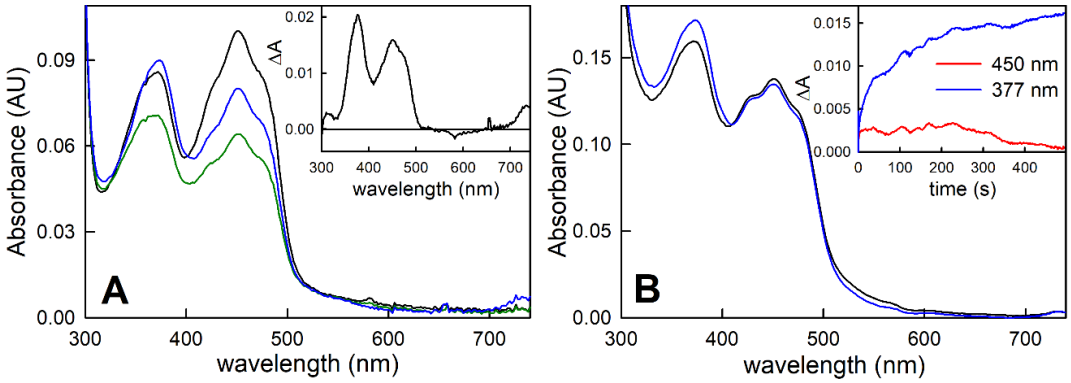

Figure 18. Intermolecular electron transfer of depleted and replete EtfAB. A, spectra of 9 μM of depleted EtfAB reacted with 4.5 μM of NADH at 25 °C. The spectra shown are oxidized (black), after mixing (green), and after 4h (blue). Inset, difference spectrum, 4 h minus after mixing. Positive feature in the 377 nm region corresponds to accumulation of FAD•⁻. B, spectra seen in the course of reaction of 7.5 μM of replete EtfAB, pre-reduced with sodium dithionite, with 7.5 μM of oxidized protein at 25 °C. The spectra shown are after mixing (black) and after 500 s (blue). Inset, the increases in absorption at 377 nm (blue) and 450 nm (red) over the course of 500 s.

4.3 Electron paramagnetic resonance confirmation of FAD•⁻ formation

In order to confirm the formation of FAD•⁻, electron paramagnetic resonance (EPR) spectra were obtained under various conditions. First, EtfAB depleted of its et FAD was titrated with dithionite to maximum absorbance at 377 nm and the EPR recorded. As shown in Figure 19A, strong SQ signal was observed when compared against a standard sample of 20 μM flavodoxin. The integrated intensity of the signal amounted to 0.6 spins per bf FAD. The replete EtfAB was reduced with either stoichiometric or excess of NADH, with the EPR sample frozen approximately 1 s after addition of substrate. Reduction of the replete protein with NADH did result in substantial FAD•⁻ formation. The EPR signals in Figure 19B integrate to ~0.2 spins per replete EtfAB. When NADH was mixed with the depleted EtfAB, there was essentially no FAD•⁻ signal observed in the first second of turnover, consistent with the lack of any increase in absorbance of ~370 nm in the course of the reaction.

That any $FAD^{\bullet-}$ was generated within ~1 s upon reduction of EtfAB with NADH was significant. With intermolecular electron transfer shown to be slow, as described previously, the only way for SQ to be formed at all in the two-electron reduced protein generated after reaction with a first equivalent of NADH was by transfer of a single electron from the now reduced bf FAD to the et FAD, meaning that both flavins in the replete protein must be present as $FAD^{\bullet-}$ in equal amounts. This in turn implied that, to the extent that $FAD^{\bullet-}$ accumulated, the half-potentials of the bf FAD must have become uncrossed. As is shown in Figure 18, the time for intermolecular electron transfer to occur was much too slow to result in the amount of $FAD^{\bullet-}$ measured during the first 1 s of turnover. This was further supported by the lack of any significant $FAD^{\bullet-}$ seen on the same timescale with the EtfAB depleted of the electron-transferring FAD. Our results indicated that this occurs in approximately 20% of the two-electron reduced protein. Thus, as with the EtfAB depleted of the et FAD, it appeared that uncrossing of the half-potentials of the bf FAD also occurred in the replete protein, although to a lesser extent than is seen in the depleted protein.

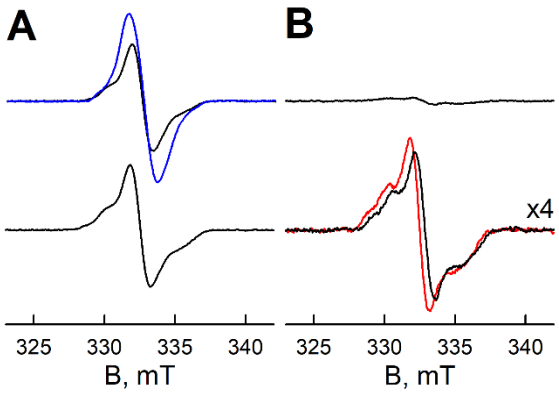

Figure 19. X-band EPR spectra of the anionic semiquinone, FAD•⁻. A, spectra of depleted EtfAB (upper, black) and replete EtfAB (lower), both titrated to maximum accumulation of semiquinone, as well as the spectrum of flavodoxin from *Azotobacer vinelandii* used as the quantification standard (upper, blue). The integrated intensity amounted to 0.6 spins/BF-FAD with the depleted EtfAB and 0.4 spins per replete EtfAB. B, spectra of depleted EtfAB reacted with 30× excess of NADH (upper) and replete EtfAB reacted with stoichiometric amount (lower, black) or 30× excess of NADH (lower, red); the integrated intensity with the replete EtfAB amounted to 0.2 spins/EtfAB.

4.4 Discussion

The et FAD was easily removed, and the reduction of the remaining bf FAD in the depleted protein exhibited a hyperbolic dependence of the observed rate constant on [NADH]. As seen previously in both the *M. elsdenii* (50) and *A. fermentans* (99) systems, we see no indication of SQ formation in the course of the kinetics of reduction by NADH or in titrations with NADH with the depleted protein (as expected, given that NADH obligatorily reduces the remaining bf FAD directly to the HQ in a two-electron process). It was important to recognize that the absence of SQ formation in these experiments did not mean that the bf FAD half-potentials have remained highly crossed in the depleted proteins, only that its midpoint potential remained sufficiently high that it was effectively reduced by NADH directly to the HQ. On the other hand, titration of the

depleted ETFs with sodium dithionite, a one-electron donor, resulted in significant accumulation of FAD•⁻, as reflected in both the UV–visible absorption spectra and observation of the expected EPR signal. The stable accumulation of FAD•⁻ on removal of the et FAD reflected that the half-potentials of the bf FAD have become uncrossed, and significantly so.

Uncrossing also appeared to occur in the replete system as well, as reflected in the transient absorption increases at 377 nm seen on the tens of milliseconds to seconds timescale in the course of reduction with NADH, again reflecting formation of FAD•⁻. This transient accumulation of FAD•⁻ had previously been observed with the EtfAB from *A. fermentans* (99) but was attributed solely to one-electron reduction of the et FAD subsequent to intermolecular electron transfer from NADH-reduced protein. Given the protein concentrations that were used, it was recognized that the observed rates of FAD•⁻ formation required that this (non-physiological) intermolecular electron transfer must occur at a bimolecular rate near the diffusion-controlled limit. In our hands, intermolecular electron transfer as determined in two different types of experiments is, in fact, extremely slow, occurring much more slowly than the transient accumulation of FAD•⁻ in the reaction with NADH. Given that NADH introduces reducing equivalents in pairs, the only partially reduced form that accumulates in the course of the reaction with NADH is the two-electron reduced $EtfAB_{2e^-}$ (one-electron and three-electron reduced forms being formed only as a result of intermolecular electron transfer). The possible

distributions of the two reducing equivalents within $EtfAB_{2e-}$ are:

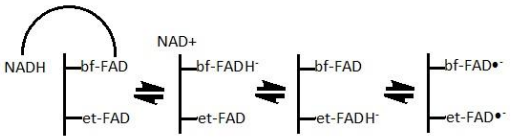

meaning that to the extent that one of the FADs is present as $FAD^{\bullet-}$, the other must be as well. Furthermore, for this distribution to be thermodynamically stable, the half-potentials for the bf FAD must have again become uncrossed, this in the replete protein. On the basis of quantification of the SQ, it appeared that during the course of reduction of the replete protein, only some 20% of the protein existed in the two-electron reduced form with two SQs, meaning that uncrossing was incomplete and suggesting that an equilibrium existed between conformational states in which the half-potentials of the bf FAD were either crossed or uncrossed.

There was, in fact, evidence in the literature that the half-potentials of the bf FAD were not always highly crossed in a bifurcating EtfAB. Whitfield and Mayhew (48), for example, showed that the FADs of EtfAB from *M. elsdenii* (not recognized at the time as being part of a bifurcating system) could be quantitatively converted to $FAD^{\bullet-}$ upon photoreduction and observed a transient increase in absorbance at ~377 nm in the course of titrations with NADH that reflected accumulation of the SQ state. Based on the work presented here, this can now be attributed to an uncrossed bf FAD, and it was clear that both the bf- and et- $FAD^{\bullet-}$ contribute to the transient SQ formation. It had not previously

been suggested that the half-potentials of a bf FAD might uncross under specific circumstances.

The kinetics of NADH reduction of replete EtfAB examined here were complex. An initial fast phase of the reaction is [NADH]-dependent and generally similar to the reduction of the depleted protein and was attributed to the initial reduction of the bf FAD by NADH. This was followed by the aforementioned intermediate phase that reflects accumulation of $FAD^{\bullet -}$ in the intermediate $EtfAB_{2e-}$ state that accumulated in the course of the reaction. The nature of this phase of course being the electron transfer to the et FAD. As discussed further, we attribute this to a reorientation of the domain containing the et FAD that resulted in uncrossing of the half-potentials of the bf FAD. This was followed by an extremely slow phase of the reduction by NADH that ultimately resulted in full reduction to $EtfAB_{4e-}$. This required that the bf FAD become fully reoxidized, meaning that the second nominally high-potential electron must pass to the et FAD (i.e., "leak" into the high-potential pathway in a non-physiological process that defeats bifurcation), followed by rapid re-reduction of the bf FAD by a second equivalent of NADH.

Chapter 5

Reduction of EtfAB via NADD and ThioNADH

5.1 Kinetics of reduction of EtfAB with NADD

With a firm understanding of the kinetics associated with reduction of EtfAB via NADH, we next investigated the reaction with NADD. As a hydride transfer mechanism is responsible for initial reduction of the bf FAD of EtfAB by NADH, with one of the two stereochemically distinct protons at the 4-position of the nicotinamide ring (pro-R or pro-S) involved. It is thus reasonable to assume that a kinetic isotope effect could be observed from the transfer of a deuteron instead. This is primarily due to the higher zero-point energy of the C – H (17.4 kJ/mol) bond compared that of the C – D (12.5 kJ/mol) (100). NADD deuterated at the pro-R or pro-S positions were synthesized as described in Chapter 2.7 and the reductive half-reaction EtfAB reacted with both deuterated forms as well as undeuterated NADH were performed on the same day as shown in Figure 20.

The traces shown in Figure 20A are for the observed reduction of EtfAB with 100 μM of each of the following substrates: NADH (black), 4-S NADD (blue) and 4-R NADD (red). The faster k_{obs} of the reaction with NADH and 4-S NADD was responsible for the difference in starting absorption when compared to the 4-R. This was due to the greater percentage of reaction occurring in the mixing dead-time. The intermediate phase of reduction (as discussed in Chapter 4.2) was found to be identical, independent of substrate. Pro-S NADD was to demonstrate that any observed decrease in rate was due to the deuterated pro-R hydrogen of the nicotinamide and not an artifact of modification.

Figure 20B shows the concentration dependencies of reacting EtfAB with increasing concentrations of the substrate. Hyperbolic fits to plots of k_{obs} versus [NADH] (black). [4-S NADD] (blue) and [4-R NADD] (red) yielded similar K_d's of 22 µM, 22 µM, and 28 µM, respectively. The limiting k_{red} as obtained by extrapolation to infinite substrate concentration in the same order were: 511 s^{-1}, 492 s^{-1}, and 209 s^{-1} all at 10 °C. The ratio of the limiting k_{red}'s for the protonated and deuterated substrates (k_H/k_D) yielded an isotope effect of 2.4, and demonstrating that EtfAB was specific for the pro-R proton of NADH.

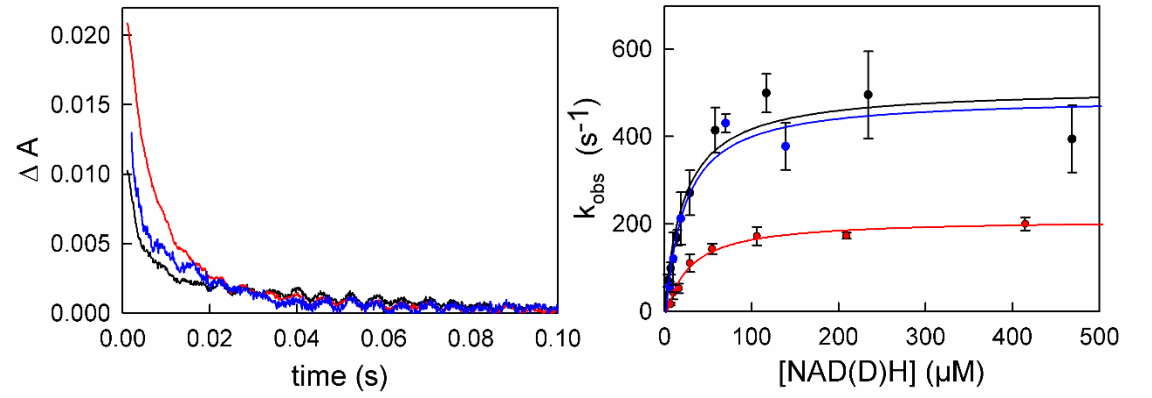

Figure 20. Concentration dependence of 5 µM oxidized EtfAB reacted with increasing concentrations of NADH, 4-S NADD, and 4-R NADD at 10 ºC. A, the 450 nm transients of 100 µM NADH (black), 100 µM 4-S NADD (blue), and 100 µM 4-R NADD (red) out to 100 ms. B, k_{obs} of 5 µM EtfAB with increasing concentrations of [NADH] (black), [4-S NADD] (blue), and [4-R NADD] (red). The K_d's and limiting k_{red}'s of the reactions are as follows: 22 µM and 511 s^{-1} for NADH, 22 µM and 492 s^{-1} for 4-S NADD, and 28 µM and 209 s^{-1} for 4-R NADD.

5.2 Reductive titrations of EtfAB with ThioNADH

Next, the nature of EtfAB reduction using thioNADH, where the carbonyl oxygen of the amide has been replaced with a sulfur, which has a reduction potential of –0.29 mV, considerably higher than the –0.32 mV potential of NADH (101). To determine if

thioNADH reduces the enzyme, anaerobic titrations were performed as shown in Figure 21. With the addition of excess thioNADH, the extent of reduction observed in Figure 21A was comparable to that seen in the titration with NADH shown in Figure 14A, although a greater excess of thioNADH was required. We did observe an initial increase at 377 nm after the first addition of ThioNADH which was consistent with the titration shown in Figure 14A, but it was later obscured towards the end of the titration due to the excess thioNADH present ($\Delta\varepsilon_{395}$ of 11.3 mM^{-1} cm^{-1}). In contrast to the titration with NADH (Figure 14A), an increase in absorbance at long wavelength (>700 nm) was observed with thioNADH, indicative of formation of a charge-transfer complex between reduced EtfAB and $thioNAD^{+}$. To further explore this, oxidized EtfAB was reacted with a large excess of thioNADH, and the broad absorbance in the long wavelength became much more apparent (Figure 21B). This was further corroborated by the positive feature of the difference spectrum in Figure 21B indicating charge-transfer.

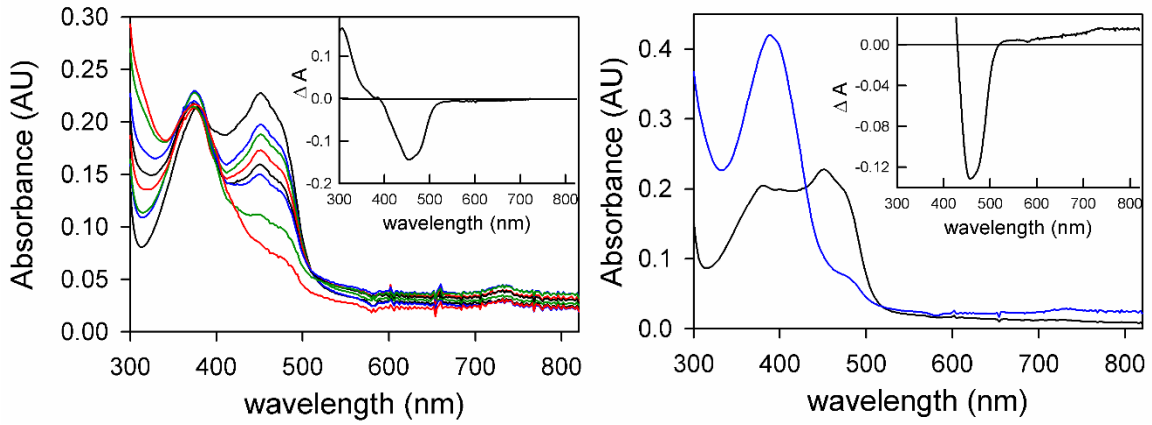

Figure 21. Reductive titrations of EtfAB with ThioNADH at 25 ºC. A, titration of 10 µM oxidized EtfAB (black) with ThioNADH. The absorbance of excess ThioNADH at 395 nm is apparent in the reduced spectrum (red) but the lack of features at 450 nm is consistent with previous titrations. The inset shows the reduced *minus* oxidized difference spectrum where the negative 450 minimum is indicative of FAD reduction. B, addition of 30 µM ThioNADH to 10 µM EtfAB, again the lack of 450 nm features is indicative of FAD reduction, note the increase in absorbance above 700 nm indicating a charge-transfer complex. The inset shows the reduced *minus* oxidized difference spectrum showing the reduction of FAD and the accumulation of the charge-transfer complex at the end of the reaction.

5.3 Kinetics of reduction of EtfAB with thioNADH

With an understanding of the behavior of EtfAB reduction by thioNADH, rapid-reaction experiments were performed next. As seen before with NADH, the reaction is biphasic, with a fast phase of reduction completed by ~10ms and the second phase progressed much the same (Figure 22A). However, unlike the reaction with NADH, even so low a concentration of thioNADH as a sevenfold excess (50 µM, compared to 7 µM EtfAB) already displayed saturating kinetics (Figure 22B). A reduced rate of reduction compared to NADH in Figure 21 (K_d and k_{red} of 22 µM and 511 s^{-1}, respectively) was observed as a hyperbolic fit to the plot of k_{obs} versus [ThioNADH] yielded a K_d and k_{red} of 11 µM and 233 s^{-1}, respectively.

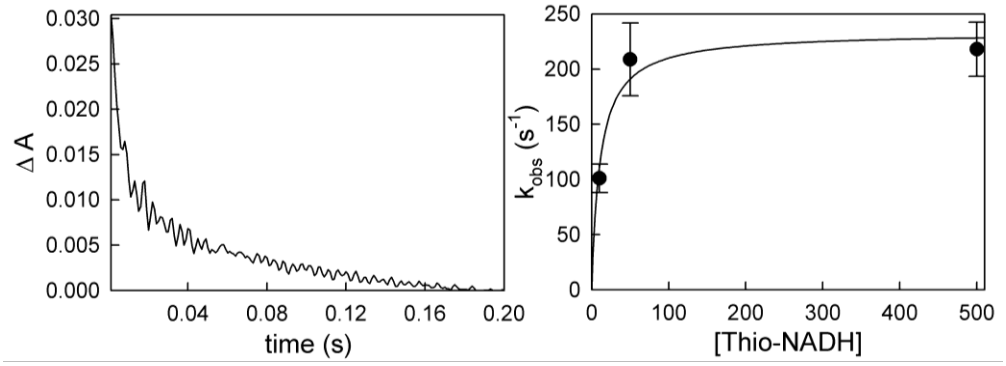

Figure 22. Concentration dependence of 7 µM oxidized EtfAB reacted with increasing [ThioNADH] at 10 ºC. A, the 450 nm trace of 50 µM ThioNADH out to 200 ms. B, k_{obs} of 7 µM EtfAB with increasing concentrations of [ThioNADH]. The K_d and limiting k_{red} of the reaction were 11 µM and 233 s^{-1}.

5.4 Discussion

When comparing the rapid-reaction kinetics of EtfAB with NADH and the two deuterated forms (4-R/S NADD), no effect on the phases of reduction out to 100 ms was observed other than the reduction in k_{red} with 4-R NADD. The k_H/k_D value of 2.4 were indicative of a kinetic isotope effect (KIE), somewhat low for the expected primary isotope effect although KIE's in the range 2-15 have been observed with yeast alcohol dehydrogenase (100 & 103). That 4-S NADD yielded identical values to the reaction with NADH clearly demonstrated that EtfAB is specific for the pro-R proton of NADH. The reaction observed only extended to include the initial phase of bf FAD reduction and the second, slower phase attributed to electron transfer to the et FAD as discussed in Chapter 4.2. The consistency in which the two phases is apparent in multiple experiments and the second phase remaining unperturbed in the reaction heavily implied that the subsequent electron transfer to the et FAD was unaffected and is a one-electron process.

In the equilibrium titration of EtfAB, an excess of thioNADH was required to fully reduce the enzyme, not unexpected given the +30 mV higher reduction potential of thioNADH relative to NADH and the fact that a small excess of NADH was also required to achieve full reduction (Figure 14A). Despite this, the rapid, initial formation of $FAD^{\bullet-}$ after the first addition of reductant was still observed in the kinetic experiment (Figure 21A blue spectrum), and full reduction of EtfAB was eventually achieved. The appearance of a weak charge-transfer complex was observed, indicating unequivocally that the $thioNADH^{+}$ had indeed bound and reacted. The difference spectrum obtained in Figure 21 insets showed that the 450 nm of FAD was still an appropriate wavelength to monitor reduction in the rapid-reaction kinetic experiments. As seen with reduction by 4-R NADD, reduction by thioNADH resulted in a decrease in rate without any perturbations to the intermediate phase of reduction, again implying that electron transfer to the et FAD within EtfAB is unaffected.

The two NADH analogues that resulted in a decrease in the rate of reduction, 4-R NADD and thioNADH, represent kinetic and thermodynamic changes to the reductive half-reaction of EtfAB, respectively. Although effects on reduction of the bf FAD were observed, the subsequent reduction of the et FAD remained the same implying that the intramolecular electron transfer between the two flavins of EtfAB is independent of reductant and overall modality of reduction as seen in Chapter 4.2 and Figures 20 & 22. Ultimately, as said reduction and generation of the low-potential bf $FAD^{\bullet-}$ remain the thermodynamic basis for flavin-based electron bifurcation, analogues that directly affect

both the kinetics and thermodynamics of reduction could prove instrumental in investigating the nature of ferredoxin reduction.

Chapter 6

Rapid-reaction kinetics of the butyryl-CoA dehydrogenase

The following work is a reprint of material published in "Rapid-reaction kinetics of the butyryl-CoA dehydrogenase component of the electron-bifurcating crotonyl-CoA-dependent NADH:ferredoxin oxidoreductase from *Megasphaera elsdenii*", July 2023 (103). The co- author Derek Nguyen assisted with experiments and helped to write and prepare the manuscript.

6.1 Reductive titrations of EtfAB with NADH and sodium dithionite

As reported previously (52,92), during reductive titrations of bcd with sodium dithionite at pH 7.5 the one-electron reduced FAD neutral semiquinone (FADH•) accumulates transiently with a characteristically broad long wavelength absorbance having a maximum at approximately 571 nm (Figure 23); this accumulation of FADH• was confirmed by EPR (6.3) and amounts to 16% total accumulation, in good agreement with the value of 19% seen previously (52). We have also undertaken titrations of bcd with sodium dithionite at pH 6.0 and 9.0 and found that, as expected, FADH• accumulates to a significantly greater extent in the course of the reductive titration at pH 6.0 than at pH 7.5, and less so at pH 9.0 (Figure 23).

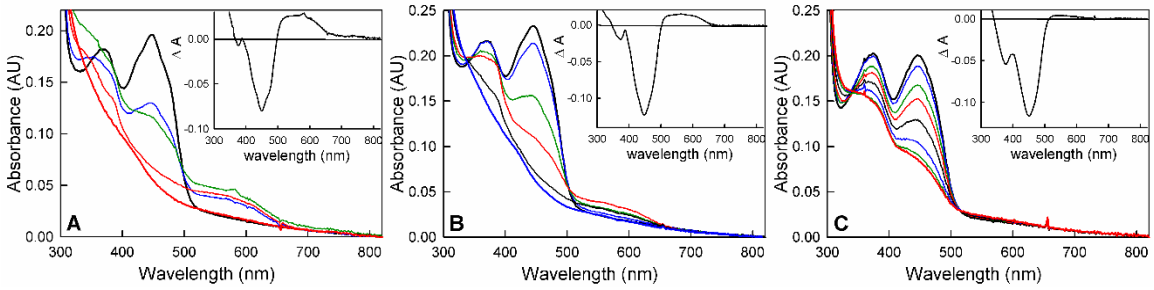

Figure 23. Reductive dithionite titrations of bcd as a function of pH. A. Titration at pH 6.0 of 17 µM bcd (bold black) in 50 mM MES, 150 mM NaCl, pH 6.0. Green and bold red spectra represent the points of largest accumulation of FADH• and full reduction, respectively, over the course of the titration. Inset, the difference spectrum between the point of greatest FADH• accumulation minus that of oxidized enzyme. B. Titration at pH 7.5 of 19 µM bcd (bold black) in 50 mM Tris-HCl, 150 mM NaCl, pH 7.5. Red and bold blue spectra represent the points of greatest accumulation of FADH• and full reduction, respectively. Inset, the difference spectrum of the point of largest FADH• accumulation minus that of oxidized enzyme. C. Titration at pH 9.0 of 17 µM bcd (bold black) in 50 mM TAPS, 150 mM NaCl, pH 9.0. Inset, the difference spectrum between the point of greatest FADH• accumulation minus that of oxidized enzyme. In all three insets, the negative features at ~450 nm reflect flavin reduction and the positive absorption in the 500-600 nm range reflect FADH• accumulation, this being greatest at pH 6.0 and least at pH 9.0. All experiments were performed at 25°C.

We next performed reductive titrations of oxidized bcd in the presence of a catalytic amount of EtfAB with both sodium dithionite and NADH at pH 7.5. As seen in Figure 24, we did not observe any major differences between the two titrations, although there was somewhat greater accumulation of FADH• in the dithionite titration. The significant accumulation of FADH• during the course of the titration with NADH indicated that a substantial portion of the electron transfer from NADH-reduced EtfAB to bcd occurred in one-electron steps.

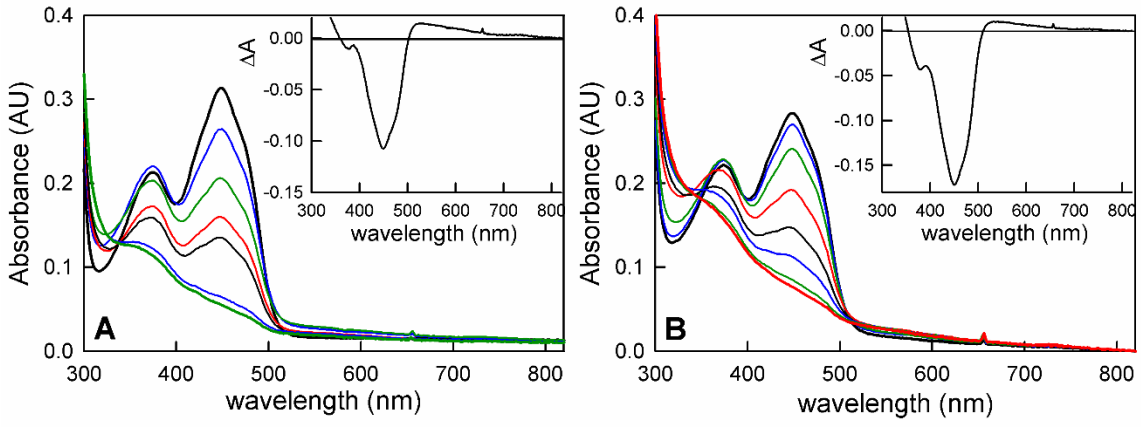

Figure 24. Reduction of bcd in the presence of catalytic amounts of EtfAB. A. Reductive titration with sodium dithionite of 27 µM bcd (bold black) bcd and 1 µM EtfAB. Inset, the difference spectrum between the point of largest accumulation of FADH• minus that of oxidized enzyme. B. Reductive titration with NADH of 25 µM bcd (bold black) bcd and 1 µM EtfAB. Inset, the difference spectrum between the point of largest accumulation of FADH• minus that of oxidized enzyme. The negative features at 450 nm reflect flavin reduction and the positive features above 500 nm reflect FADH• accumulation. Both titrations were performed in 50 mM Tris-HCl, 150 mM NaCl, pH 7.5, 25°C.

We also performed a reductive titration of bcd with butyryl-CoA (Figure 25A). This was the reverse of the physiological direction, but could be driven, if incompletely, by mass action in the presence of high concentrations of butyryl-CoA. Although the long-wavelength absorbance in the 500-600 nm range (Figure 25, insets) closely resembled the accumulation of FADH•, EPR indicated negligible semiquinone accumulation (data not shown). We attributed the long-wavelength absorbance instead to a bcd_{ox}:butyryl-CoA charge-transfer complex, by analogy to the well-characterized charge-transfer complexes of enzyme with crotonyl-CoA (51), acetoacetyl-CoA (52) and CoA persulfide (82) (see Appendix A1). A second charge-transfer complex involving reduced bcd and crotonyl-CoA was also formed transiently in the course of reacting

reduced bcd with crotonyl-CoA and the spectrum of this complex was very similar to that of the bcd_{ox}:butyryl-CoA complex (Appendix A2).

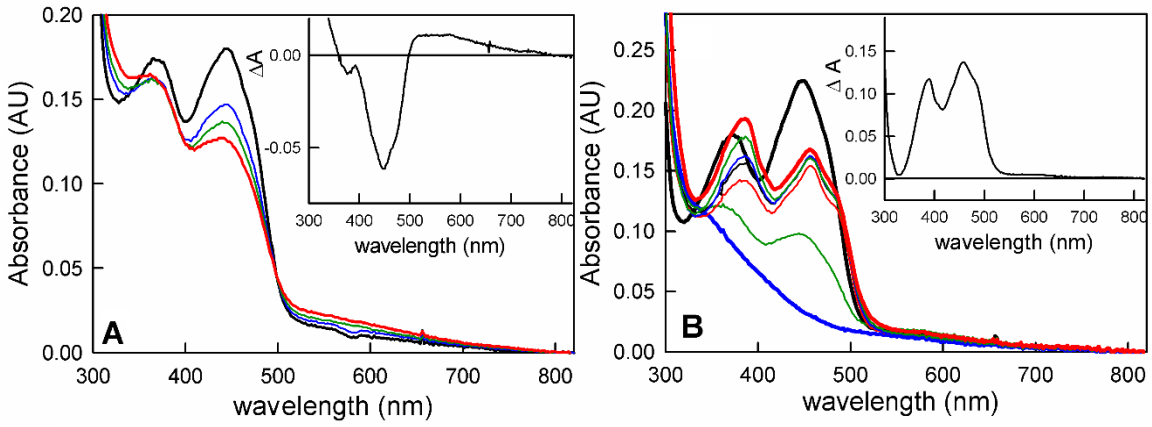

Figure 25. Reductive titration of bcd with butyryl-CoA and oxidative titration with crotonyl-CoA. A. Titration of 13 µM oxidized bcd (black) with butyryl-CoA The spectrum in red reflects the greatest extent of bcd reduction with the addition of excess (100 µM) butyryl-CoA. Inset, the difference spectrum between the point of greatest enzyme reduction minus that of oxidized enzyme. Negative features show flavin reduction with the maximum at 450 nm for FAD and positive features above 500 nm show the formation of the bcdox:butyryl-CoA charge-transfer complex (CTC) with a maximum of 571 nm. B. Reoxidation of 19 µM fully reduced bcd (bold blue) by crotonyl-CoA in 50 mM Tris-HCl, 150 mM NaCl, pH 7 to maximum reoxidation (bold red). Bold black shows fully oxidized bcd. Inset, difference spectrum, crotonyl-CoA oxidized minus reduced. Note the amount of the relative 377 nm peak is nearly the same as the 450 nm peak indicating the presence of FAD•- and the small accumulation of long-wavelength absorbance is consistent with the small amount of bcdred:crotonyl-CoA CTC. Experiments were performed in 50 mM Tris HCl, 150 mM NaCl, pH 7.5, 25°C.

Lastly, we titrated reduced bcd with crotonyl-CoA, i.e., the reaction of physiological relevance to bifurcation as catalyzed by the intact EtfAB:bcd complex. As with the reduction of bcd by butyryl-CoA, the reaction did not progress to completion (Figure 25B). In addition, there was a significant absorbance increase at 377 nm in comparison to the absorption decrease at 450 nm at the end of the reaction (compare Figure 25B with 23B), consistent with the accumulation of the anionic semiquinone, FAD•- rather than the neutral FADH• seen in the course of dithionite titrations. This

suggested, as verified by EPR below, that substrate/product binding resulted in ionization of the semiquinone oxidation state.

6.2 Kinetics of reduction of EtfAB with NADH

We next investigated the rapid-reaction kinetics of the reductive and oxidative half-reactions of bcd. This included the reaction of oxidized bcd by fully (i.e., four-electron) reduced EtfAB, the reoxidation of reduced bcd by crotonyl-CoA, and the reduction of bcd by butyryl-CoA, all by stopped-flow spectrophotometry. Previous work had shown that reduction of EtfAB by NADH is fast with a hyperbolic dependence of kobs on [NADH] and limiting k_{red} at high NADH of 590 s^{-1} (Chapter 4). The reaction of oxidized bcd with pre-reduced EtfAB involved the transfer of one or two reducing equivalents from the et FAD of EtfAB to the bcd FAD. The distinct absorption spectra of the two flavins (given the red-shifted absorption of the et FAD) allowed us to observe the reaction at 450 nm. The reaction of equimolar concentrations of fully reduced EtfAB and bcd (32 µM each) exhibited an apparent k_{red}, of 2 s^{-1} at 25 °C. The process was a well-defined monophasic exponential, as was apparent from the quality of the exponential fit to the data shown in Figure 26A, inset. The observed rate constant was independent of the equimolar protein concentrations over the range 2-70 µM, indicating that the K_d for binding EtfAB to bcd was much lower than 2 µM. The observed rate constant also did not change when the reaction was performed under approximately pseudo first-order conditions, reacting 3 µM pre-reduced EtfAB with up to 25 µM bcd, as seen in Figure 26B, suggesting that the observed kinetics did not arise from the second-order binding of the two proteins. Significantly, inspection of the observed spectral change at longer

wavelengths indicated that there is substantial accumulation of FADH• in the course of the reaction (Figure 26C). The magnitude of the absorbance increase indicated that some 40% of the total reduced bcd FAD was in the semiquinone form at the end of the reaction. This in turn meant that a significant amount of the electron transfer from the reduced EtfAB to bcd occurred in a one-electron process. 40% undoubtedly underestimates the extent of one-electron transfer as some FADH• was very likely reduced subsequently on to the hydroquinone in a second one-electron process. Given that the reduction potentials of the Q/HQ of the et FAD in EtfAB are approximately 136 mV more negative than the SQ/HQ bcd FAD it stood to reason that the two-electron transfer would be thermodynamically quite favorable (83), but since both half-potentials were more negative than the crotonyl-CoA/butyryl-CoA couple, the existence of both one- and two-election processes was not unexpected.

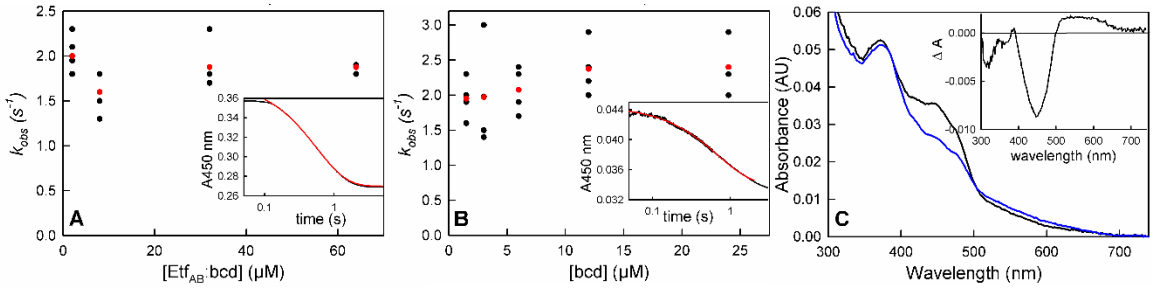

Figure 26. The reaction of reduced EtfAB with oxidized bcd. A. Reaction of pre-reduced EtfAB with oxidized bcd in a 1:1 ratio monitored at 450 nm. The average rates seen at each concentration are marked in red. The apparent k_{red} is 2 s^{-1} and is independent of absolute concentrations of the complex. Inset, a representative transient seen with 32 μM of EtfAB and bcd (black) and a single-exponential fit to the data with k_{obs} = 1.9 s^{-1} (red). B. The reaction of 3 μM pre-reduced EtfAB with increasing concentrations of oxidized bcd. The average rates of each concentration are marked in red and again the concentration-independent kred is 2 s^{-1}. Inset, a representative transient at 3 μM EtfAB and 3 μM (black) with a single-exponential fit with kobs = 2.0 s^{-1}. C. Spectral changes associated with the reaction of 3 μM pre-reduced EtfAB with 3 μM bcd. The spectra seen immediately after mixing (black) and at the end of reaction (blue) are shown. Inset, the total spectral change associated with the reaction, with positive features above 500 nm reflecting the accumulation of bcd FADH•. Experiments were performed in 50 mM Tris-HCl, 150 mM NaCl pH 7.5, 25°C.

The kinetics of the oxidative-half of the reaction were next examined, reacting pre-reduced bcd with crotonyl-CoA, the experiment being performed at 10°C given the fast kinetics that were observed. The observed kinetics were monophasic with a rate constant that was independent of [crotonyl-CoA] over the range 10-110 μM, with an apparent rate of 30 s^{-1} (Figure 27A). The bcd_{red}:crotonyl-CoA charge-transfer complex observed in the reductive titrations described above was fully formed in the mixing dead time of the stopped-flow apparatus, as shown in Figure 27B (blue), indicating extremely rapid and tight binding of crotonyl-CoA to bcd. The difference spectrum between the spectrum obtained immediately after mixing minus that of the fully reduced enzyme shown in the inset to Figure 27B illustrated formation of the charge-transfer complex (black); the difference spectrum for the overall spectral change was also shown (blue).

When reduced bcd is reacted with excess crotonyl-CoA, full reoxidation of the FAD was observed with loss of the charge-transfer complex occurring at a comparable rate, as shown in the Figure 27C.

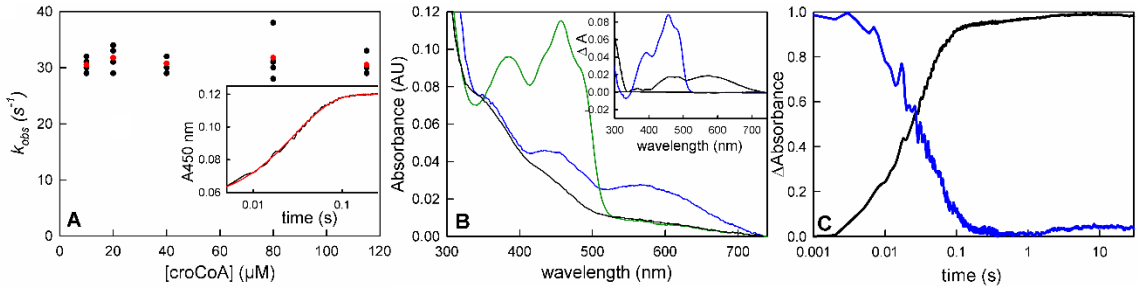

Figure 27. The oxidation of bcd by crotonyl-CoA. A. Reaction of 12 μM bcd with increasing [crotonyl-CoA] as monitored at 450 nm. The average rates of each concentration are marked in red. The apparent k_{red} is 30 s^{-1} and is independent of [crotonyl-CoA]. Inset, a representative transient seen with 112 μM crotonyl-CoA (black) and the single-exponential fit with k_{obs} = 30 s^{-1} (red). B. Spectral changes associated with the reaction of 16 μM pre-reduced bcd and 112 μM crotonyl-CoA: black, fully reduced bcd; blue the spectrum seen immediately after mixing (~1 ms); green, the final spectrum at the end of the reaction. Inset, difference spectra showing the full formation of the bcd_{red}:crotonyl-CoA charge-transfer complex (black) and full reoxidation of bcd (blue). C. The normalized kinetic transients seen at 450 nm following flavin reoxidation (black) and at 571 nm, following loss of the charge-transfer complex (blue) in the 112 μM crotonyl-CoA reacted with bcd. Reoxidation of bcd and the decay of the bcd_{red}:crotonyl-CoA complex is seen to occur concomitantly. Reactions were performed in 50 mM Tris-HCl, 150 mM NaCl, pH 7.5, 10°C.

Finally, we examined the kinetics of bcd reduction by butyryl-CoA, working again at 10°C given the fast rates that were observed. The transients were again monophasic, but unlike the reaction with crotonyl-CoA, the observed rate constant exhibited a hyperbolic dependence on [butyryl-CoA]. As shown in Figure 28A, hyperbolic fits of the plot of kobs vs [butyryl-CoA] yielded an apparent K_d of 60 μM and limiting k_{red} of 1400 s^{-1}. Given the unfavorable thermodynamics of the reaction noted above, the extent of reduction at lower concentrations of butyryl-CoA increased due to a mass action effect, but above 100 μM butyryl-CoA the extent of reduction became

independent of butyryl-CoA. The reduction potential of the crotonyl-CoA/butyryl-CoA is -10 mV (83), and consistent with this we found that in order to poise the system for the butyryl-CoA/crotonyl-CoA equilibrium a ratio of 10:1 was required, as previously reported (104). Given this, the K_d determined from the hyperbolic plot must be considered an apparent value, but the limiting k_{red} is reliable. Consistent with the results of the equilibrium titration of oxidized bcd with butyryl-CoA (Figure 25A), the reaction did not go to completion even at the highest concentrations of butyryl-CoA used, and a charge-transfer complex of butyryl-CoA with the substantial amount of enzyme that remains oxidized was seen at the end of reaction, as reflected in the extended absorption increase above 500 nm (Figure 28B).

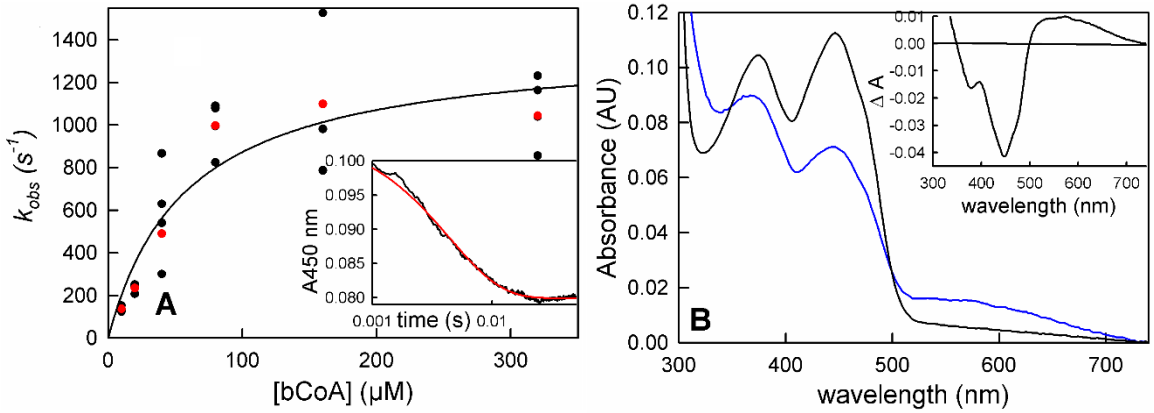

Figure 28. The reduction of bcd by butyryl-CoA. A. Reaction of 10 μM bcd with increasing [butyryl-CoA] monitored at 450 nm. The average rates of each concentration are marked in red. The K_d and limiting k_{red} from hyperbolic fits to the data are 60 μM and 1400 s^{-1}, respectively. Inset, a representative transient of 80 μM butyryl-CoA out to 0.025 s. B. The reaction of 10 μM bcd with 640 μM butyryl-CoA: black, oxidized enzyme; blue is the spectrum at the end of reaction (~ 2 ms). Inset, the difference spectrum associated with the overall reaction, where positive features represent flavin reduction, showing the full formation of the bcd_{ox}:butyryl-CoA CTC and reduction of FAD (black). Reactions were performed in 50 mM Tris-HCl, 150 mM NaCl, pH 7.5, 10°C.

6.3 Electron paramagnetic resonance confirmation of FAD•⁻ formation

As indicated in Chapters 3 & 4, the et FAD of EtfAB exhibited a thermodynamically stable anionic semiquinone in the one-electron reduced state. On the other hand, bcd exhibited a neutral semiquinone in the course of dithionite titrations, particularly at lower pH values (Figure 23). This was also the case for the bcd within the EtfAB:bcd complex (92). FADH• and FAD•⁻ could be differentiated on the basis of their different EPR linewidths (70), which fall in the range 1.9-2.2 and 1.4-1.6 mT, respectively. When bcd was reduced by one equivalent in the absence of either crotonyl- or butyryl-CoA, a 2.1 mT linewidth was seen (Figure 29A), which in conjunction with the observed long-wavelength absorbance (Figure 23) unambiguously established the semiquinone to be the neutral FADH•. On the other hand, there was a large accumulation

of absorbance at 377 nm when reduced bcd was reoxidized by crotonyl-CoA, suggesting formation of the anionic FAD•⁻ semiquinone (Figure 25B). The resulting EPR signal, shown in Figure 29B, exhibited a linewidth of 1.6 mT, indicating that FAD•- did indeed form in the presence of crotonyl-CoA. The intensity of the signal represented approximately 20% of the total enzyme as the FAD•⁻. The extent of formation of FAD•⁻ in the bound state also agreed well with the observed extent of reaction as shown in Figures 27 and 28. On the basis of these results, the binding of substrate/product resulted in ionization of the bcd semiquinone, a point discussed further below. In the case of the reductive half-reaction, the present results underscored the importance of one-electron processes in the course of electron transfer from EtfAB to bcd, as previously suggested in the context of structurally characterized motions of the et FAD-containing domain of EtfAB (Chapter 3.4). The absence of flavin semiquinone accumulation in the course of reoxidation of reduced bcd by crotonyl-CoA was consistent with the reaction occurring cleanly in a two-electron process. It was important to note, however, that there was precedent for a one-electron process with an accompanying radical on the substrate in a similar system as shown in the reaction that had previously been characterized in the dehydration of 2-hydroxy-4methylpentanoyl-CoA by *C. difficile* (105).

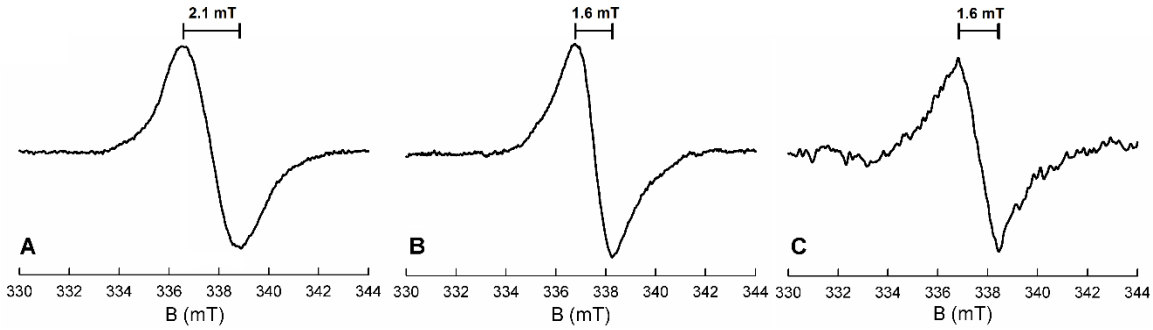

Figure 29. X-band EPR spectra of the semiquinone signal at 77 K. A. Spectra of 30 µM bcd titrated with sodium dithionite to maximum accumulation of FADH• as verified by maximum absorption at 571 nm at pH 6.0. The peak-to-trough linewidth is 21 Gauss (2.1 mT) which correlates to the UV-VIS as the neutral semiquinone. B. The spectra of 30 µM bcd fully reduced with sodium dithionite and reoxidized with 100 µM of crotonyl-CoA at pH 7.5. The linewidth is 16 Gauss (1.6 mT) and correlates to the 377 nm absorbance seen in the reoxidation above (Figure 4B). C. 100 µM bcd reacted with 1 mM butyryl-CoA at pH 7.5, as with the crotonyl-CoA reoxidized sample. The weak signal with linewidth measured at 16 Gauss (1.6 mT) represents only a small amount of $FAD•^-$ and correlates well with the absence of FADH• seen in the UV-VIS spectra (Figure 4A).

Finally, in an attempt to establish whether the long-wavelength absorbance seen during the reduction of bcd by butyryl-CoA was due to the neutral semiquinone or a charge-transfer complex, we reduced 100 µM of bcd with 1 mM butyryl-CoA (Figure 29C); there was no EPR evidence for FADH•, although a small amount of a signal with a linewidth of 16 Gauss, representative of a very small percentage of $FAD•^-$ (~2%) formed during the course of reduction by butyryl-CoA, was detected (Figure 29C). This indicated that the transient absorbance increases seen in Figures 27B and 28B were due to charge-transfer complexes and not neutral semiquinone.

6.4 Discussion

We saw transient accumulation of neutral flavin semiquinone in the course of reductive titrations of bcd with sodium dithionite, as reflected in the accumulation of long-wavelength absorbance at intermediate levels of reduction; as expected,

accumulation was greater at lower pH. Interestingly, some FADH• also accumulated in the course of reductive titrations with NADH in the presence of catalytic amounts of EtfAB, meaning that although the EtfAB was expected to be fully reduced under the reaction conditions and therefore capable of direct two-electron reduction of bcd to the fully reduced hydroquinone there was considerable one-electron transfer to the bcd. On the basis of the magnitude of the transient absorption increase at long wavelength seen in the course of the reaction (Figure 4C), the observed accumulation of FADH• was approximately 40% of the total enzyme flavin, and this undoubtedly underestimated the proportion of one-electron transfer occurring as some of the FADH• generated undoubtedly reduced on to the hydroquinone in a second one-electron event. In oxidative titrations with crotonyl-CoA and reductive titrations with butyryl-CoA, long-wavelength absorption again accumulated, although in both cases this was due to the formation of bcd_{red}:crotonyl-CoA and bcd_{ox}:butyryl-CoA complexes. Further, while significant (20%) flavin semiquinone accumulated, it is the anionic FAD•- rather than the neutral FADH• (see Figure 29B), as confirmed by EPR. Similarly, long-wavelength absorption accumulated in the course of titrations of reduced bcd with crotonyl-CoA, again due to formation of charge-transfer complexes, and again the semiquinone that accumulates is $FAD•^-$ rather than FADH•.

The observation of neutral FADH• in the absence of substrate/product and the anionic $FAD•^-$ in their presence indicated that their binding resulted in ionization of the semiquinone. Similar behavior had been observed with, e.g., trimethylamine dehydrogenase, where the anionic semiquinone was observed when the enzyme was

radiolytically reduced while the neutral form was formed after the enzyme was inactivated by ferricenium and subsequently reduced (106). In the case of bcd it had been reported that the binding of the substrate analog, acetoacetyl-CoA, resulted in a shift in the reduction potential of the enzyme by -100 mV of the free enzyme (52), illustrating the effect of substrate binding on the environment of the flavin.

The absence of anionic semiquinone accumulation in the stopped-flow experiment seen here (Figure 27B) contrasted with its significant accumulation in the course of the titration of reduced bcd with crotonyl-CoA (Figure 25B) deserves comment. Having confirmed that the observations in both the titration and stopped-flow experiments were fully reproducible, we performed two additional experiments. In a first, equal volumes of solutions of reduced bcd and crotonyl-CoA were mixed into an anaerobic cuvette, mimicking after a fashion the conditions of the stopped-flow experiment. No semiquinone, anionic or neutral, was observed and as in the stopped-flow experiment the reduced bcd was fully oxidized in a two-electron process (Appendix A3). That the long-wavelength absorbance seen transiently in the course of reoxidation was due to the bcd_{red}:crotonyl-CoA charge-transfer complex and not the neutral semiquinone, was confirmed by EPR (data not shown). In the second experiment, reduced bcd was mixed with varying small volumes of concentrated crotonyl-CoA in the stopped-flow apparatus, in a manner that mimicked additions in the course of the oxidative titration. As in the case to the titration experiment, significant amount of anionic semiquinone were indeed observed, as reflected in the transient increase in absorbance at ~380 nm and confirmed by EPR (Supplemental Figure 4). We concluded

that reoxidation of reduced bcd by crotonyl-CoA is normally a strict two-electron process, as expected and seen in the stopped-flow experiment, but that due to a mixing artifact when mixing bcd_{red} with small volumes of concentrated crotonyl-CoA some semiquinone did accumulate in the course of oxidative titrations. The above notwithstanding, it is unequivocal that under a variety of conditions when semiquinone did accumulate in the presence of crotonyl-CoA, it was the anionic rather than neutral semiquinone that was observed. The tendency of crotonyl-CoA binding to facilitate ionization of the flavin N5-H would facilitate oxidation of both FADH- and $FAD^{\bullet -}$ by crotonyl-CoA.

Electron transfer from pre-reduced EtfAB to oxidized bcd was slow, with an observed k_{red} of 2 s^{-1} that was independent of the concentration of bcd above 2 μM (Figure 26). That the rate constant was independent of [bcd] indicated that the EtfAB:bcd complex formed with a K_d smaller than 2 μM, and formed within the mixing dead time of the stopped-flow apparatus. The observed exponential behavior of the absorbance change, thus reflected the rate of intramolecular electron transfer. As discussed in Chapter 3.4, the domain containing the electron-transferring FAD of EtfAB lies with its flavin close to the bifurcating FAD in the absence of bcd, while in the intact complex the domain containing the electron-transferring FAD has swung around so that its flavin now lies in proximity to the flavin of bcd. It had been suggested that this motion served to gate electron transfer in the course of catalysis (14), and it may well limit the rate of electron transfer to bcd. We note that although a rate of 2 s^{-1} was significantly less than that of the reduction of EtfAB via NADH (k_{red} = 590 s^{-1}, Chapter 4.2) it was still

approximately an order of magnitude faster than the reported k_{cat} for ferredoxin reduction which is 0.29 s^{-1} (12). The spectral change associated with electron transfer bore the signature long-wavelength absorbance of FADH• (Figure 26C), indicating again a substantial amount of bcd reduction was a one-electron event. Sequential one-electron transfer events to bcd would serve to gate electron transfer so as to prevent low-potential reducing equivalents from progressing down the high-potential pathway (a strongly thermodynamically favorable process, but one that would short-circuit bifurcation). As been hypothesized (14), the enzyme complex during turnover was partially reduced in vivo, and the ability to clear electrons from the high-potential pathway and maintain a poised, partially reduced state, would aid in ensuring the fidelity of bifurcation. Likewise, if the EtfAB:bcd complex was to be completely and quickly reoxidized then the reducing equivalents generated from the reduction by NADH would proceed down the much more favorable high-potential pathway and again result in stopping bifurcation. This ensured that the enzyme complex can continue to facilitate turnover whenever ferredoxin was present and continue to engage in the reverse oxidation pathway. Although electrons could be transferred in pairs between FADs, this was not obligatory, as exemplified in simple ETFs that function physiologically in one-electron transfers between their physiological partners. In this way, the enzyme can also have a way to protect itself from newly generated reducing equivalents that could easily re-reduce the newly oxidized bcd.

The oxidation of reduced bcd by crotonyl-CoA occurred with an observed rate constant of 30 s^{-1} and was independent of [crotonyl-CoA] above 10 µM. The reaction

was monophasic at 450 nm, but at 600 nm there was clear evidence of the formation and decay of bcd_{red}:crotonyl-CoA and bcd_{ox}:butyryl-CoA charge-transfer complexes. While previously observed (82,51), the present work established that these complexes are kinetically competent to be catalytic intermediates. The reverse reaction, the reduction of bcd by butyryl-CoA, although thermodynamically unfavorable can be forced by mass action at high concentrations of butyryl-CoA, although reduction did not go to completion. The kinetics exhibited hyperbolic dependence on [butyryl-CoA], with an observed k_{red} of ~1400 s^{-1}. Again, the transients seen at 450 nm were monophasic but those at longer wavelengths indicated the formation of the same charge-transfer complexes as seen in the reverse (i.e., physiological) direction.

We noted that the structure of the bcd component in the *C. difficile* structure and the structure of the free bcd from the crystal structure of the *M. elsdenii* were virtually identical, as illustrated in Figure 30, with a rms deviation of C_α between the two structures of 0.585 Å. Given the lack of conformational changes in bcd on complex formation with EtfAB, we concluded that the observed kinetics of isolated bcd with crotonyl-CoA and butyryl-CoA were relevant to the complex as well.

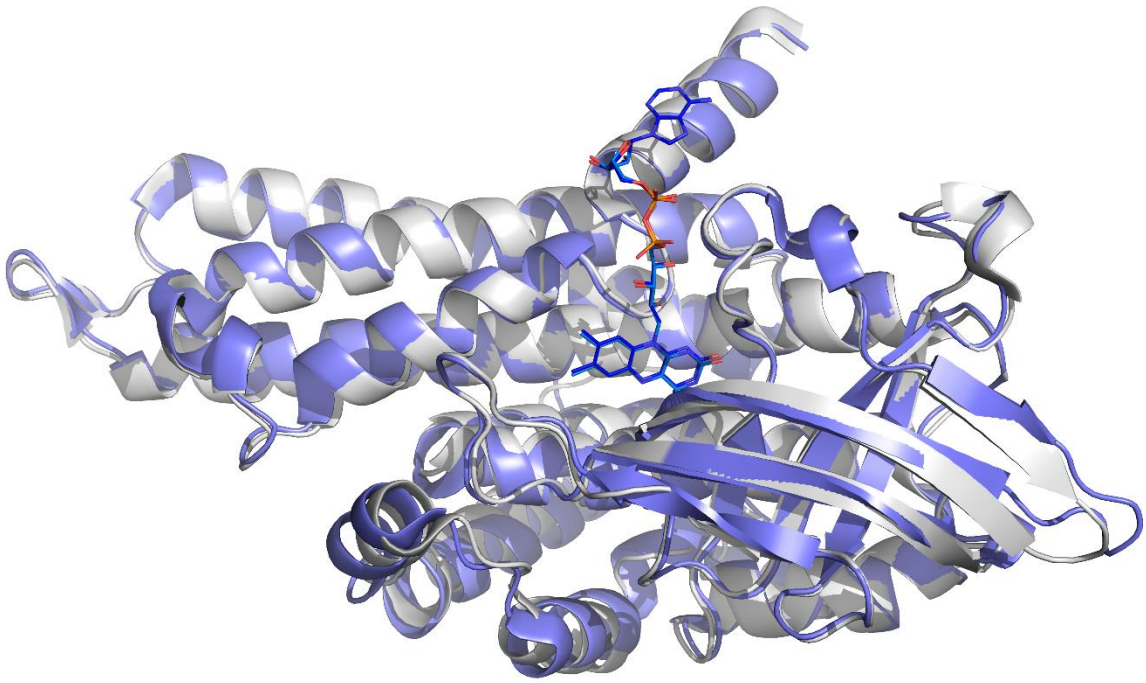

Figure 30. Alignment of the structures of EtfAB bound bcd and free bcd. Blue is the structure of the un-complexed bcd from *M. elsdenii* (PDB 1BUC) aligned with the bcd component from the *C. difficile* (PDB 5Ol2) structure.

Chapter 7

The steady-state reduction of ferredoxin

7.1 Steady-state reduction of ferredoxin

The steady-state rate of ferredoxin reduction by EtfAB:bcd has been reported by Chowdhury *et al.* as 0.29 s^{-1} at 25 ºC, using ferredoxin from *Clostridium tetanomorphum* (14). The reduction of ferredoxin was also stated to be ”tightly coupled” to the oxidation of NADH. To correlate the rate of ferredoxin reduction and overall bifurcation activity of EtfAB:bcd with the rapid-reaction kinetics discussed in the next chapter, the steady-state reaction of Chowdhury *et al.* was repeated with the [4Fe-4S] ferredoxin from *M. elsdenii*, with 15 µM of the [ferredoxin, 1 µM EtfAB:bcd, 250 µM NADH, and 50 µM crotonyl-CoA in 50 mM Tris-HCl, 150 mM NaCl, pH 7.5 at 25 ºC. As shown in Figure 31, the time course as monitored at 427 nm (Figure 31A) can be separated into two linear phases with different slopes after the addition of NADH (the large dip in absorbance at 5 – 10 s). The first extends to ~100 s and the second from 100 s to the end of the reaction (in this case approximately 290 s) when all the limiting ferredoxin has become reduced. k_{cat} was calculated using the following equation (eqn. 16):

$$k_{cat} = \frac{\Delta A_{427}}{\Delta \varepsilon_{427} \times [EtfAB]}$$

Where, ΔA_{427} was obtained by the slope of the fastest portion of the reaction (in this case the second phase) and $\Delta \varepsilon_{427}$ of 8.3 mM^{-1} cm^{-1} was used as determined by difference spectroscopy shown by Ortiz *et al.* (90). The k_{cat} with *M. elsdenii* ferredoxin as

calculated was 0.2 s^{-1}, which was in quite good agreement with the previously reported value. The spectrum after the addition of NADH at 20 s (black) and the end of reduction (blue) is shown in Figure 31B, with the difference spectrum (Figure 31B inset) representing the total ferredoxin reduced in the reaction and accounting for all the ferredoxin present, indicating complete reduction by EtfAB:bcd.

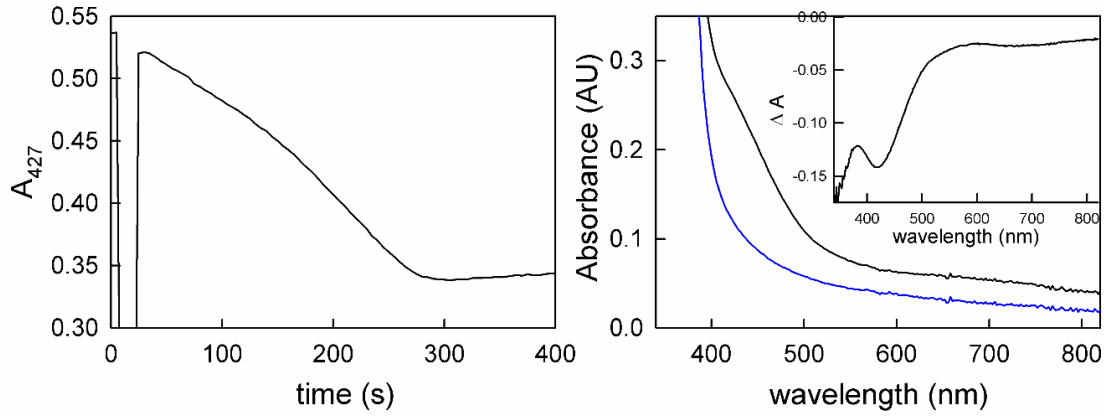

Figure 31. Steady-state ferredoxin reduction assay with NADH. A, the 427 nm transient of 15 µM *M. elsdenii* ferredoxin, 1 µM EtfAB:bcd and 50 µM crotonyl-CoA reacted with 250 µM NADH, k_{cat} = 0.2 s^{-1}. B, the spectra indicating the beginning of reaction after mixing (black) and the end of reduction (blue). Inset, the difference spectrum of blue *minus* black representing ~ 14 µM ferredoxin reduced. Reactions were performed in 50 mM Tris-HCl, 150 mM NaCl, pH 7.5 at 25 ºC.

7.2 Steady-state reduction with NADH analogues and deuterated buffer

As established in Chapter 5, the reaction of EtfAB with thioNADH and NADD resulted in a twofold decrease in rate of reduction. When NADH was substituted with either analog in the steady-state assay, however, no significant decrease in k_{cat} was observed This is shown in Figure 32 as reactions with the control (NADH), A (thioNADH), and B (NADD) had similar k_{cat}'s, 0.19 s^{-1}, 0.18 s^{-1}, 0.18 s^{-1}, respectively. This indicates that (as expected) reduction of the bf FAD is not rate-limiting to steady-state turnover. Next, assays were carried out in D_2O (50 mM Tris-DCl, 150 mM NaCl,

pH 7.5) to determine any solvent kinetic isotope effect on the steady-state reaction. As D_2O has a greater density than H_2O, a control condition containing proteated buffer in 40 % glycerol $\frac{v}{v}$ was also performed in order to exclude any viscosity effects on reduction (107-108). The D_2O (C) and 40 % glycerol (D) transients seen in Figure 32 were once again similar to the control, with k_{cat} values of 0.20 s^{-1}, 0.17 s^{-1}, respectively. In all permutations of the steady-state experiment, ferredoxin reduction occurred at the same rate within experimental error.

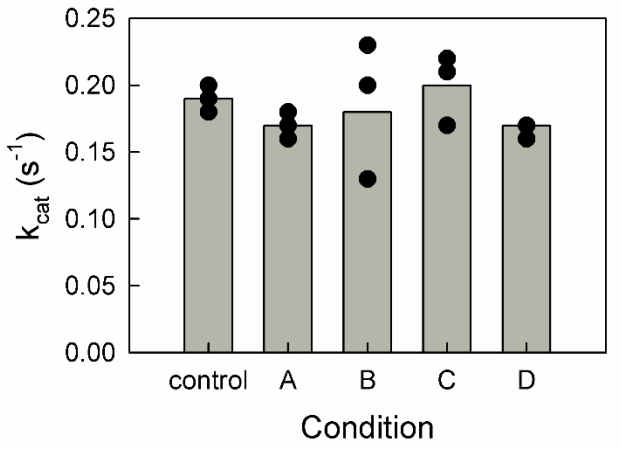

Figure 32. Steady-state assay permutations. All reaction were performed with 15 µM *M. elsdenii* ferredoxin, 1 µM EtfAB:bcd and 50 µM crotonyl-CoA. Control, standard assay with 250 µM NADH in Buffer A (50 mM Tris-HCl, 150 mM NaCl, pH 7.5), k_{cat} = 0.19 s^{-1}. A, standard reaction with 250 µM thioNADH, k_{cat} = 0.18 s^{-1}. B, standard reaction with 250 µM NADD, k_{cat} = 0.18 s^{-1}. C, standard reaction with NADH in Buffer A prepared with deuterium, k_{cat} = 0.20 s^{-1}. D, standard reaction with NADH in Buffer A in 40% glycerol, k_{cat} = 0.17 s^{-1}. Reactions were performed at 25 ºC.

7.3 Steady-state reduction of 2x[4Fe-4S] ferredoxin

All experiments presently have used ferredoxins possessing a single [4Fe-4S] cluster, including the *C. tetanomorphum* ferredoxin by Chowdhury *et al.* (14). These ferredoxins become completely reduced after a single bifurcation event , whereas a 2x[Fe-4S] ferredoxin with a pair of clusters require two successive bifurcation events in

order to fully reduce. We thus next performed the steady-state assay with 15 µM of the 2x[4Fe-4S] ferredoxin from *Pyrobaculum aerophilum* as shown in Figure 33. The 427 nm trace (Figure 33A) was indistinguishable from that of *M. elsdenii* (Figure 31A) and the k_{cat} of the reaction was similar at 0.16 s^{-1}. As in Figure 31B, Figure 33B shows oxidized ferredoxin (black) and reduced (blue), with the difference spectrum shown in the inset accounting for reduction of both clusters within the ferredoxin.

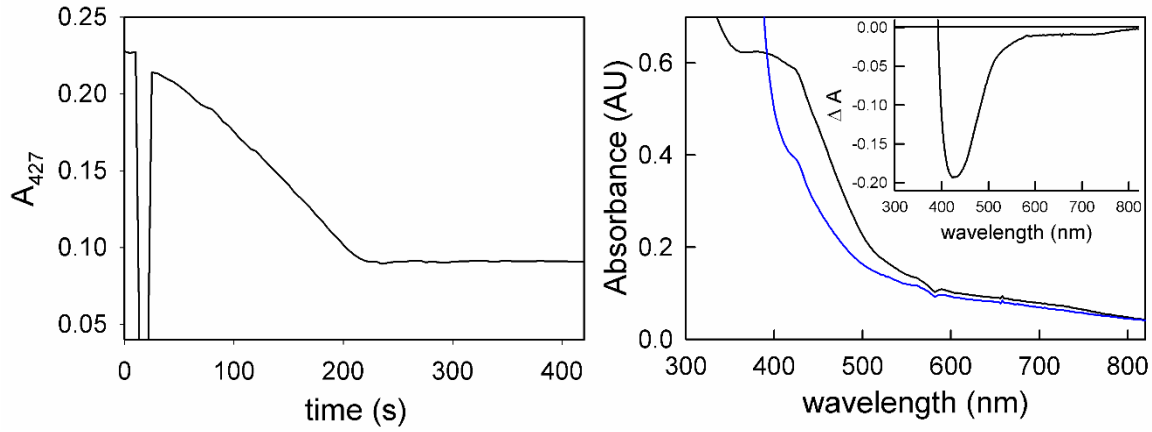

Figure 33. Steady-state assay of 2x[4Fe-4S] with NADH. A, the 427 nm transient of 15 µM *C. tetanomorphum* ferredoxin, 1 µM EtfAB:bcd and 50 µM crotonyl-CoA reacted with 250 µM NADH, k_{cat} = 0.16 s^{-1}. B, the spectra of oxidized ferredoxin (black) and the end of reduction at 210 s (blue). Inset, the difference spectrum of blue *minus* black representing ~ 14 µM ferredoxin reduced. Reactions were performed in 50 mM Tris-HCl, 150 mM NaCl, pH 7.5 at 25 ºC.

7.4 Discussion

We find that the rate of ferredoxin reduction by EtfAB:bcd is independent of the organism of origin, indicating that the binding of ferredoxin must be relatively generic. This is highlighted by the consensus in rate between the bacterial ferredoxins from *C. tetanomorphum* and *M. elsdenii* as well as the archaeal ferredoxin from *P. aerophilum*. It should be noted that the k_{cat} for ferredoxin reduction is orders of magnitude slower than the initial reduction of the bf FAD of EtfAB by NADH (k_{red} = 590 s^{-1}, Chapter 4.2), the electron transfer from EtfAB to bcd (k_{red} = 2 s^{-1} Chapter 6.2), and the oxidation of bcd by crotonyl-CoA (k_{red} = 30 s^{-1}, Chapter 6.2). We find that the slow rate of reduction is also independent of the rate of EtfAB reduction as determined by the thioNADH and NADD assays having no effect, and also note the lack of secondary isotope and viscosity effects on the rate of reduction as seen in the reaction in deuterium and 40% glycerol. This evidence supports the conclusion that the reduction of the bf FAD is not rate-limiting in the steady-state reaction.

As turnover with the EtfAB:bcd complex is more involved than just the oxidation of NADH, the intramolecular electron transfer steps involved in the coupled reaction must be heavily controlled. The rate of ferredoxin reduction remaining constant despite thermodynamic and kinetic perturbations to the reduction of EtfAB is evidence that the reduction of the bf FAD is not the controlling factor to the fidelity of bifurcation, which must be preserved through a kinetic mechanism of some sort since “tight coupling” of low- and high-potential acceptors is still observed despite the overwhelming favorability of transferring the low-potential bf $FAD^{\bullet -}$ electron into the high-potential pathway. This

sets up the investigation of ferredoxin reduction in the enzyme-monitored turnover experiments described in the next chapter.

Chapter 8

Rapid-reaction kinetics of the crotonyl-CoA-dependent NADH:ferredoxin oxidoreductase

The following work is a reprint of material published in "The Rapid-reaction Kinetics of an Electron-Bifurcating Flavoprotein. The crotonyl-CoA-dependent NADH:ferredoxin oxidoreductase", in submission. The co- author Derek Nguyen assisted with experiments and helped to write and prepare the manuscript.

8.1 The reduction of EtfAB:bcd with NADH

Reductive titration of the intact EtfAB:bcd complex (formed simply by mixing equimolar concentrations of the two separately expressed and purified recombinant components) with NADH was first performed. As shown in Figure 34A, both FADH• and $FAD^{\bullet -}$ did indeed appear transiently in the course of the titration, as reflected in the simultaneous transient absorption increases at ~570 and ~377 nm, respectively. The maxima centered around 570 nm and the ratio of the 377 nm and 450 nm minima in Figure 34A inset, implied the presence of both semiquinones at the end of titration as well. The observed accumulation of semiquinone seen with the EtfAB:bcd complex was consistent with the isolated EtfAB and bcd components (Chapters 4 and 6, respectively), and indicated that the half-potentials of a portion of the bf FAD again became uncrossed in the EtfAB:bcd_{2e-} state.

As shown in Chapter 4, the rapid-reaction kinetics for the reduction of isolated EtfAB by NADH yielded biphasic kinetics. The fast phase exhibited a spectral change

consistent with the initial rapid reaction of the bf FAD to the hydroquinone, with a hyperbolic dependence of the observed rate constant on [NADH], that yielded a limiting k_{red} of 590 s^{-1} and an apparent K_d of 30 μM. The inclusion of the bcd component to form the full complex did not significantly change the kinetics of the fast phase of the reaction, with an apparent k_{red} of 640 s^{-1} and apparent K_d of 43 μM (Figure 34B). This initial kinetic phase accounted for only approximately 1/3 of the total absorbance change (Figure 34B, inset), however, consistent with the initial reduction of only one of the three flavins present in the complex, the bf FAD. The remaining 2/3 of the absorbance change occurred on a much slower time scale, and reflected the transfer of reducing equivalents out of the bf FADH- to the et and bcd FADs, with an [NADH]-independent rate constant of 2 s^{-1} (Figure 34B inset). Figure 34C showed the spectra seen in the course of the reaction with the spectral changes associated with the two kinetic phases shown in the inset.

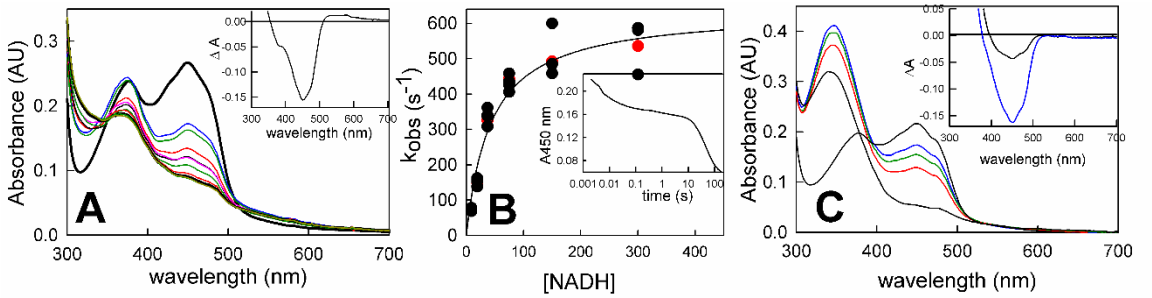

Figure 34. The reaction of oxidized EtfAB:bcd complex with NADH. Panel A, titration of 8 µM EtfAB:bcd with NADH, the spectrum in red represents the greatest accumulation of both anionic semiquinone and neutral semiquinone. Inset, difference spectrum between the oxidized and reduced showing the total absorbance change in the titration. Panel B, the rapid-reaction kinetics of 6.5 µM EtfAB:bcd with various concentrations of NADH: the apparent k_{red} is 640 s^{-1} and the apparent K_d is 43 µM. *Inset*, a representative transient at 37 µM NADH at 450 nm showing that the initial reduction of the bf FAD and the reduction of the complete system are separated temporally. Panel C, spectra seen in the course of the reaction of complex with 37 µM NADH, showing the eventual complete reduction of the system and the small accumulation and loss of anionic semiquinone demonstrated by the shift of the short wavelength maxima from 377 nm to 340 nm. Inset, difference spectra at 37 µM NADH, showing the separation of the reduction of the bf FAD (black) from the reduction of the other two flavins (blue). Both experiments were performed in 50 mM Tris HCl, 150 mM NaCl, pH 7.5. The titration was performed at 25 °C while the stopped flow experiments at 10 °C.

8.2 The reaction of fully reduced EtfAB:bcd with crotonyl-CoA

We next prepared the fully reduced EtfAB:bcd with sodium dithionite (yielding EtfAB:bcd_{6e}-) and titrated it with the high-potential acceptor crotonyl-CoA in the absence of the low-potential acceptor ferredoxin. As shown in Figure 35A, the observed spectral changes reflected a significant accumulation of anionic semiquinone in the course of the titration. This was due either to the et FAD or bcd FAD, as we have previously shown that the bcd semiquinone ionizes when a CoA substrate or analog binds (Chapter 6). It is noteworthy that the EtfAB:bcd complex was not fully reoxidized at the end of the titration even in the presence of excess crotonyl-CoA, as reflected in both the increase in absorbance at 377 nm during the course of titration and the ratio of absorption at 377 nm to 450 nm in the difference spectrum (compare Figure 35A to Figure 34A). This

incomplete reoxidation appeared to be a consequence of two things. First, the low-potential electron generated after the first electron transfer out of the bf $FADH^-$ in the course of reoxidation may leak only extremely slowly into the high-potential pathway to fully oxidize the bf FAD and allow reaction with a second (and eventually third) equivalent of crotonyl-CoA (a leakage that may indeed involve intermolecular rather than intramolecular electron transfer, which we have shown to occur on a tens of minutes time as seen in Chapter 4). Second, in the configuration in which the half-potentials of the bf FAD have become uncrossed, it may be that further reoxidation by crotonyl-CoA became unfavorable as the thermodynamics were no longer sufficient to process up the high-potential pathway.

Figure 35B showed the rapid reaction kinetics of reoxidation of dithionite-reduced EtfAB:bcd_{6e}- by crotonyl-CoA, which exhibited a [crotonyl-CoA]-independent rate constant of 30 s^{-1}, consistent with previous results using the isolated bcd, which yielded a similarly [crotonyl-CoA]-independent rate constant of 30 s^{-1} in Chapter 6. Since the reoxidation rate by crotonyl-CoA was constant at 30 s^{-1} at both stoichiometric and pseudo-first order concentrations, those are the ones that were shown (Figure 35B). Also consistent with previous results with the isolated bcd, in the presence of crotonyl-CoA, the semiquinone accumulating on the bcd FAD was the anionic rather than neutral form, the long-wavelength absorbance accumulating transiently being due to a charge-transfer complex rather than a neutral bcd semiquinone (Figure 35C inset). These complexes were between bcd_{ox}:butyryl-CoA and bcd_{red}:crotonyl-CoA.

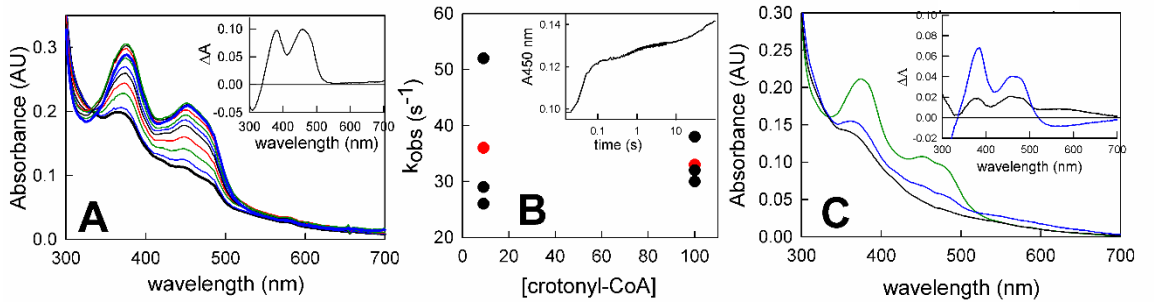

Figure 35. The reaction of fully reduced EtfAB:bcd with crotonyl-CoA. Panel A, oxidative titration of 11 µM reduced EtfAB:bcd in the absence of ferredoxin. There is an accumulation of anionic semiquinone throughout the titration. Inset, difference spectrum showing the total change throughout the titration. Panel B, rapid reaction kinetics of fully reduced EtfAB:bcd with crotonyl-CoA. The apparent k_{red} is ~ $30s^{-1}$ and there is no dependence on [crotonyl-CoA] as shown by the red points representing the average rates. Inset, transient showing the temporal separation between the reoxidation of the bcd FAD and the other FADs from EtfAB. Panel C, rapid reaction kinetics of 5 µM of pre-reduced EtfAB:bcd_{6e}- reacted with crotonyl-CoA: black, reduced EtfAB:bcd before reaction with crotonyl-CoA; blue, 0.2 seconds after mixing crotonyl-CoA; green, the endpoint of the reaction. Inset, difference spectra of the reaction: black, the difference spectrum of 0.2 seconds minus reduced; blue, the difference spectrum of 100 seconds minus 0.2 seconds. The absorbance at 377 nm is due to the anionic semiquinone while the long-wavelength absorbance is due to the charge-transfer complex of the reduced bcd and crotonyl-CoA. Both experiments were performed in 50 mM Tris HCl, 150 mM NaCl, pH 7.5. The titration was performed at 25 °C while the stopped flow experiments at 10 °C.

8.3 The reaction of EtfAB:bcd_{6e-} with crotonyl-CoA in the presence of ferredoxin

Significantly, when the equilibrium titration of EtfAB:bcd_{6e}- with crotonyl-CoA was repeated in the presence of excess ferredoxin (Figure 36A), more complete reoxidation was observed than in the absence of the low-potential acceptor (compare the relative ratio of the 377 and 450 nm peaks the oxidized-minus-reduced difference spectrum in Figure 36A inset to that in Figure 35A, and also the total absorbance changes at 450 nm in the presence and absence of the ferredoxin). With ferredoxin present, the bf $FAD•^{-}$ generated after a first (or second) successful bifurcation event occurring in the course of reoxidation reacted rapidly with the ferredoxin present, resulting in its full reoxidation.

The kinetics of the reoxidation of EtfAB:bcd_{6e-} by crotonyl-CoA were also affected by excess ferredoxin. Following the absorbance change at 427 nm to track the amount of ferredoxin that became reduced (Figure 36B, black transient), the magnitude of the absorbance change reflected the reduction of one equivalent of ferredoxin per EtfAB:bcd. Figure 36C showed the overall spectral changes for this reaction with two distinct phases. The first phase was an approach to ferredoxin reduction, and the second phase reflected ferredoxin reduction. The approach phase was the EtfAB:bcd_{6e-} complex oxidizing to reach some partially reduced state that was compatible with bifurcation. After two electron reoxidation of the bcd FAD with one equivalent of crotonyl-CoA, there existed an equilibrium between two states of the complex. One of these states having fully reduced bf and et FAD but oxidized bcd FAD, and the other with a fully reduced bf FAD, and the semiquinone on the et and bcd FADs (although semiquinone on the bcd FAD was not required), resulting from a single electron transfer from the two-electron reduced et FAD to bcd FAD. The complex bifurcated as soon as the semiquinone form was reached and reduced an equivalent of ferredoxin. Based on the amplitude at 377 nm, we can calculate that 15% of the complex was in this bifurcating state at any one time. In the absence of equilibrium, one would expect all of the protein to acquire this semiquinone state simultaneously, resulting in a much larger absorbance change at 377 nm than observed. The following phase of ferredoxin reduction is simply the rest of the protein achieving the bifurcating state and reducing ferredoxin, with no visible increase at 377 nm as it is overshadowed by the accumulation of reduced ferredoxin (Figure 36C inset, red). The 377 nm transient (Figure 36B, red) showed the

rapid accumulation of FAD•⁻ which must be due to both the uncrossing of the bf FAD as seen in the isolated EtfAB studies (Chapters 3 & 4) as well as the accumulation of the bifurcating state containing semiquinone. Since there was only a single turnover, no steady-state was achieved, and the rate of ferredoxin reduction can be determined by fitting the 427 nm transient with a single exponential giving a rate of ~0.4 s^{-1}.

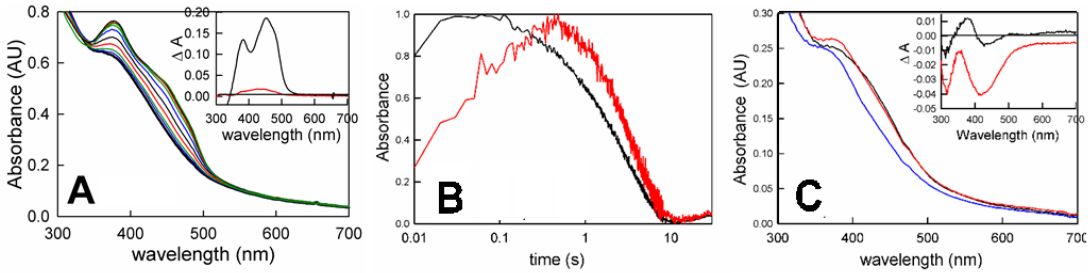

Figure 36. The reaction of fully reduced EtfAB:bcd with crotonyl-CoA in the presence of ferredoxin. Panel A, titration of 11 µM EtfAB:bcd with crotonyl-CoA in the presence of 20 µM ferredoxin: The black spectrum shows the fully reduced EtfAB:bcd alongside oxidized ferredoxin, and the light blue spectrum shows the fully oxidized EtfAB:bcd with excess crotonyl-CoA, and oxidized ferredoxin. Inset, difference spectra showing the total change throughout the titration (black) and the first addition of crotonyl-CoA (red). Panel B, rapid reaction transient at 427 nm (black) showing the extent of ferredoxin reduction and 377 nm (red) showing semiquinone accumulation when 15 µM ferredoxin is reacted with 4 µM prereduced EtfAB:bcd and 50 µM crotonyl-CoA. Panel C, the spectra of the rapid reaction of 4 µM reduced EtfAB:bcd reacted with 15 µM ferredoxin and 50 µM crotonyl-CoA, 0.01 s into the reaction (black), after 0.4 s (red), and after 12 s (blue). Inset, difference spectra showing the spectral changes associated with the approach to ferredoxin reduction (0.01 s – 0.4 s, black) and with ferredoxin reduction (0.4 s – 12 s, red). Experiments were performed in 50 mM Tris HCl, 150 mM NaCl, pH 7.5, 25 °C.

8.4 Enzyme-monitored turnover with EtfAB:bcd$_{ox}$

The steady-state kinetic behavior of EtfAB:bcd had been characterized in Chapter 7, but enzyme-monitored turnover experiments, in which spectral changes directly attributable to the enzyme complex were monitored in the course of reaction with all three substrates, were required to fully reconcile the rapid-reaction kinetics with catalytic turnover. As a preliminary to enzyme-monitored turnover studies, we first mixed

oxidized EtfAB:bcd, EtfAB:bcd$_{ox}$, with solutions containing both NADH and crotonyl-CoA but not ferredoxin, following the absorbance change at 427 nm (to mimic observations in ferredoxin-containing experiments). As shown in Figure 37A, continual flavin reduction throughout the course of the reaction was observed, as reflected in the transient at 427 nm (black transient). The enzyme-monitored turnover could be split into three phases. The initial fast phase contained mostly immediate reduction of the bf FAD by NADH as well as some electron transfer into the et FAD occurring in the first second of reaction. This is shown in the black transient in the inset of Figure 37A. Given the large excess of NADH used, the formation of anionic semiquinone, giving an absorbance increase at 377 nm (blue transient), in the first ~5 seconds of the reaction was largely obscured by the larger absorbance decreases associated with both the oxidation of NADH and reduction of the bf FAD during this portion of the reaction. A second phase occurred until about 10 seconds, consisting of reduction of the et FAD (Figure 37B inset, blue spectrum). On a much longer time scale of 10-50 seconds, however, FAD$^{\bullet-}$ did accumulate, as reflected by the absorbance increase at 377 nm in the green transient of Figure 37A and the positive 377 nm maxima in the green difference spectrum in the inset to Figure 37B. This was again a reflection of the uncrossing of the bf FAD half-potentials in a subset of the EtfAB:bcd population. The important implication is that the uncrossing of the bf FAD half-potentials previously observed with the isolated EtfAB is also seen in the EtfAB:bcd complex.

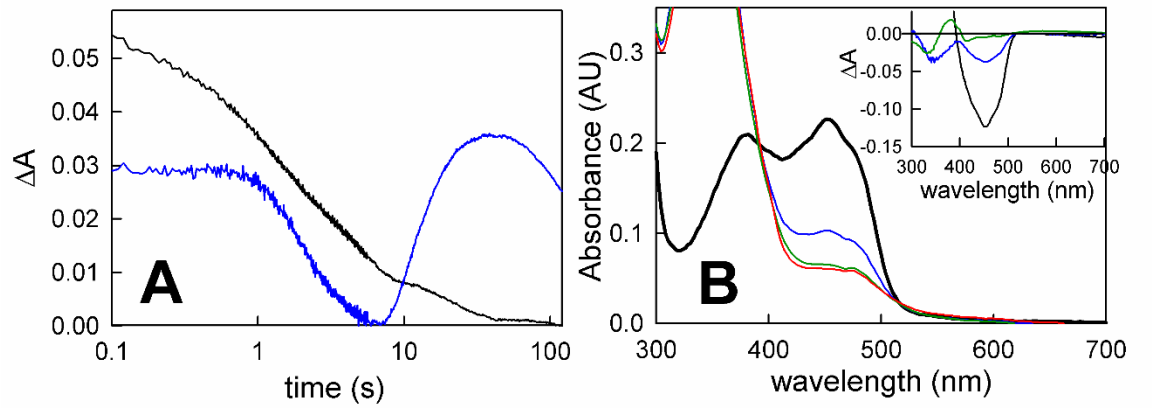

Figure 37. Crotonyl- to butyryl-CoA turnover with EtfAB:bcd$_{ox}$ and excess NADH. Panel A, the representative transients at 427 nm (black) and 377 nm (blue) of the reaction of 7 µM fully oxidized EtfAB:bcd complex with 90 µM NADH and 50 µM crotonyl-CoA shown to 120 s. Panel B, the spectra of the reaction of 7 µM oxidized EtfAB:bcd (black) with 90 µM NADH and 50 µM crotonyl-CoA at 120 seconds (red). Inset, the difference spectra showing 1 s – oxidized (black), 10 s – 1 s (blue), and 120 s - 10 s (green), negative features indicate loss while positive features represent accumulation. Experiments were performed in 50 mM Tris HCl, 150 mM NaCl, pH 7.5, 25 °C.

This was consistent with not only the titration behavior described above, but also the rapid-reaction kinetics of both the isolated reduction of EtfAB and the reoxidation of bcd as discussed in Chapters 4 & 6.

8.5 Enzyme-monitored turnover with EtfAB:bcd$_{1e^-}$

Figure 38 showed the same experiment as shown in Figure 37, but instead starting with the single electron reduced EtfAB:bcd. Utilizing the photosensitive nature of the et FAD, a semiquinone state can be imposed solely on that flavin as described in Chapter 2.9. The same phases seen in the oxidized enzyme-monitored turnover persisted in the single electron reduced complex, with an initial reduction of the bf FAD by NADH, followed by electron transfer to the subsequent FADs, and then accumulation of anionic semiquinone at longer timescales (Figure 38B inset). Again, the accumulation of

semiquinone was confirmed by the increase of absorbance at 377 nm seen in Figure 38A, albeit less so compared to the oxidized complex, as there was initial semiquinone. In both Figures 4B and 5B, the complexes equilibrated to a form with mostly hydroquinone and some semiquinone (red spectrum), demonstrating that there was some thermodynamic stability to the FAD•⁻ that accumulated at the end of reaction with excess reductant.

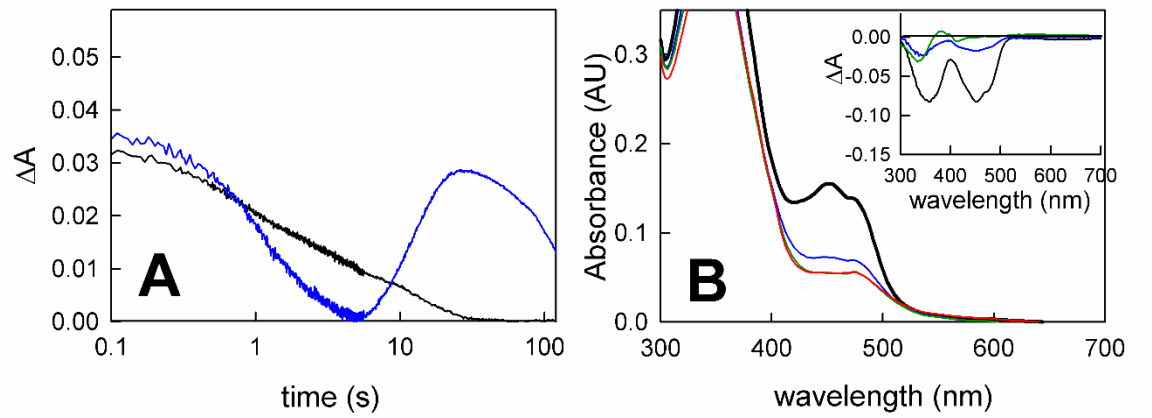

Figure 38. *Crotonyl- to butyryl-CoA turnover via excess NADH of EtfAB:bcd*$_{1e^-}$. Panel A, the representative transients at 427 nm (black) and 377 nm (blue) of the reaction of 7 µM one electron reduced EtfAB:bcd complex with 90 µM NADH and 50 µM crotonyl-CoA shown to 120 s. Panel B, the spectra of the reaction of 7 µM one electron reduced EtfAB:bcd (black) with 90 µM NADH and 50 µM crotonyl-CoA at 120 seconds (red). Inset, the difference spectra showing 1 s – oxidized (black), 10 s – 1 s (blue), and 120 s - 10 s (green), negative features indicate loss while positive features represent accumulation. Experiments were performed in 50 mM Tris HCl, 150 mM NaCl, pH 7.5, 25 °C.

For full enzyme-monitored turnover experiments, where ferredoxin was included as well as NADH and crotonyl-CoA, account must be taken of the absorbance change at 427 nm due to ferredoxin reduction ($\Delta\varepsilon$ of 7.3 mM^{-1} cm^{-1}). As shown in Figure 39, on

mixing oxidized EtfAB:bcd with a mixture of NADH, crotonyl-CoA and ferredoxin an approach to the steady-state occurred in an [EtfAB:bcd]-dependent manner over the first 10 - 20 seconds of the reaction. The spectral change associated with this approach to steady-state reflected flavin reduction to the hydroquinone which included reduction of the bf FAD, electron transfer to the et FAD and re-reduction, with characteristic negative features at 450 and 360 nm (Figure 39B, inset, black difference spectrum). There was no significant positive feature at 377 nm in this difference spectrum, as oxidation of NADH (shown as a minimum at ~350 nm) obscured any small absorbance changes that could represent $FAD^{\bullet -}$ accumulation. Importantly, no ferredoxin reduction was evident in this approach to the steady-state. The system entered a linear steady-state phase at ~10 sec that involved extensive ferredoxin reduction, as reflected in the spectral change associated with this phase having a broad minimum centered at ~405 nm (Figure 39B, inset, blue difference spectrum). There was no evidence of flavin contribution to this spectral change, indicating that the overall level of EtfAB:bcd reduction did not change significantly throughout the steady-state, particularly with regard to the level of $FAD^{\bullet -}$ (which would be manifested as a significant absorbance change in the 377 nm region in the blue difference spectrum, which was not observed). The rate of ferredoxin reduction in this steady-state phase was 0.2 s^{-1}, consistent with Chapter 7. The steady-state phase was followed by a final phase representing reduction of EtfAB:bcd by the excess NADH present upon depletion of the limiting ferredoxin in the reaction mix.

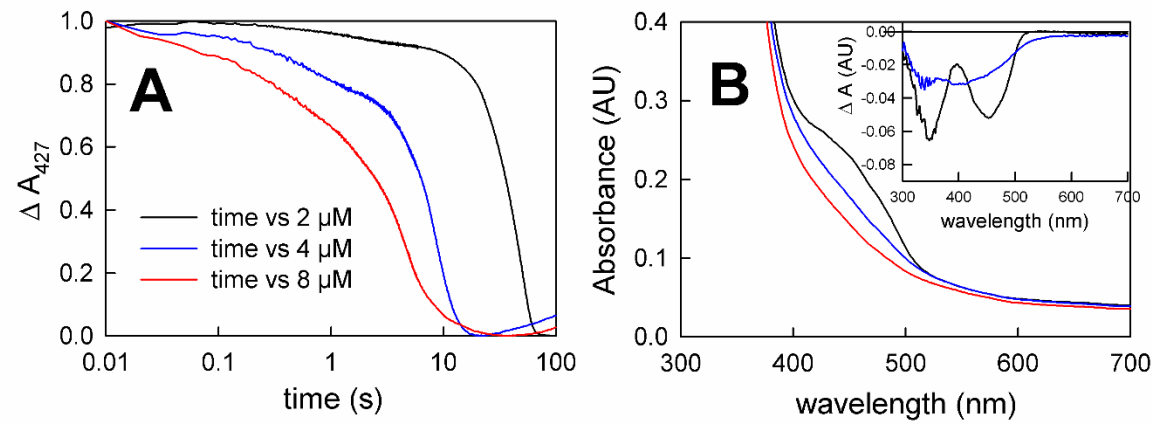

Figure 39. Enzyme monitored turnover of ferredoxin reduction with increasing $[EtfAB:bcd]_{ox}$. Panel A, transients at 427 nm normalize to 1, used to determine ferredoxin reduction at varying concentrations 2 µM (black), 4 µM (blue), and 8 µM (red) of EtfAB:bcd on reaction with a solution consisting of 90 µM NADH, 50 µM crotonyl-CoA, and 15 µM ferredoxin. The transients were normalized to the total absorbance change so that has a clearer separation between the approach and reduction phases at the lowest concentration of ferredoxin used. Panel B, the spectra of the 4µM EtfAB:bcd reaction indicating the endpoints of the distinct phases of reduction: the start being 0.01 s (black), end of flavin reduction 8 s (blue) and the end of ferredoxin reduction at 15 s (red). Inset, the difference spectra of 8 s – 0.01 s showing flavin reduction with 450 nm maxima and 15 s – 8 s showing predominately ferredoxin reduction with 420 nm maxima. Experiments were performed in 50 mM Tris HCl, 150 mM NaCl, pH 7.5, 25 °C.

We next examined the effect of changing the concentration of the high potential acceptor, crotonyl-CoA, on the kinetics of the enzyme-monitored turnover experiment. The reaction was again followed at 427 nm, using three different concentrations of 5, 50, and 150 µM crotonyl-CoA to mimic a range from stoichiometric to pseudo first-order excess relative to bcd. During the initial phase it should be noted that there were no distinguishable differences between the three concentrations as shown in Figure 40B as they were nearly identical when normalized to 1. As shown in Figure 40A, the higher concentrations of crotonyl-CoA (50 and 150 µM) exhibited comparable rates and amplitudes during the ferredoxin reduction phase of the reaction.

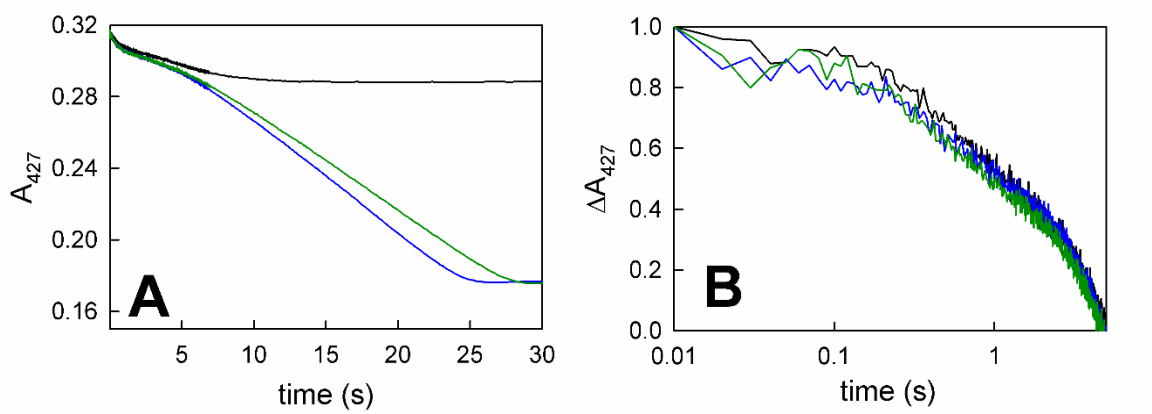

Figure 40. Enzyme monitored turnover varying crotonyl-CoA concentration. Panel A, kinetic transients of enzyme-monitored turnover experiments of 5 μM EtfAB:bcd, 15 μM ferredoxin, and 90 μM NADH reacted with crotonyl-CoA concentrations of 5, 50, 150 μM (black, blue, green, respectively) at 427 nm showing the full extent of reaction. Panel B, an expansion of the kinetic transients over the first five seconds of reaction, demonstrating that the approach to steady-state is essentially independent of [crotonyl-CoA]. Experiments were performed in 50 mM Tris HCl, 150 mM NaCl, pH 7.5, 25 °C.

At the low 5 μM concentration of crotonyl-CoA, on the other hand, a much smaller amplitude was observed due to the limiting, low crotonyl-CoA concentration. As a result, the amplitude change due to ferredoxin reduction was low and swamped by the larger spectral changes due to the flavins of EtfAB:bcd. On the other hand, the initial approach to steady-state was essentially independent of the crotonyl-CoA concentration, as shown in Figure 40B.

8.6 Enzyme-monitored turnover with ferredoxin and EtfAB:bcd$_{1e^-}$

It had been suggested that the et FAD operates principally if not exclusively through the SQ/HQ one-electron couple in shuttling high-potential electrons from the bf FAD to the bcd FAD. It was not straightforward to establish this as a requirement for bifurcation, however, as it was to be expected that the three-FAD system would become

partially reduced in the course of turnover in any case. To address the issue in the case of EtfAB:bcd, we have repeated the enzyme-monitored turnover experiment with EtfAB:bcd$_{1e}$-, where the single reducing equivalent resided predominantly on the et FAD$^{\bullet-}$. Reduction of the et FAD was accomplished by taking advantage of its uniquely photoactive nature, following its photoreduction spectrophotometrically. The et FAD$^{\bullet-}$ thus generated was stable and the electron did not transfer to the oxidized bcd FAD when the EtfAB$_{1e}$- was mixed with bcd (data not shown), so the photoreduced EtfAB and bcd could be precomplexed without difficulty. Figure 41A showed that the approach to steady-state phase when EtfAB:bcd$_{1e-}$ is mixed with all three substrates was shortened by roughly five-fold compared to that seen with the fully oxidized complex, while the steady-state involving ferredoxin reduction remained essentially unchanged, at 0.3 s^{-1}. The shortening of the approach to steady-state phase supported the hypothesis that the EtfAB:bcd must achieve some partially reduced state before reducing ferredoxin, and the et FAD$^{\bullet-}$ was either part of the primed state or allowed the system to be primed more easily. The spectral change associated with this approach to steady-state phase was changed as well, instead of an accumulation of anionic semiquinone (seen when starting with oxidized EtfAB:bcd), the difference spectrum reflects reduction of oxidized flavin to the hydroquinone state (Figure 41B inset, black difference spectrum). The absence of semiquinone accumulation in the approach to steady-state seemed to show that the et FAD$^{\bullet-}$ was indeed the preferred SQ/HQ couple when the protein was turning over. Also, the apparent inability of the electron on the et FAD$^{\bullet-}$ to transfer to the bcd supports the notion that the et FAD operates between the SQ/HQ couple.

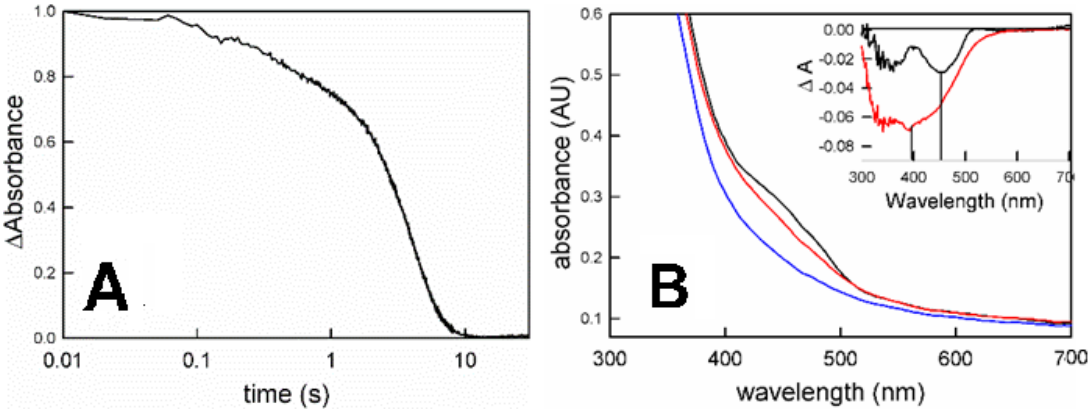

Figure 41. Enzyme-monitored turnover with EtfAB:bcd$_{1e}$-. Panel A, Transient at 427 nm normalized to 1 of the reaction of 4 µM EtfAB:bcd$_{1e}$- with 14 µM ferredoxin, 50 µM crotonyl-CoA, and 120 µM NADH used to monitor ferredoxin reduction. Panel B, spectral changes showing the break points of the different phases of the reaction: the start being 0.01 s (black), the end of flavin reduction being 1.3 s (red), and the end of ferredoxin reduction being 15 s (blue). *Inset*, difference spectra showing the extent of flavin reduction (black, 0.01 s – 1.3 s) with a minimum of 450 nm, and ferredoxin reduction (red, 1.3 s – 15 s) with a minimum of ~400 nm. Experiments were performed in 50 mM Tris HCl, 150 mM NaCl, pH 7.5, 25 °C.

8.7 Enzyme monitored turnover with ferredoxin and post-catalytic EtfAB:bcd

With the above results in mind, we were interested to know whether EtfAB:bcd that had previously undergone turnover behaved differently than the fully oxidized complex. The experiment involved reaction of EtfAB:bcd (5 µM) that had been previously exposed to excess NADH (90µM) and limiting crotonyl-CoA (50 µM), but not ferredoxin so as to generate complex that is predominately fully-reduced, but containing a small amount of anionic semiquinone (as seen in Figure 37B). When reacting this post-catalytic EtfAB:bcd with ferredoxin (15 µM), as well as more NADH (90 µM) and crotonyl-CoA (50 µM), the approach to steady-state in the enzyme-monitored turnover experiment was significantly shorter than seen with fully oxidized EtfAB:bcd.

Furthermore, the spectral change associated with this phase of the reaction was no longer predominately flavin reduction without any ferredoxin reduction (seen in Figures 39, 40, & 41), but now included a significant contribution due to ferredoxin reduction (Figure 42B inset) before the onset of linear steady-state of ferredoxin reduction. The steady-state phase remained solely due to ferredoxin reduction, as before, and the same k_{cat} was observed, 0.2 s^{-1}. This was significant as it indicates that reduction of ferredoxin depended on the overall level of reduction of the entire complex, including the bf FAD as well as the et FAD.

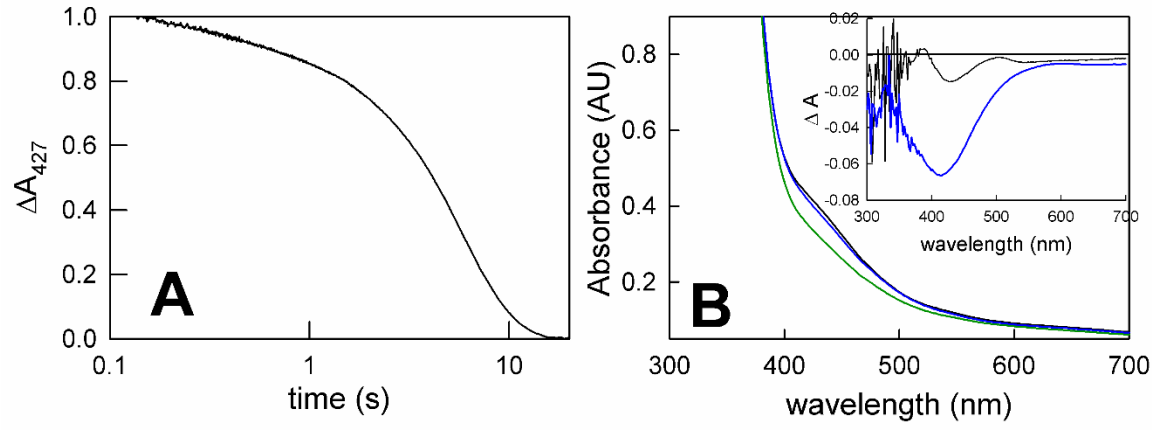

Figure 42. Enzyme monitored turnover with post-catalytic EtfAB:bcd. Panel A, kinetic transient at 427 nm normalized to 1 of EtfAB:bcd already reacted with 90 µM NADH and 50 µM crotonyl-CoA subsequently reacted with 15 µM ferredoxin, 90 µM NADH, and 50 µM crotonyl-CoA. Panel B, starting spectrum of 0.01 s (black), end of the approach phase 1 s (blue) and the end of ferredoxin reduction at 7 s (green). Inset, the difference spectra of 1 s – 0.01 s (black) and 7 s – 1 s (blue), showing reduced ferredoxin and a small amount of semiquinone formation as well as pure ferredoxin reduction, respectively. Experiments were performed in 50 mM Tris HCl, 150 mM NaCl, pH 7.5, 25 °C.

The above experiments were performed with a stoichiometric excess of ferredoxin to EtfAB:bcd (typically 3-fold) in order to ensure that binding of the oxidized ferredoxin to EtfAB:bcd was not an issue in the rate of reduction. Reacting the post-catalytic

complex with a stoichiometric amount of ferredoxin allowed for the monitoring of a single turnover. The greatest difference observed was that absent a pronounced lag, ferredoxin reduction (Figure 43A, black transient) became essentially exponential, with a rate constant of 1.8 s^{-1} (Figure 43A, red transient). This was comparable to the observed rate constant for electron transfer between the et FAD of EtfAB and the bcd FAD within the EtfAB:bcd complex, as seen in Chapter 6. The resulting absorbance changes showed ferredoxin reduction occurring concomitantly with formation of anionic semiquinone, as reflected in the negative feature at 420 nm and positive feature at 377 nm in the difference spectrum for the reaction, respectively (Figure 43B, inset).

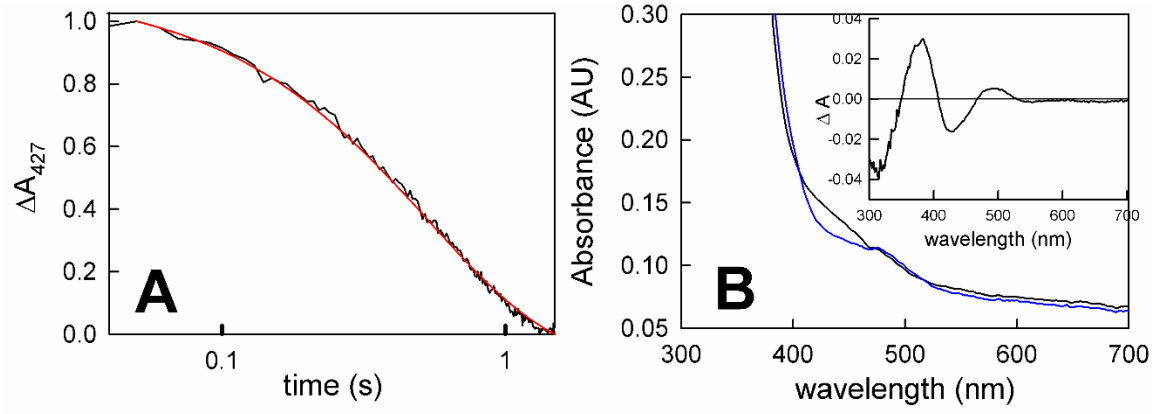

Figure 43. Stoichiometric reduction of ferredoxin with post-catalytic EtfAB:bcd. Panel A, the 427 nm transient normalized to 1 showing the 427 nm transient indicative of ferredoxin reduction (black) and the overlayed exponential fit of 1.8 s^{-1} (red) of 5 µM EtfAB:bcd pre-reacted with 90 µM NADH and 50 µM crotonyl-CoA and subsequently reacted with 5 µM ferredoxin, 90 µM NADH, and 50 µM crotonyl-CoA. . Panel B, spectra showing the start of the reaction of 0.01 s (black) and end of the reduction of ferredoxin 1.5 s (blue). Inset, the difference spectrum of 1.5 s – 0.01 s (black) showing reduced ferredoxin and an appreciable amount of semiquinone formation as shown by the negative 420 nm and the 377 nm absorbance peaks, respectively. Experiments were performed in 50 mM Tris HCl, 150 mM NaCl, pH 7.5, 25 °C.

8.8 Discussion

The present work demonstrated that the intact EtfAB:bcd complex exhibited similar kinetic behavior and oxidation-reduction properties as the isolated EtfAB and bcd components investigated in Chapters 4 & 6 of this dissertation. Starting with the reductive half-reaction, both anionic and neutral semiquinone accumulated transiently in the course of reductive titrations of EtfAB:bcd with NADH in the absence of ferredoxin (Figure 34). From the work with the isolated systems, we know that the anionic $FAD•^-$ is due to the et FAD of EtfAB (and probably also to the bf FAD, to the extent that its half-potentials have become uncrossed) and the neutral FADH• of the bcd FAD. Full reduction was not achieved at the end of the titration, with a small amount of $FAD•^-$ and FADH• persisting even in the presence of excess NADH. This was likely due to the uncrossing of half-potentials for the bf FAD in a fraction of the complex, as seen in the isolated EtfAB (Chapter 4). This uncrossing appeared to be a conserved property of EtfABs, being exhibited by EtfAB's from both bacteria (*M. elsdenii*) and archaea (*P. aerophilum)* (97). This uncrossing also occurred with the intact complex, as confirmed by EPR, showing the rapid accumulation of anionic $FAD•^-$ (Appendix A4), which can only be due to the uncrossing of the bf FAD, as electrons cannot move to the bcd FAD that quickly. The limiting k_{red} for the initial reduction of the bf FAD by NADH within the EtfAB:bcd complex complexed was 640 s^{-1}, in reasonable agreement with the 590 s^{-1} seen with the isolated *M. elsdenii* EtfAB (Chapter 4.2). The reduction of the bf FAD was followed by the much slower subsequent reduction of the et FAD and bcd FADs, with an [NADH]-independent rate constant of 2 s^{-1}. In the reduction of EtfAB, reduction of the

bf FAD accounted for approximately half of the absorbance change, while with the EtfAB:bcd complex, this was reduced to one third, as expected given the presence of the bcd FAD in the complex. This slower phase of reduction was similar in rate with both the isolated EtfAB and EtfAB:bcd complex, at 2 s^{-1} (Chapter 6.2).

For the oxidative half-reaction, the reaction of fully reduced EtfAB:bcd_{6e-} with crotonyl-CoA, just as in the reoxidation of isolated bcd, resulted in the rapid formation and decay of long-wavelength absorbing charge-transfer complexes consisting of reduced bcd:crotonyl-CoA and oxidized bcd:butyryl-CoA. In contrast to the reaction with isolated bcd, however, reaction of the EtfAB:bcd complex with crotonyl-CoA did not result in its full re-oxidation, even with an excess of crotonyl-CoA. Notably, a significant amount of $FAD•^-$ persisted at the end of reaction in both equilibrium titration and rapid reaction experiments, as reflected in the residual absorbance at 377 nm (Figure 35). The rate constant for the fast phase of the reaction, reflecting the reoxidation of the bcd $FADH^-$ within the fully reduced complex, was essentially identical to that seen with isolated bcd, with a [crotonyl-CoA]-independent k_{ox} of 30 s^{-1}. With the complex, however, a subsequent slow phase was observed, which necessarily involved the slow and rate-limiting electron transfer out of the EtfAB component of the complex to the bcd with a rate constant of 2 s^{-1} (followed by the more rapid reoxidation of the now re-reduced bcd component of the complex). This electron transfer was incomplete due to the difficulty of reoxidation of the bf FAD in the absence of the low-potential acceptor ferredoxin, and at least a portion of the complex appeared trapped in a configuration in which the bf FAD's half-potentials had become uncrossed and the reducing equivalents in

the resulting bf FAD•⁻ and et FAD•⁻ were unable to transfer to the bcd FAD, presumably due to unfavorable thermodynamics. In the presence of ferredoxin, on the other hand, the equilibrium titration of reduced EtfAB:bcd with crotonyl-CoA resulted in more complete reoxidation (compare Figure 36A to Figure 35A), as the presence of ferredoxin allowed effective bifurcation and full reoxidation of the bf FAD. On the other hand, the persistence of absorption in the 377 nm region at the end of the titration with crotonyl-CoA suggested that the et FAD remained partially reduced as the FAD•⁻ at the end of the titration, even in the presence of ferredoxin.

Working with the intact complex allowed investigation of the key aspect of electron bifurcation, the reduction of the low-potential ferredoxin. The steady-state rate of reduction of ferredoxin by EtfAB:bcd reported in Chapter 7 at 0.2 s^{-1}, was much slower than either the initial reduction of the bf FAD by NADH or the reoxidation of the reduced bcd FAD by crotonyl-CoA in rapid-reaction kinetic experiments with both the isolated EtfAB and bcd components, and the intact EtfAB:bcd complex, as demonstrated here (Figures 1B and 2B). Using an enzyme-monitored turnover approach, we found two distinct phases in the course of the reaction of enzyme with all three substrates under multiple-turnover conditions. The first phase was an approach to a steady-state that occurred on a comparable time scale to the 2 s^{-1} process involving electron transfer from the bf FAD to the et FAD within EtfAB. There was no ferredoxin reduction in this phase of the reaction. The second phase of the enzyme-monitored turnover experiment represented a brief steady-state in which EtfAB:bcd turned over all three substrates until the limiting substrate (ferredoxin) was consumed, with little change in the steady-state

levels of flavin reduction in the complex but abundant reduction of ferredoxin (and presumably also oxidation of crotonyl-CoA to butyryl-CoA) at rates consistent with the previous published steady-state parameters (Figure 39). Oxidation of the low-potential bf FAD•– formed upon electron bifurcation by the ferredoxin present permitted the very rapid re-reduction of the now fully reoxidized bf FAD by another equivalent of NADH. Bifurcation appeared to be rate-limited by the initial slow transfer of the first, high-potential electron from the bf FADH-, once reduced by NADH, to the et FAD, meaning that the bf FAD was expected to be predominantly reduced throughout the steady-state. Consistent with rate-limiting electron transfer out of the bf FAD, varying the concentration of the high-potential acceptor crotonyl-CoA in these enzyme-monitored turnover experiments had little to no effect on the observed kinetics (Figure 40). Importantly, when EtfAB:bcd6e- was reacted with crotonyl-CoA in the presence of ferredoxin (Figure 36), the rate of ferredoxin reduction remains unaltered in the absence of NADH, demonstrating that NADH and crotonyl-CoA need not bind simultaneously to the complex for effective bifurcation and reduction of ferredoxin.

In a single-turnover experiment with fully reduced EtfAB:bcd_{6e-} and one equivalent of ferredoxin, reduction of the low-potential acceptor occurred exponentially with a rate constant of 0.4 s^{-1} (Figure 36). Although the initial phase persists in the observed kinetics, the spectral changes were significantly altered compared to the experiment with fully oxidized EtfAB:bcd and reflect a significant accumulation of FAD•$^{-}$ in the course of the reaction. The duration of this initial phase was also significantly shortened with the reduced complex, indicating that there was some partially

reduced state that the complex needed to achieve before ferredoxin reduction can begin. That this is the case was also demonstrated in enzyme monitored experiments with pre-reduced complex, either photoreduced to EtfAB:bcd_{1e-} (Figure 41) or previously exposed to NADH and crotonyl-CoA (Figure 42), in which the approach to steady-state phase of the reaction was either significantly reduced or eliminated, with the onset of ferredoxin reduction occurring much earlier in the course of the reaction. In the case of the photoreduced EtfAB:bcd_{1e-}, while the length of the approach to steady-state phase and the onset of ferredoxin reduction was significantly reduced compared to oxidized protein, it was still longer than when starting with the fully reduced complex. This means that the et $FAD^{\bullet -}$ was necessary but not sufficient for bifurcation. Also, when photoreduced $EtfAB_{1e-}$ containing et $FAD^{\bullet -}$ was mixed with oxidized bcd FAD, no electron transfer was observed, which also supports the hypothesis that the et FAD operates between the SQ/HQ couples in transferring electrons to the bcd FAD. When post-catalytic complex was used in the enzyme-monitored turnover experiment, the approach to steady-state phase was significantly shorter in duration and, significantly, the onset of ferredoxin reduction was immediate. The spectral change associated with this approach to steady-state phase was in fact mainly due to ferredoxin reduction, although features due to anionic semiquinone were also present in the difference spectrum (Figure 42B and 43B). It was clear that this post-catalysis form of the complex was "primed" for effective bifurcation and ferredoxin reduction.

In considering the structural basis for the slow electron transfer from the bf FAD to the et FAD, it was known that while the structure of the bcd does not change

significantly on binding to EtfAB, the domain possessing the et FAD of EtfAB undergoes a significant reorientation relative to the remainder of the protein, amounting to a ~80° rotation. It was not clear at this point whether this domain simply "clicked" between the two crystallographically observed orientations or instead continuously swung between them with multiple intermediate orientations populated to a significant degree in solution. This same motion has been implicated in the uncrossing of the bf FAD half-potentials, although this has not been proven.

Chapter 9

Conclusions

9.1 Introduction

The constituent flavoproteins of the crotonyl-CoA-dependent NADH:ferredoxin oxidoreductase from *Megasphaera elsdenii* (EtfAB and bcd) have been extensively studied for their role in butyrate synthesis in the bovine and ovine rumen, with EtfAB being implicated as involved in H_2 gas production as early as the 1960s, well before the discovery of flavin-based electron bifurcation (42-46, 48-53). This organism conserves energy by coupling endergonic reduction of ferredoxin to exergonic reduction of crotonyl-CoA (12-13). Although the thermodynamics were well understood, the kinetics of the reaction, including the discrete steps of electron transfer were not. A kinetic manifestation of bifurcation must be integral to its function as, *a priori,* electron transfer into the high-potential pathway would be preferred thus disfavoring bifurcation. The present work has focused on kinetics of the discrete steps of electron transfer in the complex and their role in preserving bifurcation activity. The modular nature of the EtfAB:bcd complex proved pivotal in assessing the redox behavior of each component as well as the kinetics of reaction. In Chapter 3, we have identified and deconvoluted the spectral contributions of the three discrete oxidized FADs and the one-electron reduced semiquinones of the et FAD ($FAD^{\bullet -}$) and bcd FAD ($FADH^{\bullet}$).

9.2 Successful deconvolution of the spectral contributions of each FAD discovers uncrossing of the bf FAD's half-potentials

As described in Chapter 2, both proteins were separately expressed making it possible to assign the oxidized and reduced forms of the bcd FAD including its transient accumulation of FADH•. The assignment of the spectral contributions of FAD in EtfAB were simplified using a method described in Chapter 2 in which the et FAD was readily removed after incubation in KBr leaving a form of EtfAB depleted of its et FAD modified from Sato *et al* (49). Difference spectra between the replete (both bf FAD and et FAD) and depleted (bf FAD) forms allowed us to assign features of the et FAD that are distinct from the other two FADs in the system as the oxidized et FAD exhibited a significant red shift of the absorption envelope typically centered around 360 nm to now around 410 nm. Titration of the replete enzyme with both NADH (an obligate two-electron donor) and sodium dithionite ($SO_2^{\bullet-}$, a one-electron donor) gave rise to the et $FAD^{\bullet-}$ as confirmed by photoreduction described in Chapter 2. Lastly, the reduced EtfAB did not form charge-transfer complex with NAD^+ which was not unexpected.

Next, we have identified that upon removal of the et FAD from EtfAB the remaining bf FAD's half-potentials become uncrossed. As identified by the near quantitative accumulation of $FAD^{\bullet-}$ during reductive titrations with sodium dithionite. This uncrossing is significant, as the second electron leaving the reduced FAD (SQ/Q) can no longer reduce ferredoxin and is non-bifurcating.

9.3 Kinetics of the RHR are multiphasic and uncrossing of the bf FAD's half-potentials occurs during turnover

Before investigating the kinetics of reduction by NADH, we performed equilibrium titrations with both NADH and sodium dithionite to determine the characteristics of reduction in both forms of EtfAB. What we found, in contrast to the transient accumulation of $FAD^{\bullet -}$ during titration with sodium dithionite when reduced with NADH no accumulation $FAD^{\bullet -}$ was observed. This was expected as there was no path of egress for electrons in the depleted enzyme and although the half-potentials were uncrossed the midpoint potential of the bf FAD was still sufficiently high that NADH still fully reduced the enzyme. During reductive titrations with both NADH and sodium dithionite of the replete enzyme transient accumulation of $FAD^{\bullet -}$ was observed as expected. With a firm understanding of behavior of reduction in both forms of the enzyme stopped-flow experiments were then performed.

The reduction by NADH for both forms of the enzyme was by far the fastest reaction of the complex with limiting k_{red} of 590 s^{-1} and 1600 s^{-1} and K_d of 30 μM and 96 μM for the replete and depleted forms of the enzyme, respectively. When stoichiometric amounts of NADH were reacted with replete EtfAB we noticed accumulation of $FAD^{\bullet -}$ within 100 ms. This represented an uncrossing of the bf FAD's potential that occurred during catalysis and not just when the enzyme was depleted. The extent of uncrossing (20 %) as verified by EPR represents $FAD^{\bullet -}$ accumulation on both bf FAD and et FAD as the intermolecular electron transfer of the enzyme occurred on the hundreds of seconds time-scale. The kinetic transients of the reaction with excess [NADH] revealed a

multiphasic reaction where the first being 50% of the total amplitude change occurring in the first 20 ms as the bf FAD is reduced by NADH. The second phase extending to approximately 1 s represented the slow electron transfer to the et FAD and accumulation of bf and et FAD•⁻. The full reduction of the enzyme occurs after 100 s and makes up the final phase illustrating slow et of the low-potential electron into the high-potential pathway. When the reaction was repeated with both thioNADH and 4-R NADD we did observe a two-fold decrease in the k_{red}, but the intermediate phase remained unperturbed despite thermodynamic and kinetic effects on the reduction of the bf FAD, again confirming the [reductant] independence of electron transfer to the high-potential pathway.

9.4 Characterization of OHR kinetics reveals tight binding of complex formation and evidence for one-electron transfer in the high-potential pathway

As with the isolated EtfAB component, reductive titrations of bcd were performed. What we observed was transient accumulation of FADH• and full reduction with both sodium dithionite and NADH (using catalytic amounts of EtfAB). Reductive and oxidative titrations with the physiological substrates (butyryl- and crotonyl-CoA) yielded incomplete reaction and resulted in the change in ionization of FADH• to FAD•⁻.

Rapid-reaction kinetics revealed a [crotonyl-CoA] independent rate of reoxidation of reduced bcd of 30 s^{-1}, nearly one-twentieth the rate of EtfAB reduction but still orders of magnitude faster than the rate of ferredoxin reduction. Oxidized bcd reacted with

four-electron reduced EtfAB revealed the nature and intramolecular rate of electron transfer from EtfAB to bcd, being predominately one-electron and occurring at 2 s^{-1}. Interestingly, the rate of reduction was also concentration independent of either [EtfAB] or [EtfAB:bcd] implying rapid complex formation (with a functional K_d as low as 2 μM). The slow rate of electron transfer despite tight binding of the complex served as a reasonable rate-limiting step as the domain motion of the α subunit could throttle the flow of electrons into the high-potential pathway.

9.5 Steady-state reduction of ferredoxin remain indiscriminate of thermodynamic and kinetic effects to turnover of EtfAB:bcd

The steady-state reduction of ferredoxin by EtfAB:bcd in our hands was consistent regardless of ferredoxin type, organism of origin, or midpoint electron donor. With a k_{cat} of 0.2 s^{-1}, observed rate of ferredoxin reduction was orders of magnitude slower than the reduction of EtfAB, reoxidation of bcd, and reduction of bcd. With both thioNADH and 4-R NADD we observed similar rates of ferredoxin reduction similar to NADH. Demonstrating the rate of bifurcation was not influenced by the rate or extent of reduction of the bf FAD and rather preserved through other means.

9.6 The reductive properties of the isolated components remain relatively unchanged when complexed while oxidative differences were observed

The observed kinetics of EtfAB:bcd reduction by NADH comported well with the isolated EtfAB, with a limiting k_{red} of 640 s^{-1} and accumulation of $FAD^{\bullet -}$ observed during the first 100 ms of the reaction indicating uncrossing in the intact complex.

Reduction to the six-electron reduced EtfAB:bcd (EtfAB:bcd$_{6e}^-$) occurred after 200 s which was reflective of the slow rate of electron transfer into the high-potential pathway. The fast phase of reoxidation in EtfAB:bcd$_{6e}^-$ was again [crotonyl-CoA] independent with a rate of 30 s^{-1}. In contrast to the isolated bcd experiment, full reoxidation did not occur and instead accumulation of both et and bcd FAD•$^-$ was observed. Most likely a result of uncrossing of the bf FAD leaving only bf and et FAD•$^-$ that are unable to transfer to the bcd FAD due to unfavorable thermodynamics. Resulting in limited egress into the high-potential pathway.

9.7 Enzyme monitored turnover of the intact complex in the absence and presence of ferredoxin provided insight into the preservation of bifurcation

Surprisingly, when EtfAB:bcd was reacted with excess NADH and limiting crotonyl-CoA in an enzyme monitored turnover experiment, full reduction was not observed as the accumulation of FAD•$^-$ persisted even after 120 s. Although this did differ from the reaction with NADH, it aligned with the crotonyl-CoA experiment as even though reducing equivalents are introduced and removed from the system in pairs the intermediary steps are single-electron transfers. This was supported by the same experiment repeated with one-electron reduced complex, EtfAB:bcd$_{1e}^-$ (where the et FAD was reduced to FAD•$^-$ leaving oxidized bf and bcd FAD), in which the same persistence of FAD•$^-$ was observed at the end of reaction.

When enzyme monitored turnover experiments of oxidized EtfAB:bcd were performed in the presence of ferredoxin several aspects of the reaction were observed. The first is reduction proceeded in a two-stage fashion, where the first phase consisted of an "approach to steady-state" in which FAD reduction was observed without any ferredoxin reduction and lasted several seconds. The "steady-state" phase of ferredoxin reduction followed and consisted of only ferredoxin reduction with a k_{cat} of 0.2 s^{-1}. The reaction performed with EtfAB:bcd_{1e^-} only resulted in a five-fold decrease to the onset of ferredoxin reduction and did not impact the rate of reduction. When EtfAB:bcd_{6e^-} was reacted with crotonyl-CoA and ferredoxin the same "two-stage" behavior was observed, however the approach phase of reduction consisted of $FAD\bullet^-$ accumulation before ferredoxin reduction. Observation of ferredoxin reduction absent NADH illustrated that bifurcation was strictly dependent on the electron transfer into the high-potential pathway and wasn't driven by reduction of the bf FAD as supported by Chapter 7.

The experiment with EtfAB:bcd reacted with NADH/crotonyl-CoA (post-catalysis EtfAB:bcd) and then re-reacted with NADH/crotonyl-CoA and ferredoxin proved to be vital in understanding ferredoxin reduction. Other permutations of the reaction had the onset of ferredoxin reduction occurring after FAD reduction. However, in the case of the post-catalysis enzyme immediate ferredoxin reduction was observed. This was then followed by the steady-state reduction of ferredoxin as before with the same k_{cat}. In contrast to the reaction with EtfAB:bcd_{1e^-} where only the et FAD is in the semiquinone oxidation state, the post catalysis enzyme was predominately in the hydroquinone with a small portion in semiquinone oxidation state. This evidence

supported the proposal that the et FAD must be reduced prior to effective bifurcation and operated exclusively between the SQ/HQ couple during catalysis. The et FAD being unable to reduce the bcd FAD and the reaction with EtfAB:bcd_{1e^-} only decreasing the approach to ferredoxin reduction reinforces this further.

9.8 Future directions

In the present work, we have firmly established the kinetics of several discrete electron transfer steps of the reaction and determined that the reduction of ferredoxin is preserved through controlled, slow electron transfer into the high-potential pathway. The et FAD serves as the first site in the high-potential pathway and is operating exclusively between the hydroquinone and semiquinone oxidation states, thus limiting transfer from bf FAD to a single electron transfer at any point. As discussed above, reduction of the et FAD and its large domain movement play a vital role in electron transfer and serves as the gatekeeper for electrons into the high-potential pathway. It is also implicated as involved in the uncrossing behavior of the bf FAD's half-potentials as shown when nearly quantitative bf $FAD^{\bullet -}$ accumulation was observed when the et FAD was removed. There is also crystallographic evidence of interaction between the α subunit and bf FAD as illustrated in the *A fermentans* EtfAB structure (96).

With this, two key experiments to probe the dynamics of the domain motion and mutation studies could be performed. The first being solution-state NMR, as there are only two tryptophan residues in EtfAB, one on the α subunit proximal to the et FAD and the other being in the interface between α and ß subunits near the bf FAD. The

characteristic NMR spectra can be used to probe the effects of domain movements in per-deuterated enzyme. The second being mutational studies, in which the α and ß domains are joined via chemical ligations. If EtfAB proves to be stable with both domains linked together then the reactions with NADH could be repeated and compared to determine if domain movement effects the percentage of bf FAD that becomes uncrossed during catalysis. If ligation could be performed after removal of the et FAD then the effect of uncrossing could also be determined by sodium dithionite titration in the absence of the et FAD (but still interacting with the α domain). Lastly, reduction of precomplexed EtfAB:ferredoxin and NADH could be performed via stopped-flow and with rapid freeze quench EPR to observe if any ferredoxin reduction occurs at the rate of intrinsic electron transfer in the case of ligated enzyme.

Chapter 10

References

1. Wikström, M.K. and Berden, J.A. (1972). *Biochimica et Biophysica Acta (BBA)-Bioenergetics*, 283, 403-420, https://doi.org/10.1016/0005-2728(72)90258-7

2. Herrmann, G., Jayamani, E., Mai, G., Buckel, W. (2008). Energy conservation via electrontransferring flavoprotein in anaerobic bacteria, *J. Bacteriol*. 190 784–791, https://doi.org/10.1128/JB.01422-07

3. Buckel, W., Thauer, R.K. (2018). Flavin-Based Electron Bifurcation, ferredoxin, flavodoxin and anaerobic respiration with protons (Ech) or NAD+ (Rnf) as electron acceptors: a historical review, *Front. Microbiol.* 9 article # 401, https://doi.org/10.3389/fmicb.2018.00401

4. Buckel, W., Thauer, R.K., (2018), Flavin-based electron bifurcation, A new mechanism of biological energy coupling, *Chem. Rev*. 118 3862–3886, https://doi.org/10.1021/acs.chemrev.7b00707

5. Buckel, W., Thauer, R.K., (2013). Energy conservation via electron bifurcating ferredoxin reduction and proton/Na+ translocating ferredoxin oxidation, *Biochim. Biophys. Acta Bioenerg.* 1827 94–113, https://doi.org/10.1016/j.bbabio.2012.07.002

6. Kaster, A.-K., Moll, J., Parey, K., & Thauer, R. K. (2011). Coupling of ferredoxin and heterodisulfide reduction via electron bifurcation in hydrogenotrophic methanogenic archaea. *Proceedings of the National Academy of Sciences of the United States of America*, 108(7), 2981–2986. https://doi.org/10.1073/pnas.1016761108

7. Wang, S. N., Huang, H. Y., Kahnt, J., Mueller, A. P., Kopke, M., & Thauer, R. K. (2013). NADP-specific electron-bifurcating FeFe -hydrogenase in a functional complex with formate dehydrogenase in *clostridium autoethanogenum* grown on CO. *Journal of Bacteriology*, 195(19), 4373–4386. https://doi.org/10.1128/jb.00678-13

8. Crane, F.L., Beinert, H., (1954). A link between fatty acyl CoA dehydrogenase and cytochrome c: a new flavin enzyme1. *J. Am. Chem. Soc* 76 , 4491–4491, https://doi.org/10.1021/ja01646a076

9. Gorelick, R.J., Mizzer, J.P., and Thorpe C., (1982). Purification and Properties of Electron-Transferring Flavoprotein from Pig Kidney, *Biochem.* 21, 6936-6942 https://doi.org/10.1021/bi00269a049

10. Leys, D., Basran, J., Talfournier, F., Sutcliffe, M. J., & Scrutton, N. S. (2003). Extensive conformational sampling in a ternary electron transfer complex. *Nature Structural & Molecular Biology,* 10(3), 219–225. https://doi.org/10.1038/nsb894

11. Feng, X., Schut, G. J., Lipscomb, Adams, M. W. W. (2020), Cryoelectron microscopy structure and mechanism of the membrane-associated electron-bifurcating flavoprotein Fix/EtfABCX, *Biochem*. 118 (2) https://doi.org/10.1073/pnas.2016978118

12. Chowdhury, N. P., Kahnt, J., & Buckel, W. (2015). Reduction of ferredoxin or oxygen by flavin ‐ based electron bifurcation in *Megasphaera elsdenii*. *The FEBS Journal*, 282(16), 3149 ‐ 3160. Portico. https://doi.org/10.1111/febs.13308

13. Toogood, H. S., Leys, D., & Scrutton, N. S. (2007). Dynamics driving function - new insights from electron transferring flavoproteins and partner complexes. *FEBS Journal*, 274(21), 5481–5504. https://doi.org/10.1111/j.1742-4658.2007.06107.x

14. Demmer, J. K., Chowdhury, N. P., Selmer, T., Ermler, U., & Buckel, W. (2017). The semiquinone swing in the bifurcating electron transferring flavoprotein/butyryl-CoA dehydrogenase complex from *Clostridium difficile*. *Nature Communications*, 8, 1–10. https://doi.org/10.1038/s41467-017-01746-3

15. Abbas C, A, Sibirny A, A. (2011). Genetic control of biosynthesis and transport of riboflavin and flavin nucleotides and construction of robust biotechnological producers. *Microbiol Mol Biol Rev*. 75(2):321-60. https://doi.org/10.1128/MMBR.00030-10

16. Warburg, O., and Christian, W., (1932). Über ein neues Oxydationsferment und sein Absorptionsspektrum. Biochemische Zeitschrift. 254: 438–458

17. Theorell, H., (1935). Das gelbe Oxydationsferment. Biochemische Zeitschrift. 278: 263–290

18. Theorell, H., (1937). Die freie Eiweisskomponente des gelben Ferments und ihre Kupplung mit Lacto-flavinphosphorsaure. Biochemische Zeitschrift. 290: 293–303

19. Warburg, O., and Christian, W., (1938). Isolierung der prosthetischen Gruppe der d-Aminosaureoxydase. Biochemische Zeitschrift. 298: 150–155

20. Hayashi, H. (2013). *Historical Context of Vitamin B. In B Vitamins and Folate Chemistry, Analysis, Function and Effects* (pp. 6–8). essay, *The Royal Society of Chemistry*.

21. Fischer, M., & Bacher, A. (2010). Biosynthesis of riboflavin. *EcoSal Plus*, 4(1). https://doi.org/10.1128/ecosalplus.3.6.3.2

22. Kaiser, J., Schramek, N., Eberhardt, S., Püttmer, S., Schuster, M., & Bacher, A. (2002). Biosynthesis of vitamin B2. *European Journal of Biochemistry*, 269(21), 5264–5270. https://doi.org/10.1046/j.1432-1033.2002.03239.x

23. Richter, G., Fischer, M., Krieger, C., Eberhardt, S., Lüttgen, H., Gerstenschläger, I., & Bacher, A. (1997). Biosynthesis of riboflavin: Characterization of the bifunctional deaminase-reductase of *Escherichia coli* and *Bacillus subtilis*. *Journal of Bacteriology*, 179(6), 2022–2028. https://doi.org/10.1128/jb.179.6.2022-2028.1997

24. Richter, G., Krieger, C., Volk, R., Kis, K., Ritz, H., Götze, E., Bacher, A., (1997). *Biosynthesis of riboflavin: 3,4-dihydroxy-2-butanone-4-phosphate synthase*, *Methods in Enzymology, Academic Press*, Volume 280, Pages 374-382, ISSN 0076-6879, ISBN 9780121821814, https://doi.org/10.1016/S0076-6879(97)80128-0

25. Richter, G., Fischer, M., Krieger, C., Eberhardt, S., Lüttgen, H., Gerstenschläger, I., & Bacher, A. (1997). Biosynthesis of riboflavin: Characterization of the bifunctional deaminase-reductase of *Escherichia coli* and *Bacillus subtilis.* *Journal of Bacteriology*, 179(6), 2022–2028. https://doi.org/10.1128/jb.179.6.2022-2028.1997

26. Eberhardt, S., Richter, G., Gimbel, W., Werner, T., & Bacher, A. (1996). Cloning, sequencing, mapping and hyperexpression of the *ribc* gene coding for riboflavin synthase of *Escherichia coli*. *European Journal of Biochemistry*, 242(3), 712–719. https://doi.org/10.1111/j.1432-1033.1996.0712r.x

27. Kearney, E. B., Goldenberg, J., Lipsick, J., & Perl, M. (1979). Flavokinase and FAD synthetase from *Bacillus subtilis* specific for reduced flavins. *Journal of Biological Chemistry*, 254(19), 9551–9557. https://doi.org/10.1016/s0021-9258(19)83550-0

28. Efimov, I., Kuusk, V., Zhang, X., & McIntire, W. S. (1998). Proposed Steady-State Kinetic Mechanism for *Corynebacterium ammoniagenes* FAD Synthetase Produced by Escherichia coli. *Biochemistry*, 37(27), 9716–9723. https://doi.org/10.1021/bi972817j

29. Abbas, C. A., & Sibirny, A. A. (2011). Genetic control of biosynthesis and transport of riboflavin and flavin nucleotides and construction of robust biotechnological producers. *Microbiology and Molecular Biology Reviews*, 75(2), 321–360. https://doi.org/10.1128/mmbr.00030-10

30. Müller, F. (1983). The flavin redox-system and its biological function. In: *Radicals in Biochemistry. Topics in Current Chemistry*, vol 108. Springer, Berlin, Heidelberg. https://doi.org/10.1007/3-540-11846-2_3

31. Kao, Y.-T., Saxena, C., He, T.-F., Guo, L., Wang, L., Sancar, A., & Zhong, D. (2008). Ultrafast Dynamics of Flavins in Five Redox States. *Journal of the American Chemical Society*, 130(39), 13132–13139. https://doi.org/10.1021/ja8045469

32. Chosrowjan, H., Taniguchi, S., Mataga, N., Tanaka, F., & Visser, A. J. W. G. (2003). The stacked flavin adenine dinucleotide conformation in water is fluorescent on picosecond timescale. *Chemical Physics Letters*, 378(3–4), 354–358. https://doi.org/10.1016/s0009-2614(03)01339-3

33. Anderson, R. F. (1983). Energetics of the one-electron reduction steps of riboflavin, FMN and FAD to their fully reduced forms. *Biochimica et Biophysica Acta (BBA) - Bioenergetics,* 722(1), 158–162. https://doi.org/10.1016/0005-2728(83)90169-x

34. Libby, W. F. (1952). Theory of electron exchange reactions in aqueous solution. The *Journal of Physical Chemistry*, 56(7), 863-868 https://doi.org/10.1021/j150499a010

35. Marcus, R. A. (1956). On the Theory of Oxidation-Reduction Reactions Involving Electron Transfer. I. *Journal of Chemical Physics*, 24(5), 966–978. https://doi.org/10.1063/1.1742723

36. Marcus, R. J., Zwolinski, B. J., and Eyring, H., (1954) The Electron Tunnelling Hypothesis for Electron Ex-change Reactions. *The Journal of Physical Chemistry 58* (5), 432-437 https://doi.org/10.1021/j150515a013

37. Marcus, R. J., Zwolinski, B. J., and Eyring, H., (1955), Inorganic Oxidation-Reduction Reactions in Solution Electron Transfers. *Chemical Reviews* 55 (1), 157-180 https://doi.org/10.1021/cr50001a004

38. Wardman, P. (1989). Reduction potentials of one‐electron couples involving free radicals in aqueous solution. *Journal of Physical and Chemical Reference Data*, 18(4), 1637-1755. https://doi.org/10.1063/1.555843

39. Elsden, S. R., & Lewis, D. (1953). The production of fatty acids by a gram-negative coccus. *The Biochemical journal*, 55(1), 183–189. https://doi.org/10.1042/bj0550183

40. Gutierrez, J., Davis, R. E., Lindahl, I. L., & Warwick, E. J. (1959). Bacterial changes in the rumen during the onset of feed-lot bloat of cattle and characteristics of *Peptostreptococcus elsdenii* n. sp. *Applied microbiology*, 7(1), 16-22 https://doi.org/10.1128/aem.7.1.16-22.1959

41. Rogosa, M. (1971). Transfer of Peptostreptococcus elsdenii Gutierrez et al. to a new genus, *Megasphaera [M. elsdenii* (Gutierrez et al.) comb. nov.]. *International journal of systematic and evolutionary microbiology*, 21(2), 187-189. https://doi.org/10.1099/00207713-21-2-187

42. Elsden, S. R., Volcani, B. E., Gilchrist, F. M. C., & Lewis, D. (1956). Properties of a fatty acid forming organism isolated from the rumen of sheep. *Journal of bacteriology*, 72(5), 681-689. https://doi.org/10.1128%2Fjb.72.5.681-689.1956

43. Hino, T., Miyazaki, K., & Kuroda, S. (1991). Role of extracellular acetate in the fermentation of glucose by a ruminal bacterium, *Megasphaera elsdenii*. *The Journal of General and Applied Microbiology*, 37(1), 121-129. https://doi.org/10.2323/jgam.37.121

44. Hungate, R. F., (1966). *The rumen and Its Microbes*. *Academic Press Inc*., New York p. 76-77 https://doi.org/10.1016/c2013-0-12555-x

45. Valentine, R. C., & Wolfe, R. S. (1963). Role of ferredoxin in the metabolism of molecular hydrogen. *Journal of Bacteriology*, 85(5), 1114-1120. https://doi.org/10.1128/jb.85.5.1114-1120.1963

46. Baldwin, R. L., & Milligan, L. P. (1964). Electron transport in *Peptostreptococcus elsdenii*. *Biochimica et Biophysica Acta (BBA)* - Specialized Section on Enzymological Subjects, 92(3), 421–432. https://doi.org/10.1016/0926-6569(64)90001-x

47. PEEL J. L. (1958). The separation of flavins by paper electrophoresis and its application to the examination of the flavin contents of micro-organisms. *The Biochemical journal*, 69(3), 403–416. https://doi.org/10.1042/bj0690403

48. Whitfield, C. D., & Mayhew, S. G. (1974). Purification and Properties of Electron-transferring Flavoprotein from *Peptostreptococcus elsdenii. Journal of Biological Chemistry*, 249(9), 2801–2810. https://doi.org/10.1016/s0021-9258(19)42700-2

49. Sato, K., Nishina, Y., and Shiga, K. (2003). Purification of Electron-Transferring Flavoprotein from *Megasphaera elsdenii* and Binding of Additional FAD with an Unusual Absorption Spectrum. *Journal of Biochemistry*, 134(5), 719–729. https://doi.org/10.1093/jb/mvg199

50. Sato, K., Nishina, Y., & Shiga, K. (2013). Interaction between NADH and electron-transferring flavoprotein from *Megasphaera elsdenii. Journal of Biochemistry*, 153(6), 565–572. https://doi.org/10.1093/jb/mvt026

51. Engel, P. C., & Massey, V. (1971). The purification and properties of butyryl-coenzyme A dehydrogenase from *Peptostreptococcus elsdenii. Biochemical Journal*, 125(3), 879–887. https://doi.org/10.1042/bj1250879

52. Fink, C. W., Stankovich, M. T., & Soltysik, S. (1986). Oxidation-reduction potentials of butyryl-CoA dehydrogenase. *Biochemistry*, 25(21), 6637–6643. https://doi.org/10.1021/bi00369a046

53. Stankovich, M. T., & Soltysik, S. (1987). Regulation of the butyryl-CoA dehydrogenase by substrate and product binding. *Biochemistry*, 26(9), 2627–2632. https://doi.org/10.1021/bi00383a033

54. Weiss, M. C., Preiner, M., Xavier, J. C., Zimorski, V., & Martin, W. F. (2018). The last universal common ancestor between ancient Earth chemistry and the onset of genetics. *PLOS Genetics*, 14(8), e1007518. https://doi.org/10.1371/journal.pgen.1007518

55. Pearce, B. K. D., Tupper, A. S., Pudritz, R. E., & Higgs, P. G. (2018). Constraining the Time Interval for the Origin of Life on Earth. *Astrobiology*, 18(3), 343–364. https://doi.org/10.1089/ast.2017.1674

56. Martin, W. F., Bryant, D. A., & Beatty, J. T. (2018). A physiological perspective on the origin and evolution of photosynthesis. *FEMS Microbiology Reviews*, 42(2), 205–231. https://doi.org/10.1093/femsre/fux056

57. Poudel, S., Dunham, E. C., Lindsay, M. R., Amenabar, M. J., Fones, E. M., Colman, D. R., et al. (2018). Origin and evolution of flavin-based electron bifurcating enzymes. *Frontiers in Microbiology*, 9, 1–26. https://doi.org/10.3389/fmicb.2018.01762

58. Jheeta, Sohan. 2017. "The Landscape of the Emergence of Life." *Life* 7 (2): 27. https://doi.org/10.3390/life7020027

59. O'Sullivan C, Tompson FW (1890) Invertase: a contribution to the history of an enzyme or unorganized ferment. *J Chem Soc* (London) 57:834–931 https://doi.org/10.1039/CT8905700834

60. Brown AJ (1902) Enzyme action. *J Chem Soc* (Trans) 81:373–388 https://doi.org/10.1039/ct9028100373

61. Henri V (1903) Lois generals de l'action des diastases. Hermann, Paris https://doi.org/10.1038/068221d0

62. Michaelis, L., & Menten, M. L. Die Kinetic der Invertinwirkung, 1913. *Biochem*. Z, 49, 333.

63. Johnson, K. A., & Goody, R. S. (2011). The Original Michaelis Constant: Translation of the 1913 Michaelis–Menten Paper. *Biochemistry*, 50(39), 8264–8269. https://doi.org/10.1021/bi201284u

64. Briggs, G. E., & Haldane, J. B. (1925). A Note on the Kinetics of Enzyme Action. The *Biochemical journal*, 19(2), 338–339. https://doi.org/10.1042/bj0190338

65. Hartridge H. and Roughton Francis J. W., (1923) The kinetics of hæmoglobin.—II. The velocity with which oxygen dissociates from its combination with hæmoglobin *Proc. R. Soc. Lond.* A104395–430 http://doi.org/10.1098/rspa.1923.0117

66. Hartridge H. and Roughton Francis J. W., (1923) A method of measuring the velocity of very rapid chemical reactions *Proc. R. Soc. Lond*. A104376–394 http://doi.org/10.1098/rspa.1923.0116

67. Hartridge, H., & Roughton, F. J. W. (1924). Improvements in the Apparatus for Measuring the Velocity of very rapid Chemical Reactions. *Mathematical Proceedings of the Cambridge Philosophical Society*, 22(3), 426–431. https://doi.org/10.1017/S030500410001433X

68. Thomas, N. C. (1991). The early history of spectroscopy. *Journal of chemical education*, 68(8), 631. https://doi.org/10.1021/ed068p631

69. Fasella, P. (1967). Pyridoxal phosphate. *Annual Review of Biochemistry*, 36(1), 185-210. https://doi.org/10.1146/annurev.bi.36.070167.001153

70. Edmondson, D.E., Tollin, G. (1983). Semiquinone formation in flavo- and metalloflavoproteins. In: *Radicals in Biochemistry. Topics in Current Chemistry*, vol 108. Springer, Berlin, Heidelberg. https://doi.org/10.1007/3-540-11846-2_4

71. Gibson, Q. H., & Milnes, L. (1964). Apparatus for rapid and sensitive spectrophotometry. *The Biochemical journal*, 91(1), 161–171. https://doi.org/10.1042/bj0910161

72. Gibson, Q. H., Swoboda, B. E. P., & Massey, V. (1964). Kinetics and Mechanism of Action of Glucose Oxidase. *Journal of Biological Chemistry*, 239(11), 3927–3934. https://doi.org/10.1016/s0021-9258(18)91224-x

73. Strickland, S., & Massey, V. (1973). The Mechanism of Action of the Flavoprotein Melilotate Hydroxylase. *Journal of Biological Chemistry*, 248(8), 2953–2962. https://doi.org/10.1016/s0021-9258(19)44100-8

74. Strickland, S. & Palmer, G & Massey, V. (1975). Determination of dissociation constants and specific rate constants of enzyme substrate (or protein ligand) interactions from rapid reaction kinetic data. *The Journal of biological chemistry*. 250. 4048-52. https://doi.org/10.1016/S0021-9258(19)41384-7

75. Gay-Lussac, H. L. *Ann. Chim*. 1815, 95, 172.

76. Gomberg, M. (1900). AN INSTANCE OF TRIVALENT CARBON: TRIPHENYLMETHYL. *Journal of the American Chemical Society*, 22(11), 757–771. https://doi.org/10.1021/ja02049a006

77. Zavoisky, E. K., Paramagnetic Relaxation of Liquid Solutions for Perpendicular Fields Zhur. Eksperiment. i *Theoret. Fiz*., Vol.15, pp.344–350, 1945

78. Roessler, M. M., and Salvadori, E. (2018). Principles and Applications of EPR Spectroscopy in the Chemical Sciences. *Chemical Society Reviews* 47 (8): 2534–53. https://doi.org/10.1039/C6CS00565A

79. Rowlands, C. C., and Murphy, D. M., (1999). EPR Spectroscopy, Theory. *In Encyclopedia of Spectroscopy and Spectrometry*, 445–56. Elsevier. https://doi.org/10.1006/rwsp.2000.0080

80. Palmer G., Mueller F., Massey V., (1971). Electron paramagnetic resonance studies on flavoprotein radicals, in: H. Kamin (Ed.), *Flavins and Flavoproteins*, University Park Press, Baltimore, 132–140.

81. Edmondson, D.E., Tollin, G., (1983). Semiquinone formation in flavo- and metalloflavoproteins, Radicals in Biochem. Topics in Current Chem. 109–138, https://doi.org/10.1007/3-540-11846-2_4

82. Williamson, G., Engel, P. C., Mizzer, J. P., Thorpe, C., and Massey, V. (1982) Evidence that the greening ligand in native butyryl-CoA dehydrogenase is a CoA persulfide. *J. Biol. Chem.* 257, 4314 https://doi.org/10.1016/s0021-9258(18)34723-9

83. Djordjevic, S., Pace, C. P., Stankovich, M. T., and Kim, J. J. P. (1995) 3-Dimensional structure of butyryl-CoA dehydrogenase from *Megasphaera elsdenii. Biochemistry* 34, 2163–2171 https://doi.org/10.2210/pdb1buc/pdb

84. Jaganaman, S., Pinto, A., Tarasev, M., & Ballou, D. P. (2007). High levels of expression of the iron–sulfur proteins phthalate dioxygenase and phthalate dioxygenase reductase in *Escherichia coli*. *Protein Expression and Purification*, 52(2), 273–279. https://doi.org/10.1016/j.pep.2006.09.004

85. Aliverti, A., Curti, B., & Vanoni, M. A. (n.d.). *Identifying and Quantitating FAD and FMN in Simple and in Iron-Sulfur-Containing Flavoproteins. Flavoprotein Protocols*, 9–24. https://doi.org/10.1385/1-59259-266-x:9

86. Kozioł, J. (1971). Fluorometric analyses of riboflavin and its coenzymes. *Methods in Enzymology*, 253–285. https://doi.org/10.1016/s0076-6879(71)18089-5

87. Viola, R. E., Cook, P. F., & Cleland, W. W. (1979). Stereoselective preparation of deuterated reduced nicotinamide adenine nucleotides and substrates by enzymatic synthesis. *Analytical Biochemistry*, 96(2), 334–340. https://doi.org/10.1016/0003-2697(79)90590-6

88. Toogood, H. S., Leys, D., & Scrutton, N. S. (2007). Dynamics driving function−new insights from electron transferring flavoproteins and partner complexes. *The FEBS Journal*, 274(21), 5481–5504. Portico. https://doi.org/10.1111/j.1742-4658.2007.06107.x

89. Niks D., Hille R., (2018). Reductive activation of CO2 by formate dehydrogenases, *Methods Enzymol*. 613 277–295, https://doi.org/10.1016/bs.mie.2018.10.013

90. Ortiz, S., Niks, D., Wiley, S., Lubner, C. E., & Hille, R. (2023). Rapid-reaction kinetics of the bifurcating NAD+-dependent NADPH:ferredoxin oxidoreductase NfnI from *Pyrococcus furiosus. Journal of Biological Chemistry*, 299(12), 105403. https://doi.org/10.1016/j.jbc.2023.105403

91. Aono, S., Bryant, F. O., & Adams, M. W. (1989). A novel and remarkably thermostable ferredoxin from the hyperthermophilic archaebacterium *Pyrococcus furiosus. Journal of Bacteriology*, 171(6), 3433–3439. https://doi.org/10.1128/jb.171.6.3433-3439.1989

92. Vigil, W., Niks, D., Franz-Badur, S., Chowdhury, N., Buckel, W., & Hille, R. (2021). Spectral deconvolution of redox species in the crotonyl-CoA-dependent NADH:ferredoxin oxidoreductase from *Megasphaera elsdenii*. A flavin-dependent bifurcating enzyme. *Archives of Biochemistry and Biophysics*, 701, 108793. https://doi.org/10.1016/j.abb.2021.108793

93. Nitschke, W., & Russell, M. J. (2011). Redox bifurcations: Mechanisms and importance to life now, and at its origin. *BioEssays*, 34(2), 106–109. Portico. https://doi.org/10.1002/bies.201100134

94. Metcalf, W. W. (2016). Classic Spotlight: Electron Bifurcation, a Unifying Concept for Energy Conservation in Anaerobes. *Journal of Bacteriology*, 198(9), 1358–1358. https://doi.org/10.1128/jb.00185-16

95. Lubner, C. E., & Peters, J. W. (2017). Electron Bifurcation Makes the Puzzle Pieces Fall Energetically into Place in Methanogenic Energy Conservation. *ChemBioChem*, 18(23), 2295–2297. Portico. https://doi.org/10.1002/cbic.201700533

96. Chowdhury, N. P., Mowafy, A. M., Demmer, J. K., Upadhyay, V., Koelzer, S., Jayamani, E., Kahnt, J., Hornung, M., Demmer, U., Ermler, U., & Buckel, W. (2014). Studies on the Mechanism of Electron Bifurcation Catalyzed by Electron Transferring Flavoprotein (Etf) and Butyryl-CoA Dehydrogenase (Bcd) of *Acidaminococcus fermentans. Journal of Biological Chemistry*, 289(8), 5145–5157. https://doi.org/10.1074/jbc.m113.521013

97. Vigil, W., Tran, J., Niks, D., Schut, G. J., Ge, X., Adams, M. W. W., & Hille, R. (2022). The reductive half-reaction of two bifurcating electron-transferring flavoproteins. *Journal of Biological Chemistry*, 298(6), 101927. https://doi.org/10.1016/j.jbc.2022.101927

98. Pace, C. P., & Stankovich, M. T. (1987). Redox properties of electron-transferring flavoprotein from Megasphaera elsdenii. *Biochimica et Biophysica Acta (BBA) - Protein Structure and Molecular Enzymology*, 911(3), 267–276. https://doi.org/10.1016/0167-4838(87)90067-7

99. Sucharitakul, J., Buckel, W., & Chaiyen, P. (2021). Rapid kinetics reveal surprising flavin chemistry in bifurcating electron transfer flavoprotein from *Acidaminococcus fermentans. Journal of Biological Chemistry*, 296, 100124. https://doi.org/10.1074/jbc.ra120.016017

100. Fersht, A. (1999). *Chemical Catalysis. In Structure and Mechanism in Protein Science: A Guide to Enzyme Catalysis and Protein Folding* (pp. 96–96). W.H. Freeman.

101. Yakovlev, G., & Hirst, J. (2007). Transhydrogenation Reactions Catalyzed by Mitochondrial NADH−Ubiquinone Oxidoreductase (Complex I). *Biochemistry*, 46(49), 14250–14258. https://doi.org/10.1021/bi7017915

102. Klinman, J. P. (1972). The Mechanism of Enzyme-catalyzed Reduced Nicotinamide Adenine Dinucleotide-dependent Reductions. *Journal of Biological Chemistry*, 247(24), 7977–7987. https://doi.org/10.1016/s0021-9258(20)81798-0

103. Vigil, W., Nguyen, D., Niks, D., & Hille, R. (2023). Rapid-reaction kinetics of the butyryl-CoA dehydrogenase component of the electron-bifurcating crotonyl-CoA-dependent NADH:ferredoxin oxidoreductase from *Megasphaera elsdenii. Journal of Biological Chemistry*, 299(7), 104853. https://doi.org/10.1016/j.jbc.2023.104853

104. Ghisla, S., Thorpe, C., & Massey, V. (1984). Mechanistic studies with general acyl-CoA dehydrogenase and butyryl-CoA dehydrogenase: evidence for the transfer of the .beta.-hydrogen to the flavin position N(5) as a hydride. *Biochemistry*, 23(14), 3154–3161. https://doi.org/10.1021/bi00309a008

105. Kim, J., Darley, D. J., Buckel, W., & Pierik, A. J. (2008). An allylic ketyl radical intermediate in clostridial amino-acid fermentation. *Nature*, 452(7184), 239–242. https://doi.org/10.1038/nature06637

106. Anderson, R. F., Jang, M.-H., & Hille, R. (2000). Radiolytic Studies of Trimethylamine Dehydrogenase. *Journal of Biological Chemistry*, 275(40), 30781–30786. https://doi.org/10.1074/jbc.m001256200

107. Harris, K. R., & Woolf, L. A. (2004). Temperature and Volume Dependence of the Viscosity of Water and Heavy Water at Low Temperatures. *Journal of Chemical & Engineering Data*, 49(6), 1851–1851. https://doi.org/10.1021/je049668

108. Volk, A., & Kähler, C. J. (2018). Density model for aqueous glycerol solutions. Experiments in Fluids, 59(5). https://doi.org/10.1007/s00348-018-2527-y

Appendix A

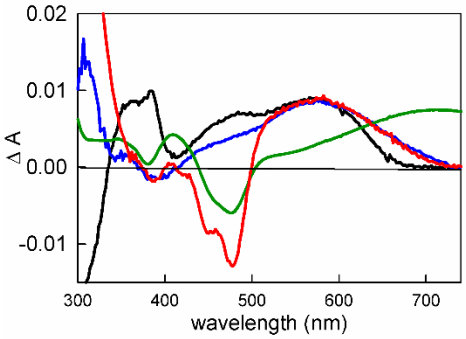

Appendix A1. Long wavelength absorbance of bcd. Black is the FADH• as extracted from the sodium dithionite titration at pH 6.0. The main absorbance maxima are 370 nm, 470 nm and at 574 nm. All subsequent pure spectra were obtained by selecting points via inspection as done in Chapter 3, during the course of titration or reaction. Blue is the bcdred:crotonyl-CoA CTC which was extracted from the rapid reaction kinetics experiment. The absorption maxima centered at 574 nm is in the same as the FADH• signal but is missing the 370 nm maxima. Green is the persulfide-CoA bound bcd as seen during purification, the absorbance maxima is centered around 700 nm. Lastly, red is the difference between oxidized bcd and then mixed with excess acetoacetyl-CoA, again we find an absorbance maximum at 574 nm, the negative features at 470 nm and 450 are a result of a shift in the FAD absorbance upon binding.

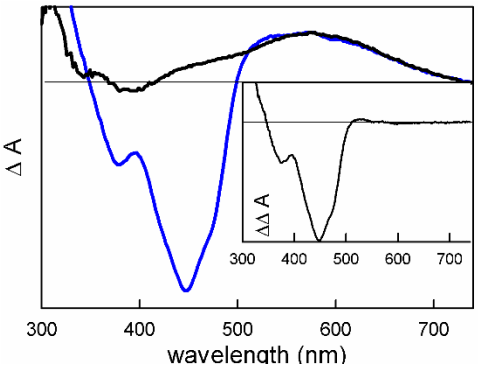

Appendix A2. CTC spectra of bcd and the appropriate crotonyl/butyryl-CoA. Black spectra resulting from the binding of reduced bcd and crotonyl-CoA after 1 ms showing full formation of the bcd_{red}:crotonyl-CoA CTC upon binding. Blue shows the absorbance from reacting oxidized bcd and butyryl-CoA, bcd_{ox}:butyryl-CoA CTC, negative features are a result of FAD reduction in bcd during the mixing dead time of the stopped flow. Inset, is the difference spectra of bcd_{red}:crotonyl-CoA CTC minus bcd_{ox}:butyryl-CoA CTC, the unperturbed FAD spectra seen in the resulting difference spectra is illustrates that the two CTCs are indistinguishable from each other at any reasonable concentration.

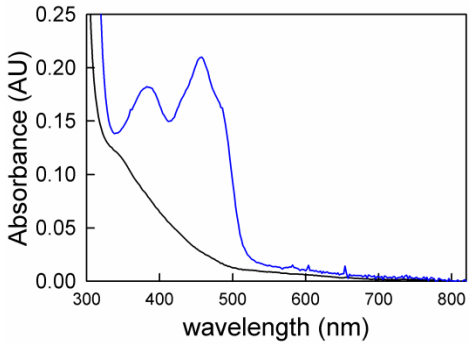

Appendix A3. Mimicking reoxidation of bcd by crotonyl-CoA with stopped-flow mixing in an anaerobic cuvette. In a Hewlett-Packard 8452A diode-array spectrophotometer, a 500 µL solution of 10 µM bcd was titrated to max reduction by sodium dithionite in an anaerobic cuvette, then is taken up into a 500 µL Hamilton syringe. Another Hamilton syringe filled with 500 µL of 200 µM crotonyl-CoA pierces the anaerobic cuvette, both syringes are simultaneously ejected into the anaerobic cuvette and spectra are taken in kinetics mode, mimicking the equal volume mixing seen in the stopped-flow. The black spectrum shows the fully reduced bcd and the blue spectrum shows reoxidized bcd after mixing with crotonyl-CoA, without the presence of $FAD^{\bullet -}$.

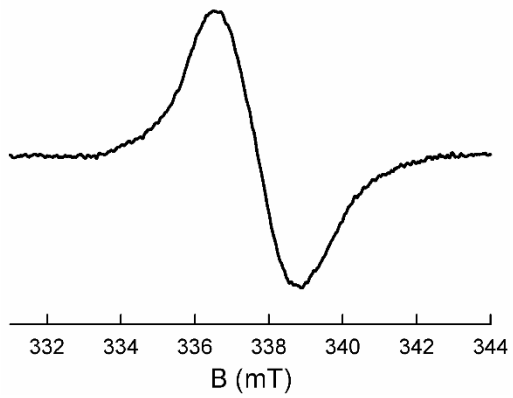

Appendix A4. 77 K EPR of EtfAB:bcd reduction by NADH at short timescales in the presence of crotonyl-CoA. Spectra of 16 µM EtfAB:bcd, reacted with an excess (250 µM) of NADH and 100 µM crotonyl-CoA, frozen at ~0.5s after mixing. The rapid formation of anionic semiquinone (1.6 mT) must be due to the uncrossing of the bf FAD, creating semiquinone on both the bf and et FADs, which has been reported in the isolated EtfAB NADH reduction. Rapid freezing was achieved by chilling an anaerobic solution of EtfAB:bcd in a sealed EPR tube on ice, then after injecting and mixing the solution of NADH and crotonyl-CoA (via Hamilton syringe), the tube was quickly frozen in a dry ice/ethanol bath. The EPR sample was observed at 77 K using liquid nitrogen